*Author:*
**Lawal, Aminu M**

*Title:*
**Anthropogenic and lithological controls on production and bioavailability of mineral nutrients in agricultural karst critical zones**

# ANTHROPOGENIC AND LITHOLOGICAL CONTROLS ON PRODUCTION AND BIOAVAILABILITY OF MINERAL NUTRIENTS IN AGRICULTURAL KARST CRITICAL ZONES


Aminu Muhammad Lawal

Supervisors: Heather L. Buss; Penny J. Johnes

A dissertation submitted to the University of Bristol in accordance with the requirements for award of the degree of Doctor of Philosophy in the Faculty of Science

School of Earth Sciences
July 2021

Word count: 41609

# ABSTRACT

Over geological timescales, the functions and shape of the Earth's critical zone (CZ), the region that extends from the top of the vegetation canopy to the bottom of the weathering zone, have been governed by its responses to natural (tectonic and climatic) forcings. Recently, however, anthropogenic activities, occasioned by increasing population (human and livestock) and demand for resources such as food and fibre, have emerged as major drivers of changes in the critical zone. This demand for resources has led to unsustainable land use practices and loss of soil quality especially in karst environments where lithology contributes to the slow formation of nutrient deficient soils.

This thesis investigated the impacts of anthropogenic activities and bedrock lithology in the production, distribution, and bioavailability of mineral nutrients in two karst CZs in Guizhou, China and Crete, Greece, both impacted by intensive agricultural activities but under different timescales and seasonality.

This thesis identifies lithological control on the production, distribution, and abundance of the bulk and bioavailable mineral nutrients in both CZs. In addition, this thesis also identifies the influence of atmospheric dust deposition to the abundance and distribution of bulk mineral nutrients consistent with earlier findings and establishing that bedrock age and climate variability have no significant influence in the production of mineral nutrients in these carbonate environments.

The thesis also establishes that lithology and atmospheric deposition control the abundance and distribution of bioavailable mineral nutrients in both CZs. However, atmospheric deposition is more prominent in the Greek CZ than the Chinese CZ. Recovery of mineral nutrient bioavailability after perturbation was also established to take longer than 5 years, which has previously been shown for forested, silicate bedrock soils, but not agricultural, carbonate bedrock soils.

# Author's Declaration

I declare that the work in this dissertation was carried out in accordance with the requirements of the University's Regulations and Code of Practice for Research Degree Programmes and that it has not been submitted for any other academic award. Except where indicated by specific reference in the text, the work is the candidate's own work. Work done in collaboration with, or with the assistance of, others, is indicated as such. Any views expressed in the dissertation are those of the author.

.....

Aminu Lawal

July 23, 2021

# Acknowledgments

This thesis is a culmination of a long, arduous march along a thorny road to the fulfilment of a lifelong dream. A huge number of people have contributed in various ways to achieve this dream, some of which I may not be able to appreciate in this brief acknowledgement.

First, I want to thank my supervisors Dr Heather Buss and Professor Penny Johnes who accepted my deficiencies, tolerated my inadequacies, and helped make this work a reality. It was a pleasure working with, especially Dr Buss, without whose mix of tenderness and firmness this work would have been impossible. I am grateful.

In addition to my supervisors, I want to say a big thank you to Drs Adam McAleer, Oliver Moore, Nicholas Hayes and Evangelos Mouchos, Ben Buse and Stuart Kearns who have in various ways contributed to the success of this work. I also want to thank our UK, Chinese and Greek collaborators especially Sophia Green, Tim Quine, Zhaoliang Song, Chenlong Tu, Maria Lilli, and Nikolaos Nikolaidis.

To my Head of School and my supervisor-in-law, Professor Richard Pancost, words cannot be enough, so I will simply say thank you. You have been a model and an inspiration.

Back home, I want to thank my wife, Fatima for holding the home front while I was away, and my children Hafsah, Umar and Halima for enduring the long absence of their father.

Finally, to my leader, Dr Ahmad Galadima, I hope this achievement makes you proud.

# COVID-19 Impact Statement

At around March 2020, national lockdowns due to Covid-19 pandemic restricted access to my data and some pending laboratory analyses. This situation was further compounded when I contracted Covid-19 in mid-April 2019. As a result, I lost about six months of laboratory (especially the SEM analyses due to laboratory restrictions) and write-up time. On a visit home in Nigeria, I also contracted the virus again delaying my eventual return to the UK to continue analysing and writing my thesis.

In all, this thesis was greatly impacted by the time lost due to lockdown and my contracting the virus (twice).

# Contents

# List of Figures

# List of Tables

# Chapter 1

## Introduction to the Critical Zone Science, Critical Zone Observatories and Karst Geology

## 1.1 Critical Zone Science and Critical Zone Observatories

The global human population has crossed the 7 billion mark and is projected to reach 9 billion by 2050 (Millennium Assessment Board, 2005). This increase in population has led to increases in the demand for resources such as food and fibre leading to rapid urbanisation, intensive agricultural activities, and deforestation (Foley et al., 2005). The cumulative effects of these activities have transformed, water, vegetation and climate and increased the pressure being exerted on the Earth's surface (Anderson et al., 2010; Brantley et al., 2007), specifically the outer skin called the Critical Zone (Fig. 1, Brantley et al., 2017) which was defined by the National Research Council as 'the heterogeneous, near-surface environment in which complex interactions involving rock, soil, water, air, and living organisms regulate the natural habitat and determine the availability of life-sustaining resources' (NRC, 2001). However, the scope of the definition of the Critical Zone has been reviewed over time to properly outline what environments (such as desert, polar/arctic) constitute the CZ (Giardino and Houser, 2015). The CZ is now generally defined as the region extending from the top of the vegetation canopy to the bottom of the groundwater zone (Brantley and Lebedeva, 2011).

The functions (and shape) of the Critical Zone have been controlled over geological timescales by natural forcings (such as climate change and tectonic shift), however, recently, historical and ongoing anthropogenic changes are negatively impacting the environment leading to substantial loss of ecosystem functions (Lin et al., 2011; Moravec and Chorover, 2020). In the Critical Zone, a complex interplay of processes involving interactions between water, biota and minerals from rocks, which re-equilibrate with surface conditions (Brantley et al., 2007), sustain terrestrial lifeforms by providing energy and nutrients to the living organisms (Anderson et al., 2007; Brantley et al., 2006b; Lin et al., 2011; Moravec and Chorover, 2020). These coupled physical, chemical, and biological processes, such as weathering and erosion, drive the evolution of the Critical Zone and its response to natural (tectonic and climatic) and anthropogenic forcings (Brantley et al., 2007; Brantley et al., 2006b). Responses to these forcings make the CZ susceptible to changes over timescales that range from milliseconds to millions of years, which makes it difficult to understand how the CZ can simultaneously sustain the increase in human population and deliver essential ecosystem services (Brantley et al., 2017; White et al., 2017).

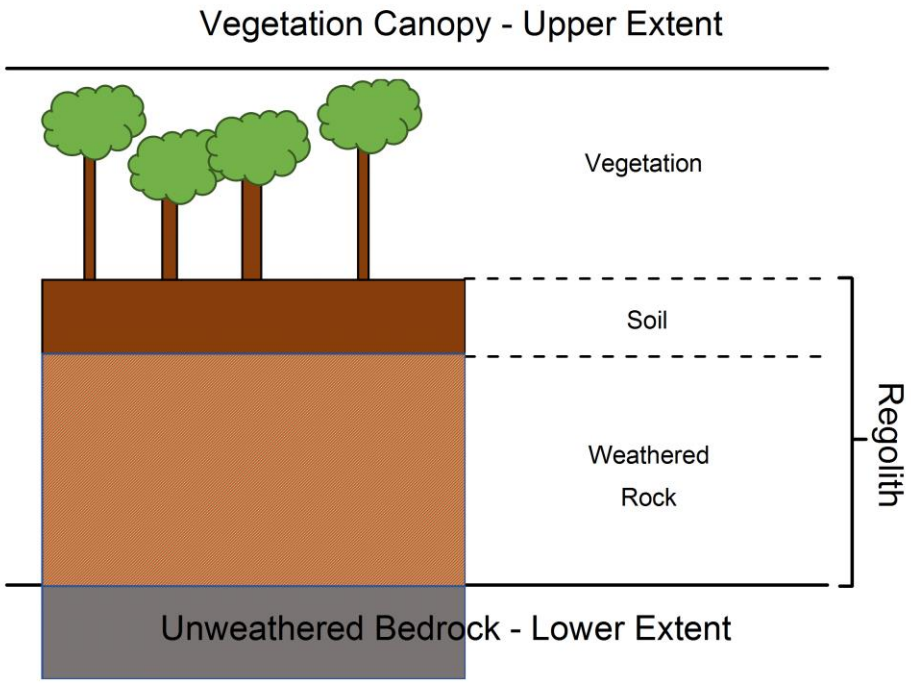


**Figure 1.1:** Schematic diagram, taken from Hayes (2019), representing the extent and depth of the Critical Zone, typically, from the top of the vegetation canopy to the bottom of the weathering zone.

The threat to the sustainability and the complexity of the CZ requires an extensive study of the CZ properties, evolution, and functions (Anderson et al., 2008; Goddéris et al., 2013; White et al., 2017). However, our knowledge of the CZ as a sustainable system that responds to human perturbations (increasing demands for resources due to growing population and decreasing soil quality, maintaining Earth's biodiversity and provision of ecosystem services) is limited (Brantley et al., 2007; Giardino and Houser, 2015). There is little understanding of how processes such as climate variability and land use changes control hydrological as well as biogeochemical fluxes from watersheds (Sekhar et al., 2016) or how the processes control the resilience, response and recovery of the CZ to anthropogenic perturbations (Giardino and Houser, 2015). This complexity and lack of adequate knowledge led to the development of a new field of research known as the Critical Zone Science.

Critical zone scientists integrate spatial and temporal scales to study the evolution of the CZ and its response to human perturbations by integrating various fields of science such as geology, geochemistry, geomorphology, soil science, biology and hydrology, coupling the complex (bio)geochemical, physical and hydrological processes that combine to break down rocks into soil (the process known as weathering), produce nutrients and control carbon sequestration (Anderson et al., 2008; Anderson et al., 2007; Lin et al., 2011; Moravec and Chorover, 2020). Soil, which is the relatively mobile part of the regolith that is easily impacted by human activities (Alekseev et al., 2018), has been recognised by researchers as the principal link through which matter, energy and organisms are exchanged between different Earth systems (such as biosphere, lithosphere and atmosphere, Alekseev et al., 2018; Anderson et al., 2008). Soils, as part of the regolith (Fig. 1), defined by Brantley and Lebedeva (2011) as 'the mantle of physically, chemically and biologically altered material that overlies non-weathered rock' have also long been recognised as records of interactions between different components of the CZ (Brantley and Lebedeva, 2011; Minasny et al., 2008) on both short-term (e.g. days-years) and long-term (years-millennia) timescales and are useful in understanding of both evolution and function of the CZ as well as its response to anthropogenic perturbations.

A major focus in CZ science is to understand what controls the resilience of the CZ and how it responds to historical and ongoing anthropogenic perturbation (Brantley et al., 2006b; Giardino and Houser, 2015) by understanding the mechanisms of, and feedback from, the coupled biogeochemical processes that govern the evolution of the CZ to predict (or 'earthcast') the response of the CZ, through these processes, to increasing human perturbations in the future (Goddéris et al., 2013). To facilitate such interdisciplinary studies focusing on a wide range of timescales, CZ science utilises Critical Zone observatories (CZOs, as 'watershed laboratories' (White et al., 2017). Critical Zone Observatories promote global scale coordination of data collected from different locations and/or environmental gradients (Anderson et al., 2010). They serve as vehicles through which the resilience of the CZ and its response to perturbation is being actively monitored (Giardino and Houser, 2015). In addition, the CZOs provide the platform to integrate the individual disciplines (such as geology, geochemistry, ecology, geomorphology etc) to understand the interactions

between matter, energy and different earth systems and the coupled biogeochemical and physical processes that drive them (Anderson et al., 2010; 2008).

As a global network of sites representing gradients across key environmental parameters (lithology, biology, climate, topography, disturbance and time) that intersect at 'nodes' (Fig. 2), there are several CZOs established in specific environments around the world where research projects are aimed at addressing key scientific questions that mainly couple biogeochemical processes and their response to human perturbations such as land use (Anderson et al., 2010; Anderson et al., 2008; Giardino and Houser, 2015). The focus of this thesis is on two CZOs located in carbonate or karst environments.

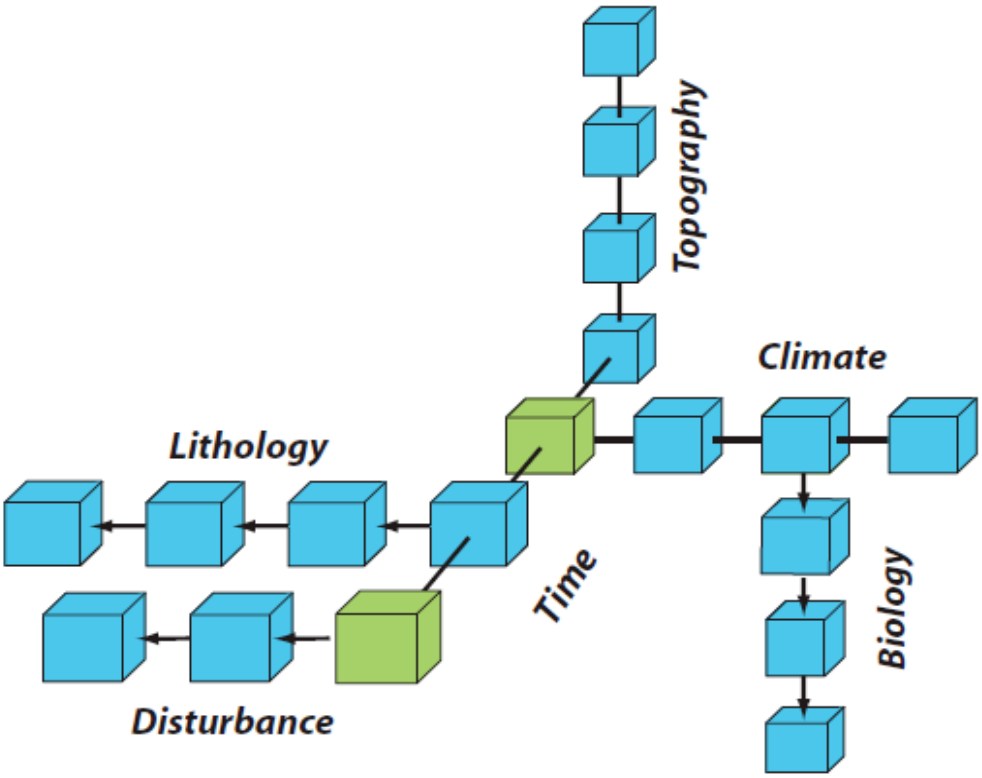


**Figure 1.2:** A diagram, taken from Brantley et al. (2006b) illustrating the environmental gradients represented by the global network of CZOs. Sites coloured in green are designed for a longer more extensive studies of CZ processes than the sites in blue.

### 1.2 Karst Critical Zone

About 25% of the global land surface is covered by carbonate (karst) landscapes dominated by limestones and dolostones and are characterised by thin soil, low water retention

capacity, low nutrient content and surface and subsurface flow paths (Daoxian, 2001; Jiang et al., 2014). Depending on age and regions, karst limestones have different porosities. For example, in China the limestone in the pre-Triassic carbonate rocks have about 1% porosity while the dolostone has about 5% (Daoxian, 2001). On the other hand, other karst environments around the world have significantly higher porosities than Chinese karst. In the Caribbean region for example, carbonate rocks have porosities as high as 16% for limestone and up to 44% for dolomite (Daoxian, 2001; Jiang et al., 2014). The difference in porosities in different karst environments is largely attributed to sedimentation processes, diagenesis and other physical characteristics such as steep karst landforms (Daoxian, 2001).

Many carbonate environments globally are affected by karst rocky desertification due to fragility of the ecosystem, inappropriate land usage and population pressure (Jiang et al., 2014) leading to the loss of large expanses of arable land (Jiang et al., 2014; Wang et al., 2014). Karst rocky desertification has been described as a process of progressive loss of soil quality and land degradation that results in loss of vegetation and exposure of bedrocks (Ye et al., 2011). According to Wang et al. (2004b) karst rocky desertification has led to the loss of cultivated lands (Fig. 3) in China and contributed significantly in reduction to food production and increasing poverty of local populations and drastically changed the hydrological and ecological properties of the soil.

**Figure 1.3**: Karst rocky desertified soil in Chenqi, Guizhou Province, southwestern China. Human activities, such as agriculture, have increased pressure on the fragile karst landscape leading to loss of soil, nutrients, and associated ecosystem services.

In karst environments, arable lands are especially scarce due to the shallowness of the soil, lack of nutrients, adequate vegetation cover and low water retention capacity (Wang et al., 2004a; 2004b). In an environment where the local population are poor and dependent on agriculture, pressures exerted on these soils could lead to significant degradation, loss of fertility and rocky desertification. Extensive human perturbations such as agricultural practices accelerate loss of soil biodiversity and vegetation cover resulting in rocky desertification. Loss of soil biodiversity especially algae and moss makes vegetation recovery in rocky desertified karst environments difficult due to their importance in water retention (Cao et al., 2009). Loss of vegetation cover is likely to affect the abundance of the scarce mineral nutrients in the soil by reducing water retention capacity, increasing overland flow and infiltration (Cao et al., 2009; Jiang et al., 2014; Wang et al., 2004a). Increased overland flow and infiltration increases removal and export of the scarce nutrient elements from the soils in karst systems through weathering.

## 1.3 Weathering in the Critical Zone

Chemical weathering is dominated by the dissolution of minerals from rocks as they reequilibrate to surface conditions, releasing chemical elements that are either retained or removed from the regolith (Brantley et al., 2007; Chapela Lara et al., 2018; Frings and Buss, 2019) and transported to the rivers and oceans through runoff or groundwater. Weathering, both chemical and physical, is the principal process that shapes landscapes, regulate climate and drive production of mineral nutrients and soil formation and development (Chapela Lara et al., 2018; Maher, 2010; Moore et al., 2019; West et al., 2005). The formation of soil and the production of mineral nutrients (as well as the release of soil mineral nutrients such as Ca, Mg, K, Fe) from weathering reactions are seen as the most important processes that drive the creation and the sustenance of the CZ (Brantley et al., 2006a; Chapela Lara et al., 2018). Understanding weathering processes and rates is therefore important in improving our understanding of the CZ evolution and response to pertubation.

### 1.3.1 Weathering Controls – Lithology, Climate, Vegetation and Land Use

Although weathering is the key process through which soils are formed, different factors (such as climate, vegetation, land use and lithology) can affect the rate of soil formation and production, mobilisation, and distribution of mineral nutrients. In terms of lithology, different rock types (such as silicate and carbonate rocks) have different weathering rates as well as mineral composition. Silicate rocks which constitute about 90% of rocks on the global surface (Garrels and MacKenzie, 1971; White and Buss, 2014) weather slower than other rocks such as carbonates and/or evaporites (Jiang et al., 2014; Viers et al., 2014). Lithology also strongly influences weathering rates by influencing the availability of fresh minerals of varying reactivity for weathering reactions. For example, in silicate weathering, mafic (basaltic) lithologies are generally more reactive than felsic (granitic) lithologies and have a wider proportion of minerals containing Ca and Mg (such as apatite, feldspars and amphiboles) to drive carbonate formation in marine sediments (Chapela Lara et al., 2018; Hayes et al., 2020; Oliva et al., 2003). Although felsic lithologies have similar minerals, albeit in lower proportions compared with mafic silicates, it could be said that mafic lithologies

exhibit greater control on silicate weathering rates, long-term climate regulation and faster soil forming processes and mineral production rates (Brantley et al., 2013; West et al., 2005). In carbonate weathering on the other hand, the rocks are usually dominated either by limestone or dolostone with small quantities of other minerals often regarded as 'impurities' (Jiang et al., 2014; Moraetis et al., 2011; Wang et al., 2004b). Because the dominant minerals (calcite in limestone and dolomite in dolostone) are highly soluble (Dere et al., 2016), carbonate rocks are reported to drive regional weathering (Oliva et al., 2003). For example, in the mountainous Himalayas in Pakistan, Blum et al. (1998) established that weathering is driven by carbonate minerals even though they consist of only 1% of the area. Also in the carbonate landscapes in Mallorca, Spain, Muhs et al. (2010) established that carbonate minerals, calcite and dolomite, dissolve faster thereby leaving the soils enriched with silicate mineral residues such as quartz, feldspar and kaolinite.

Weathering of silicate rocks has also been credited with the regulation of long-term climate through the drawdown of atmospheric $CO_2$ over geological timescale (Berner et al., 1983). Dissolution of silicate minerals such as plagioclase through acidic precipitation sequesters $CO_2$ from the atmosphere through carbonate-silicate cycle (Berner et al., 1983) and produces metal ions such as $Ca^{2+}$ and bicarbonate ions $HCO_3^-$ which are then transported through rivers to the ocean (Dupré et al., 2003; Oliva et al., 2003; Viers et al., 2014). Equations 1.1 – 1.3 explained the process of plagioclase weathering by acidified rainwater and the subsequent deposition of calcite in the oceans:

$$CO_{2(g)} + H_2O_{(aq)} \rightarrow H_2CO_{3\,(aq)} \quad \text{.....1.1}$$

$$CaAl_2Si_2O_{8(s)} + 2CO_{2(g)} + 3H_2O_{(l)} \rightarrow Ca^{2+}_{(aq)} + 2HCO_3^-{}_{(aq)} + Al_2Si_2O_5(OH)_{4(s)} \quad \text{....1.2}$$

$$Ca^{2+}_{(aq)} + 2HCO_3^-{}_{(aq)} \rightarrow CaCO_3(s) + CO_{2(g)} + H_2O_{(l)} \quad \text{.....1.3}$$

High atmospheric $CO_2$ concentrations block the outflux of radiation from Earth into space by acting as a greenhouse and warms the atmosphere thereby increasing the rate of evaporation and acid precipitation which, in turn, increases silicate dissolution and $CO_2$ removal from the atmosphere (Walker et al., 1981). On the other hand, low atmospheric $CO_2$ concentrations cool down the atmosphere and reduce the evaporation and, by extension, precipitation rates which, in turn, slow down silicate dissolution (Viers et al., 2014). However, weathering of carbonate rocks does not affect atmospheric $CO_2$

concentrations over geological timescales due to the release of $CO_2$ during the formation of marine sediments (Blum et al., 1998; Viers et al., 2014).

Several studies have examined different components of climate such as temperature, precipitation and run-off to unravel the effect of climate on weathering rates (e.g., Dupré et al., 2003; Egli et al., 2008; Egli et al., 2003; Hayes et al., 2020; Oliva et al., 2003). For example, Gislason et al. (2009) reported that increase in temperature and run-off increased weathering rates in Iceland over 40 years. Also, White and Blum (1995) in a study of 68 small watersheds established that temperature and precipitation are the major drivers of weathering rates. Oliva et al. (2003) also reported that temperature and run-off control weathering rates in granitic rocks. In alpine regions, precipitation was found (Egli et al., 2003) to have greater influence of weathering rates than temperature and vegetation. Similarly, West et al. (2005) postulated that although warmer environments should have higher weathering rates, some warm environments have low cation weathering rates and water fluxes strongly influence weathering rates in such environments. Hayes et al. (2020) also established that precipitation has greater control on weathering rates in temperate forests than temperature and erosion.

Vegetation has also been reported to impact weathering rates. While the low pH in the root zone from microbial respitation and vegetation degradation increases the dissolution of minerals and weathering rates (Augusto et al., 2000; Marie-Pierre et al., 2009), vegetation also reduces erosion rates, encouraging formation of thick soils which block the bedrock from interaction with water, thereby reducing weathering rates at depth (Oliva et al., 2003). In a study of African rivers, Gaillardet et al. (1995) established that thick soils resulting from dense vegetation are responsible for slow weathering in the Congo region in central Africa. Edmond et al. (1995) reported similar findings in the Amazonian forests of Venezuela and Brazil. In addition, mineral nutrient elements in acidic soils are more significantly weathered around the root zone than deeper in the soil and more nutrient elements are depleted around the root zone (Augusto et al., 2000; Marie-Pierre et al., 2009). However, nutrient mobilisation and distribution in the soil is essential in providing the nutrient needs of the vegetation. As such, root exudates contribute in restructuring the microbial activity and distribution and enhance the dissolution of minerals (Calvaruso et al., 2010; Napieralski et al., 2019). Mycorrhizal fungi associated with plant roots develop symbiotic relationships

with some microbial species, mostly bacteria, that are more efficient in mineral weathering and ensure faster mineral dissolution especially in forest ecosystems (Calvaruso et al., 2010; Marie-Pierre et al., 2009). Marie-Pierre et al. (2009) also established that microbes in the rhizhosphere enhance the dissolution of Ca-bearing minerals such as apatite in nutrient deficient soils.

In addition to the chemical and microbial activities that hasten mineral dissolution in the rhizosphere, plant roots also contribute to the weathering rates by physically breaking up rocks and soil aggregates, thereby increasing access of fresh minerals to water which increases weathering rates (Jobbagy and Jackson, 2004) or by directly absorbing nutrients such as P from the rocks (Lambers et al., 2017).

Although anthropogenic activities such as land use change are expected to impact weathering and denudation rates, Oliva et al. (2003) reported no correlation between weathering rates and land usage in granitic environments. However, in carbonate environments, land use was reported to impact on the weathering rates by enhancing elemental denudation and rocky desertification (Jiang et al, 2915). Alekseev et al. (2018) reported that land use in different soil profiles around the Moscow region in Russia affects the weathering and the distribution of minerals and elements by affecting the distribution of chemical elements between different subfractions of clay and silt between 50 – 150 years.

### 1.3.2 Weathering and Nutrient Cycling

Soils, formed during weathering reactions, contribute significantly to the global biogeochemical cycling of elements (Derry and Chadwick, 2007). Depending on the environment, the distribution of mineral elements (e.g. Ca, Fe, P, Mg, K) is usually dependent on processes such as weathering, atmospheric deposition, leaching and/or vegetation (plant) cycling (Dawson et al., 2020; Derry and Chadwick, 2007; Porder et al., 2007a; Uhlig et al., 2017; Uhliq and Blanckenburg, 2020) acting together or in isolation (Porder et al., 2007b). Weathering enriches the soil with nutrient elements derived from lithospheric sources such as rocks (Buss et al., 2017; Buss et al., 2010; Frings and Buss, 2019; Porder et al., 2015) and controls the depth and distribution of nutrient inputs (Buss et al.,

2010; Dawson et al., 2020; Kirkby, 1985; Moore et al., 2017; Moore et al., 2005; Porder et al., 2007b; Uhlig et al., 2017).

In environments where the rate of removal of soil by erosion is faster than dissolution of minerals through weathering, the nutrient elements provided in the soil by weathering are removed, becoming unavailable for vegetation, The cycling of mineral nutrients is usually then controlled by other processes such as atmospheric deposition and/or vegetation cycling (a process in which plants recycle mineral nutrients through litterfall and throughfall) (Dawson et al., 2020; Derry and Chadwick, 2007; Jobbagy and Jackson, 2004). In addition to these processes, leaching removes the mineral nutrient elements released by weathering in environments where removal of nutrient elements through erosion is slower than mineral dissolution, also making the elements unavailable for vegetation (Dawson et al., 2020; Porder et al., 2015). In these weathering-limited environments, nutrient elements such as P, K and, in some cases, Ca (which becomes the limiting mineral nutrient element in soils where P and K are either too low or absent, Tanner et al., 1998; Uhlig et al., 2017; Uhliq and Blanckenburg, 2020) tend to be more concentrated near the surface than elements such as Mg and Na (Dawson et al., 2020; Jobbagy and Jackson, 2001; Porder et al., 2007a; Porder et al., 2007b) due to biolifting (a process in which plants scavenge for nutrients at depth and concentrate them on the surface) and/or vegetation cycling (Dawson et al., 2020; Uhlig and von Blanckenburg, 2019). Although K and P are the major mineral nutrient elements, in soils and limit plant growth, environments where both are either two low or absent, Ca becomes the more widely distributed mineral nutrient element in the soil and thus regulate plants' growth and development. Globally, according to Jobbagy and Jackson (2001) Ca is the most widely distributed mineral elements in soils that are deficient in K and P.

### 1.4 Soil Formation and Degradation

The amount of the soil formed during weathering depends on the type and the composition of the rock (Marzaioli et al., 2010; Porder et al., 2007a; Porder et al., 2015). Carbonate soils are formed either from the dissolution of the 'impure' carbonate bedrock interbedded with silicates or from the deposition of parent materials or both (Durn et al., 1999; Muhs and Budahn, 2009). However, it is not known whether these major sources of soil in carbonate

environments directly correspond to the available mineral nutrients in the soil. For example, in the granitic and andesitic watersheds in Puerto Rican rainforest, although the soils are formed from the weathering of the nutrient-rich silicate bedrock, thick and highly weathered, the majority of the mineral nutrient elements used by vegetation were deposited from atmospheric dust (Buss et al., 2017; 2008; Pett-Ridge, 2009). Similarly, at the SPECTRA and Koiliaris CZOs, there are no reported studies that investigated the relationship between seasonality, temperature and/or precipitation and their effects on mineral nutrient contents in the soil**.** Although effects of temperature and precipitation on weathering (and thus, mineral nutrients production and distribution) are still being debated, wetter and/or warmer climates are found to promote rapid weathering and, by extension faster mineral nutrient production (e.g., Hayes et al., 2020; Strakhov et al., 1972).

Dominant minerals (calcite and dolomite) in carbonate environments weather away easily and leave the soil matrix enriched in soil forming aluminosilicates and other metal (hydr)oxides often regarded as impurities. These shallow, nutrient-poor soils lead to loss of biomass and vegetation cover increasing the susceptibility of the soils to rocky desertification especially in environments where extensive anthropogenic activities, such as agriculture, are taking place.

Anthropogenic activities such as land use and land cover change have transformed soils globally and accelerated soil degradation (loss of nutrients etc) resulting in the loss of about 33% of global land resources at about 0.5% annual rate (Foley et al., 2005). In an environment where the local population is poor and dependent on agriculture, pressures exerted on these soils could lead to significant degradation, loss of fertility and rocky desertification (Jiang et al., 2014; Wang et al., 2004b).

## 1.5 Thesis Aims and Objectives

To establish the mineral nutrient production processes as well as the factors that control the bioavailability of the mineral nutrients in the karst landscapes, I studied soils and underlying carbonate bedrock in cultivated and formerly cultivated sites that have been abandoned for various lengths of time, representing gradients in recovery. The sites were located at two CZ

observatories, with similar MAT and MAP, but with opposite seasonality. This research work aims to answer the following questions:

1. Are long-term mineral nutrient release processes on karst terrains controlled by the distribution of silicate-rich clastic rocks interbedded in the carbonates (or silicate minerals present as impurities in the carbonate rocks)?

   I hypothesize that the abundance of silicate minerals in the bedrock, which are lower in abundance than the dominant carbonate minerals (calcite and dolomite), are primarily responsible for the production and distribution of mineral nutrient elements in these soils with climate, and/or atmospheric deposition as minor negligible factors.

2. Is the soil quality and nutrient bioavalability across the watersheds dominantly controlled by land use, silicate mineral distribution, or climate seasonality?
   I hypothesize that the bioavailability of nutrient elements in these soils is controlled primarily by land use (extent of recovery) and bedrock lithology.

To address these questions, soils were studied in two agricultural karst CZOs: the SPECTRA Critical Zone Observatory (CZO), in Guizhou, China, which has warm-wet summers and cool-dry winters, and the Koiliaris CZO in Crete, Greece, which has warm-dry summers and cool-wet winters (Chapter 2). Bulk elemental profiles with depth in soils and rocks were analysed to identify mineral nutrient production via weathering processes over soil-formation timescales (Chapters 3 and 4). Ammonium-acetate-extractable cations with depth in the soils were analysed to assess mineral nutrient bioavailability over agricultural timescales (Chapters 5 and 6). Differences in lithology as well as lithological and climatic controls on weathering on mineral nutrient production and abundance were discussed (Chapter 7). Thesis summary, conclusion and further work were explained in Chapter 8.

# Chapter 2

## Field Sites, Methods and Data Analysis

**Author contributions and declaration:** Field work and sample collection at the SPECTRA CZO was led by Heather L. Buss and colleagues from the UK and China in autumn 2016 and summer 2017. Sample collection and field work in Koiliaris were led and conducted by Aminu Lawal under the guidance of Heather L. Buss with assistance from Maria Lilli and Nikolaos Nikolaidis in Autumn 2019.

## 2.1 Introduction

This chapter outlines the field settings, experimental and analytical methods employed, including sampling and laboratory measurements such as bulk elemental chemistry, bioavailable cations extractions, and scanning electron microscopy (SEM) to achieve the objectives of this research work. The chapter also details the techniques used to analyse the data such as mass transfer analysis.

## 2.2 Field Sites

### 2.2.1 SPECTRA Critical Zone Observatory

SPECTRA Critical Zone Observatory is situated in Puding, Guizhou province, in southwestern China. It is one of the four critical zone observatories taking part in the broader UK-China Critical Zone Observatory programme, funded jointly by the UK National Environmental Research Council (NERC) and the Chinese National Science Foundation (CNSF). The programme aims to understand and provide possible solutions to the challenges associated with China's increasingly intensive land use and land cover changes and the resultant effects in ecosystem service delivery. The SPECTRA CZO was established to study the effects of anthropogenic perturbations on a karst CZ.

Guizhou province is situated at the centre of the South Asian karst zone with carbonate rocks covering about 62% or about 130,000 $km^2$ (Tang et al., 2012; Wang et al., 2014; 2004b) of the total land surface of the province. Within Puding County, however, about 79.2% or 863.7 $km^2$ of the total land area is composed of exposed carbonate rocks (Jiang et al., 2014; Wang et al., 2004b). The county is characterised by humid climate with monsoon-type rainfall, mean annual ambient temperature of 15$^oC$ (Wang et al., 2014) with annual precipitation levels of between 850 – 1600 mm and an elevation of up to 1470 m a.s.l. Within Puding County, our research focused on three watersheds namely: Chenqi, Chenjiazhai and Tianlong.

The main site for this study is Chenqi (Fig. 1), a small (1.31 $km^2$) watershed impacted by intensive agriculture, which is situated between $105^042'$ – $105^043'$E and $26^014'$ – $26^015'$N, overlying a mid-Triassic Guanling formation (Zhao et al., 2010). As with the wider province, it is characterised by monsoon-type rainfall with an annual average of 1314.6 mm (80% of which occurs between May and October) with an elevation that ranges from 1365 – 1481 m.

The main geomorphological feature in the area is a karst valley covered with loose Quaternary deposits (Wang et al., 2014; Zhao et al., 2010). The site has a four layered (ranging from the Upper Sinian Dengying formation at the base to Lower Middle Triassic at the top formation), 8 km thick carbonate rock deposit interbedded with clastic rocks from the late Neoproterozoic to the late Triassic (Wang et al., 2004b). The lower hillslopes have been transformed into terraced farmlands (Cheng et al., 2019). The sedimentary rocks in Chenqi have largely horizontal layered formations of limestone, dolostone and marls. The primarily clay soil type is thicker and deeper at the hill bottom due to soil erosion (Cheng et al., 2019). The main land uses in Chenqi are the sloping farmlands which are still being actively farmed, abandoned farmlands which were abandoned for about a year at the time of sampling and secondary forest which consists of mainly olive trees.

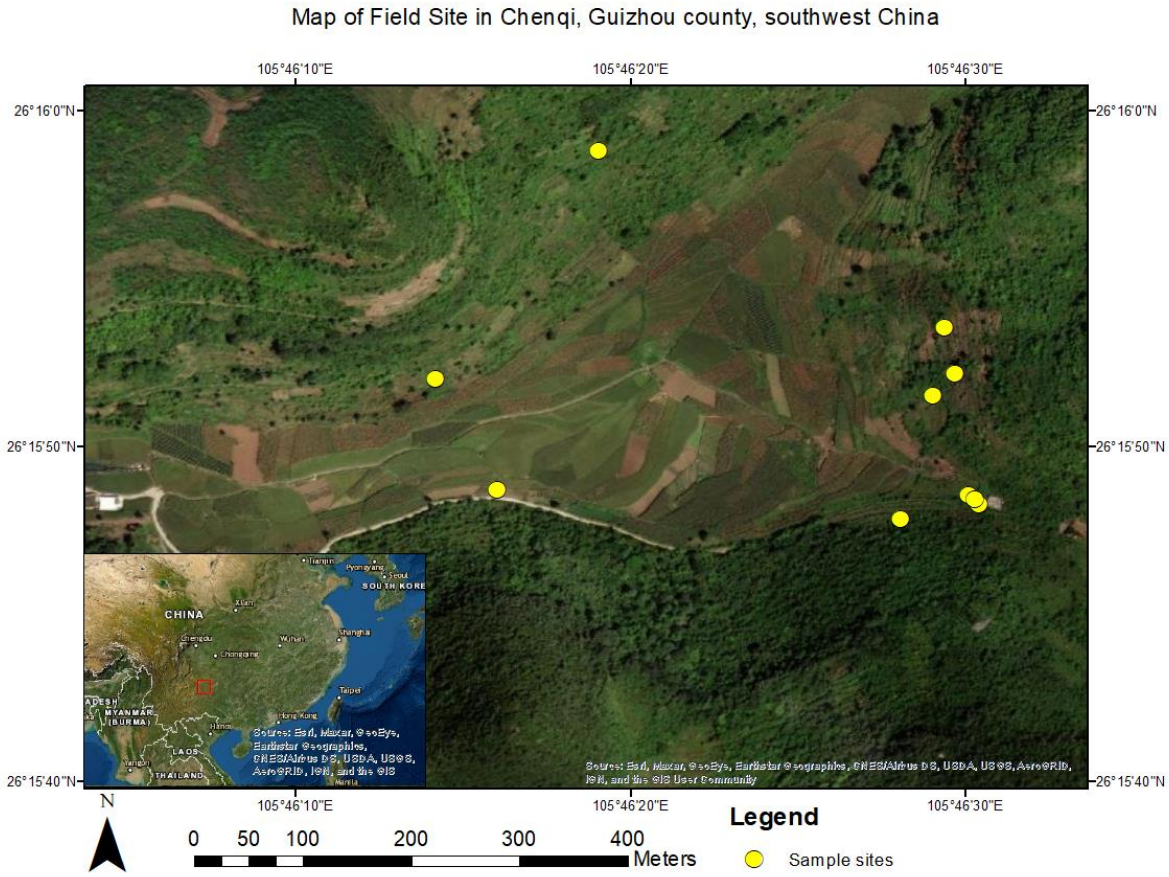


**Figure 2.1:** Map of Field Site in Chenqi indicating some of the sampling sites.

Chenjiazhai is a 1.5 km$^2$ recovering agricultural catchment also situated between 105$^0$42' – 105$^0$43'E and 26$^0$14' – 26$^0$15'N with similar geological formation as Chenqi. Lower hillslopes are largely abandoned but recovering farmlands with thicker soils, due to soil erosion, than hilltop. The main land use in Chenjiazhai is the sloping farmland. Tianlong on the other hand, is a less disturbed mountainous forest located between 26$^0$14.8'N and 105$^0$45.8'E. This site represents a near-pristine environment, whilst the other two represent mainly degrading (Chenqi) and recovering (Chenjiazhai) environments. The Tianlong watershed overlies the same geological formation as Chenqi and Chenjiazhai and the forest has a vegetation density of about 40 species per 100 m$^2$ (Liu et al., 2019).

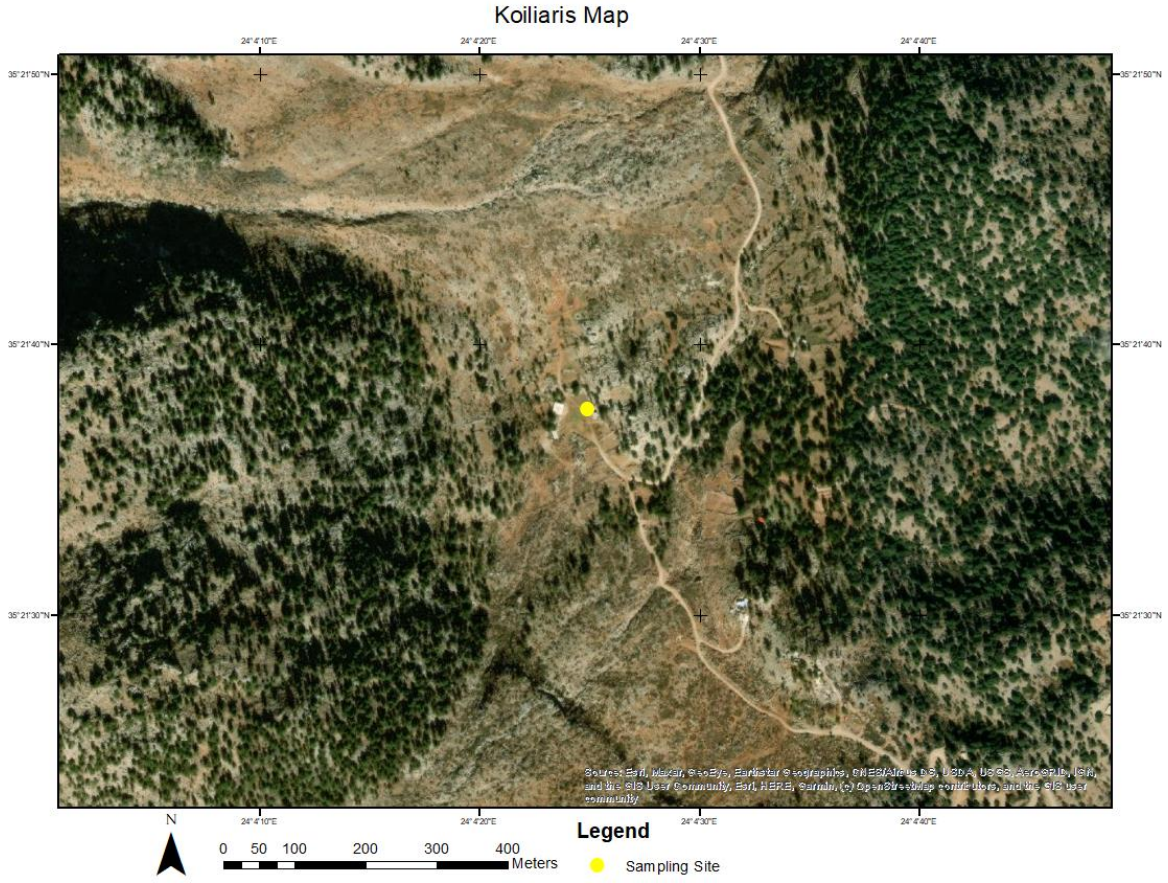


**Figure 2.2:** Map of Field Site in Koiliaris indicating one of the sampling sites

### 2.2.2 Koiliaris Critical Zone Observatory

The Koiliaris Critical Zone Observatory is part of Soil Transformation in European Catchments (SoilTrEC; Banwart et al., 2011) situated in the Koiliaris River watershed located about 25 km east of Chania in the north-western part of the island of Crete, Greece (Lilli et al., 2020; Moraetis et al., 2011; Tsiknia et al., 2014). The watershed has an area of about 132 $km^2$ and is characterised by intense geomorphology with an elevation of 2120 m, annual rainfall of between 500 - 900 mm and the annual mean temperature of about $9.6^0C$ (Moraetis et al., 2011; Tsiknia et al., 2014). Like Guizhou, the geological formations in Koiliaris are principally made up of limestone and dolostone (Plattenkalk, Tripoli and Trypali series) with cherty intercalations (Moraetis et al., 2015). The karst system is characterised by fast infiltration with significant number of sinkholes and caves and a karstic system that is comprised mainly of limestones and dolostones from the Mesozoic period and the calcaric marls of the Neogene formation (Moraetis et al., 2015; Moraetis et al., 2011; Stamati et al., 2011).

Over several centuries, intensive agricultural activities such as clearing of forest and natural vegetation for cropping and overgrazing has degraded the soil (Moraetis et al., 2011) leading to significant loss of soil organic matter (Tsiknia et al., 2014) making the soil susceptible to erosion. The soils in Koiliaris also represent typical Mediterranean soils facing serious threat of desertification due to climate change (Moraetis et al., 2015).

In Koiliaris Critical Zone Observatory, the primary sites for this research were sites K4 and K5 reported in Moraetis et al. (2015). Both sites were developed on cherty limestones. Site K4 has manmade terraces with about 50-year-old olive trees and in the past, the main land use is thought to have been production of wheat and animal grazing (Lilli et al., 2020). Site K5, which also consists of abandoned terraces, was mainly an agricultural site for crop production and animal grazing (Moraetis et al., 2015).

## 2.3 Sample Collection

Soil samples were collected from the Chenqi watershed (Fig. 1) in Guizhou province in southwestern China. In June 2016, soil pits were dug (30 pits, 197 samples) from horizons O

- A and samples collected at different depths (from 14 cm – 120 cm) and elevation (between 1320 and 1345 m) by PhD supervisor H. L. Buss with SPECTRA collaborators from University of Exeter, Rothamsted Research, and the Chinese Academy of Sciences. At the same time, 23 rock samples were collected from outcrops across the catchment. Sixty cores were drilled in Chenqi through the overlying soil (where present) and 3 meters of underlying rock by Chinese Academy of Sciences collaborators in autumn 2016 from which the UK team obtained 21 cores (183 samples). All the samples were collected at the three major land uses in the province – sloping farmlands (88 pits, 56 cores), abandoned farmlands (48 pits, 57 cores) and secondary forests (61 pits, 70 cores). In Chenjiazhai, soil pits (9 pits, 99 samples) were dug by collaborators from the University of Exeter and Rothamsted Research in June 2017, with samples collected at different depths (ranging from 16 cm – 26 cm) from the three slope positions. Also in June 2017, the same team dug 6 soil pits in Tianlong and 47 samples were collected at different depths (ranging between 5 cm to 9 cm). No rock samples were collected at either Chenjiazhai and Tianlong.

**Figure 2.3**: The bottom slope of the Chenqi watershed. This showed one of the sloping farmlands in Chenqi (picture credit: H. L. Buss).

In Koiliaris, with collaborators from the Technical University of Crete and PhD supervisor H. L. Buss, I collected samples from sites K4 and K5 (Moraetis et al. (2015) as they share similar

characteristics (bedrock lithology, land use) with Chenqi and Chenjiazhai in the SPECTRA CZO. Pits (2 pits, 24 samples) were dug at different depths (up to 30 cm) and rock outcrops (5 each from the two sites) were collected from these sites. Chenqi, Chenjiazhai and Koiliaris are karst environments with soils that have been degraded (to various degrees) by historical and ongoing agriculture. The Chinese sites have slightly higher MAP and MAT than the Greek sites, but opposite seasonality, with the Chinese sites having hot-wet summers and cool-dry winters while the Greek sites have hot-dry summers and cool-wet winters.

**Figure 2.4**: Images of the sample collection and initial processing a) the rock samples collected in the cores and (b) pit soil samples were air dried before shipment to the UK (picture credit: Dr H. L. Buss).

## 2.4 Analytical Methods

### 2.4.1 Extraction and Measurement of Exchangeable Cations

Exchangeable cations were extracted by mixing, 1 g of the soil with 30 ml of 1 M $NH_3$-Ac (pH adjusted to 8) solution and shaken for 16 hrs. The mixture was then centrifuged at 4500 rpm and dried down to near dryness and made up to 25 cm with 1 M $HNO_3$ before analysis using ICP-OES (Agilent 7110 Series) at the University of Bristol. The extraction was conducted by adding 10 ml of 1 M $NH_3$-Ac to 0.33 g of soil sample and mixed for 16 h. The mixture was heated at about $60^0$C to remove excess ammonia and the mixture was then reflux with 1 M $HNO_3$ and filled to the mark in 25 cm volumetric flask before analysis. As there was lack of literature on the method for extraction of exchangeable cations, this method was developed

by me in conjunction with senior technician Dr Adam McAleer at the University of Bristol. The samples were analysed in triplicate by ICP-OES with standards run between blocks of samples for drift correction. Detection limits were assessed by measuring blanks and repeat analyses of low concentration standards. Internal calibration quality checks were performed. Standard deviations of the replicate measurements were calculated and reported.

### 2.4.2 Bulk Elemental Chemistry of Rock and Soil Samples

Soil samples from Chenqi were first sterilized with an autoclave at a temperature of 120$^{o}$C and 15 bars for 30 minutes to remove DEFRA foreign soil restrictions on the samples, which was not required for the Koiliaris soils. All soils were then ground using pestle and mortar and sieved before sending them to a commercial laboratory (ALS; Loughrea, Ireland) for further pulverization followed by Li-metaborate fusion digestion and ICP-AES analysis of major and some trace elements. Quality control (QC) was performed by ALS by analysis of several rock and soil standards, blanks, and replicate measurements of the samples. We conducted QC by including additional standards and previously analysed rock and soil samples labelled as part of the sample set. ALS Loughrea is an INAB accredited testing laboratory (Reg. No. 173T).

### 2.4.3 Scanning Electron Microscopy (SEM)

Selected rock cores were analysed for mineralogy and mineral distribution by scanning electron microscopy (Hitachi S-3500N) coupled with a backscattered electron (BSE) mode and energy dispersive spectrometry (Thermo Scientific 10 mm$^2$ Silicon Drift Detector) operated at 20 kV. Mineral identification was conducted using EDS analysis of relative elemental abundances of selected points. Rock porosity and mineral volume was determined from phase analysis of X-ray elemental maps produced using Noran System Seven (NSS) 3.2 software, which groups pixels that have similar chemical ratios. Approximately 15-20 samples were analysed to determine the dominant mineralogy for each land use.

## 2.5 Mass Transfer Analysis

The mass transfer coefficient ($\tau$) is a useful parameter for analysing mobilisation of elements during weathering because it reflects mass changes not only of a given component, but also relative to other components (Brimhall and Dietrich, 1987). The mass transfer of the mobile elements was determined by normalising the concentrations of the mobile elements to an assumed immobile element (Zr in this case, e.g. Buss et al., 2017; White and Buss, 2014) and the net gain or loss of mass of the immobile element is then determined relative to the parent material (in this study, the deepest sample in a given pit or core) using the equation reported by Anderson et al. (2002):

$$\tau_{i,j} = \left(\frac{C_{j,w}C_{i,p}}{C_{j,p}C_{i,w}}\right) - 1 \quad (2.1)$$

Where $\tau$ is the mass transfer coefficient, $C$ is concentration of a given element, mobile = *i*, immobile = *j* in the parent sample, p, and a weathered sample, w. A $\tau$ value of 0 indicates no mobilisation of the mobile element has occurred relative to the parent sample, whereas a value of -1 indicates total depletion of the mobile element relative to the parent sample. Positive values indicate that the mobile element is enriched relative to the parent. Elements that are totally depleted ($\tau = -1$) at the top of a weathering profile are said to have completely developed profiles while those that are partially depleted are said to have incompletely developed profiles (Brantley et al., 2007).

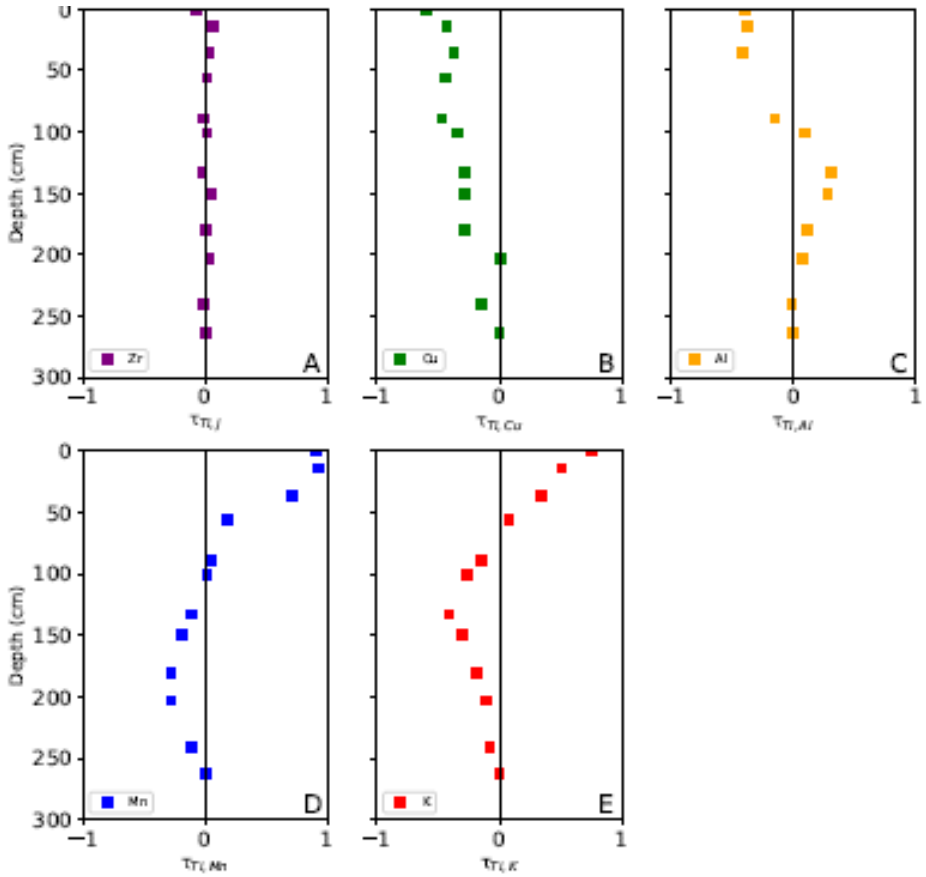


**Figure 2.5:** The concentrations of the mobile elements (from Hayes, 2019) are normalised to the concentration an assumed immobile element (Zr in our case but Nb and Ti are also usually used) relative to the bedrock or deepest sample. Normalisation of elemental profile around the middle line indicates neither enrichment nor depletion (immobile profile, Fig. 4a), tilting to the left side (depletion profile, Fig. 4b) indicates depletion while tilting to the right (enrichment or addition profile, Fig 4d) indicates enrichment of the mobile elements. Figures 4c and 4e indicated depletion-enrichment and biogenic profiles.

Mass transfer profiles can be categorised with four endmember (Brantley et al., 2007) profiles (Fig. 2.3) namely: immobile profile (Fig. 2.3a) in which the element shows no mobility and exhibit the same mass transfer coefficient as the parent material or the deepest sample; depletion profile (Fig. 2.3b) in which the element exhibits a decreasing mass transfer coefficient (loss) from depth towards the surface due, mainly, the mineral dissolution; depletion-enrichment profiles (Fig. 2.3c) that show enrichment of an element at depth but depletion towards the surface which occurs mostly due to changes in soil pH and/or organic ligands; enrichment profile (Fig. 2.3d) in which the element revealed higher mass transfer coefficient than the bedrock or the deepest sample which could be due to external sources or bioturbation; and biogenic profile (Fig. 2.3e) which results due to the dissolution of minerals at depth and redistribution at the surface from biolifting (a process

in which plants scavenge for nutrients and concentrate them at the surface, Amundson et al., 2007; Jobbagy and Jackson, 2001).

# Chapter 3

# Mechanism of Mineral Weathering and Mass Transfer in the SPECTRA Critical Zone Observatory

**Author contributions and declaration:** Rock cutting preparatory to thin sections was conducted by Aminu Lawal and the thin sections were made by Chris Blake Mineralogy Consulting. Soil samples were prepared by Aminu Lawal and ICP-OES was conducted by ALS Geochemistry Loughrea. All SEM analyses were conducted by Aminu Lawal under the guidance of Stuart Kearns, and Evangelos Mouchos. Sections of this work have been presented at Goldschmidt (Lawal et al., 2020; Appendix B) and some of it will be presented at the OSZCAR-TERENO (Lawal et al., 2021; Appendix C).

## 3.1 Introduction

Chapter 1 provided an overview of weathering and its importance in the removal of atmospheric $CO_2$, landscape development, mineral nutrient production, retention, cycling, and soil formation and development. Carbonate dissolution is known to be the major driver of weathering in karst environments and, since the dissolution of the minerals (carbonates) is congruent, soils formed in karst environments are thin and deficient in nutrients. In this chapter, I provide results from SEM and bulk chemical analyses of the soil pits and cores (Chapter 2) from different land uses and slope positions from three Chinese catchments (Chenqi, Chenjiazhai and Tianlong, representing degrading, recovering and pristine soil environments, respectively) to explain the mechanism and controls on weathering and mineral nutrient production (and retention) in these subtropical karstic catchments. The results will provide insights on whether the distribution and abundance of silicate impurities found in the dominant carbonate bedrocks in the karstic catchments controls the production and retention of mineral nutrients, and soil formation and development.

## 3.2 Results

### 3.2.1 Bedrock Mineralogy in Guizhou

SEM images (Chapter 2.4.3) of the bedrock cores confirm the predominance of calcite and dolomite with significant but variable distributions of non-carbonate minerals including quartz, pyrite, hematite, apatite, kaolinite, orthoclase, fluorite, illite and celestine, consistent with previous studies of regional bedrock (Chen and Bi, 2011; Moore et al., 2017; Wang et al., 2004b). Some of these minerals (e.g. hematite, Fig. 3.1), are found along cracks, pores, or weathering veins in association with clay minerals (mostly kaolinite and illite) especially in the sites dominated by calcite. After calcite, dolomite then quartz is the most abundant and evenly distributed minerals (Tables 3.1 and 3.2) in the bedrock.

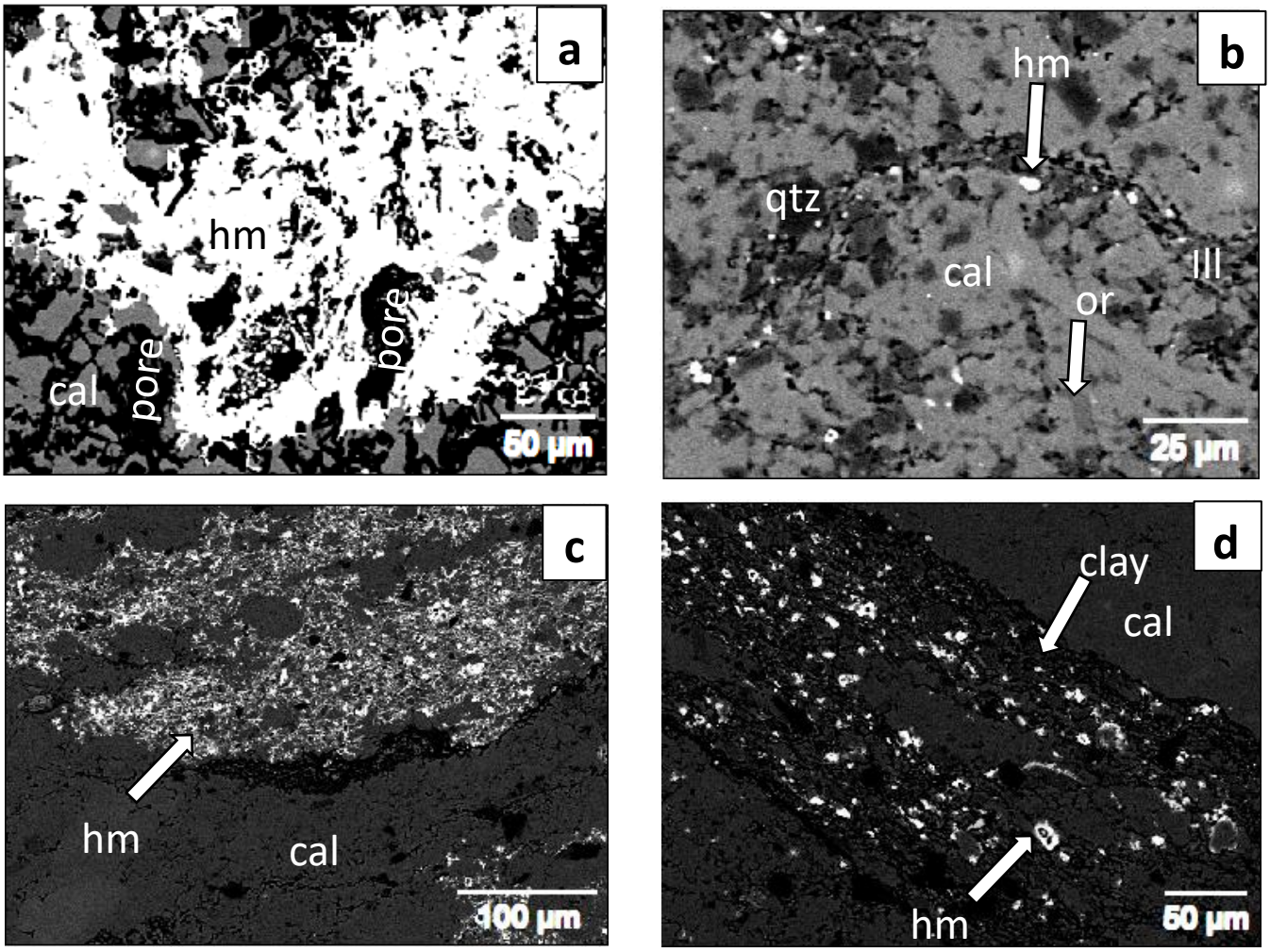


**Figure 3.1:** Scanning electron microscopic (SEM) image site CQ64 (top slope, secondary forest) showing hematite (hm) on a calcite (cal) dominated bedrock. b) Site CQ54 (top slope, abandoned farmlands) showing hematite is almost always found associated with weathering veins and pores in a calcite (cal) dominated bedrock with quartz (qtz), hematite (hm) and clay (ill), found, along the weathering vein. Also, in the image is orthoclase (or) which is not as significantly or evenly distributed in the bedrock as quartz or hematite. c) CQ1 (middle slope, abandoned farmlands) showing cal domination in the bedrock with significant distribution of hm around small pores and d) CQ45 (bottom slope, sloping farmlands) showing clay and hm along the weathering vein on a cal dominated bedrock.

Bedrock samples with calcite as the dominant mineral (determined by SEM and confirmed by Mg/Ca ratio, Table 3.2) have less porosity and a wider variety of minerals than bedrock dominated by dolomite (porosity visibly observed in SEM images consistent with Wang et al. (2004b), which reported an average porosity of 2% for limestone and 4% for dolostone in the region). Hematite is found more associated with calcite while pyrite is found more with dolomite.

Bedrock abundances of Si, Al, Fe, Ca, Mg and K (Table 3.1) showed variability between slope positions (and between sites in the same slope positions and within land uses), although the abundances of the elements are mostly within uncertainty with each other in some of the sites. On the other hand, Na and P, which are also mostly present at similar abundances within uncertainty, show little variability between sites and slope positions except for site CQ55 (abandoned farmlands, mid slope) which showed a significantly high abundance of P compared to the other sites in all the different land uses.

The Mg/Ca ratios (Table 3.2) used to determine the dominant carbonate mineral in the bedrock shows variability and mostly within uncertainty of each other in all the sites (within and between slope positions and land uses) except for site CQ17 (middle slope, secondary forest), which has a higher ratio than the other sites in the catchment. Assuming that all the Ca in the bedrock comes from the calcite and dolomite, the carbonate contents of the bedrock can be estimated from the sum of CaO and MgO and the content of silicate 'impurities' as the sum of $SiO_2$ and $Al_2O_3$ (Table 3.2) both of which showed variability in the different land uses and slope positions with most of the abundances mostly being within uncertainty of each other.

### 3.2.2 Soil Mineralogy in Guizhou

Abundances of Si (Table 3.3 and 3.4) in Chenqi and Chenjiazhai (Table 3.5) are higher than Si in Tianlong (a pristine forest that is largely unaffected by anthropogenic perturbation, Chapter 2.2.1, Table 3.7). The Tianlong soils, however, show similarity with the abundances of Si in the secondary forest in Chenqi. On the other hand, Al in Chenqi (Table 3.3) show similarity in abundance with Chenjiazhai (Table 3.5) but lower than Tianlong (Table 3.7) while Fe abundances are lower in Tianlong than

Chenjiazhai but higher than Chenqi. Also, Ca, Mg and Na abundances were higher in Tianlong soils than in Chenjiazhai but similar to Chenqi while K is lower in Tianlong than in Chenqi but similar to Chenjiazhai. Abundances of P are similar in the soils of all three catchments.

**Table 3.1:** Bedrock bulk chemistry of Chenqi

| Site | Sample | [a]$SiO_2$ | $Al_2O_3$ | $Fe_2O_3$ | CaO | MgO | $Na_2O$ | $K_2O$ | $P_2O_5$ | Zr | n[b] |
|---|---|---|---|---|---|---|---|---|---|---|---|
| [d]**SFB** | [c]**CQ7** | 6.70 ± 5.3 | 2.50 ± 2.00 | 1.00 ± 0.60 | 48.4 ± 5.4 | 1.00 ± 0.3 | 0.04 ± 0.02 | 0.80 ± 0.60 | 0.03 ± 0.01 | 15.0 ± 10.7 | 7 |
| | **CQ41** | 1.50 ± 1.3 | 0.50 ± 0.40 | 0.40 ± 0.30 | 53.6 ± 1.3 | 0.70 ± 0.3 | 0.02 ± 0.01 | 0.20 ± 0.20 | 0.03 ± 0.01 | 3.00 ± 0.00 | 11 |
| | **CQ43** | 10.9 ± 7.0 | 3.00 ± 2.50 | 1.40 ± 0.60 | 38.5 ± 7.6 | 6.40 ± 6.7 | 0.05 ± 0.03 | 1.20 ± 0.90 | 0.07 ± 0.03 | 28.8 ± 22.8 | 12 |
| | **CQ45** | 0.80 ± 0.4 | 0.20 ± 0.08 | 0.20 ± 0.10 | 54.7 ± 0.8 | 0.50 ± 0.1 | 0.02 ± 0.00 | 0.08 ± 0.05 | 0.01 ± 0.00 | nd | 8 |
| | **CQ61** | 0.70 ± 0.6 | 0.10 ± 0.10 | 0.10 ± 0.03 | 55.0 ± 0.6 | 0.40 ± 0.2 | 0.02 ± 0.00 | 0.07 ± 0.09 | 0.01 ± 0.00 | 5.00 ± 0.00 | 12 |
| **SFM** | **CQ37** | 5.70 ± 1.9 | 1.50 ± 0.70 | 0.90 ± 0.20 | 47.5 ± 2.6 | 3.90 ± 2.5 | 0.06 ± 0.01 | 0.70 ± 0.20 | 0.04 ± 0.01 | 13.8 ± 6.40 | 6 |
| **AFB** | **CQ38** | 6.60 ± 4.0 | 2.70 ± 0.60 | 0.70 ± 0.40 | 49.0 ± 4.0 | 1.80 ± 0.9 | 0.05 ± 0.01 | 1.00 ± 0.60 | 0.04 ± 0.02 | 20.0 ± 9.60 | 6 |
| **AFM** | **CQ1** | 14.0 ± 4.8 | 4.70 ± 1.80 | 1.80 ± 0.60 | 36.3 ± 9.8 | 5.60 ± 5.0 | 0.05 ± 0.01 | 1.70 ± 0.50 | 0.05 ± 0.01 | 34.8 ± 12.5 | 10 |
| | **CQ40** | 5.30 ± 0.3 | 1.00 ± 0.20 | 0.70 ± 0.10 | 49.7 ± 0.1 | 1.40 ± 0.3 | 0.03 ± 0.00 | 0.60 ± 0.06 | 0.02 ± 0.00 | 9.70 ± 7.40 | 8 |
| | **CQ46** | 6.00 ± 3.0 | 1.90 ± 0.90 | 0.80 ± 0.40 | 47.0 ± 4.3 | 3.80 ± 2.6 | 0.04 ± 0.01 | 0.90 ± 0.40 | 0.03 ± 0.02 | 18.8 ± 5.00 | 9 |
| | **CQ55** | 4.70 ± 3.0 | 1.50 ± 1.20 | 1.20 ± 0.50 | 35.3 ± 5.7 | 13.8 ± 4.5 | 0.05 ± 0.02 | 0.70 ± 0.50 | 9.80 ± 6.80 | 0.04 ± 0.03 | 11 |
| **AFT** | **CQ54** | 9.60 ± 4.5 | 2.90 ± 1.40 | 1.40 ± 0.20 | 31.0 ± 6.0 | 14.3 ± 6.4 | 0.06 ± 0.00 | 1.30 ± 0.70 | 0.05 ± 0.02 | 20.8 ± 12.0 | 13 |
| **SeFB** | **CQ16** | 2.60 ± 0.8 | 0.70 ± 0.40 | 0.30 ± 0.10 | 52.5 ± 1.8 | 1.50 ± 1.0 | 0.03 ± 0.01 | 0.30 ± 0.10 | 0.02 ± 0.00 | 8.00 ± 4.60 | 6 |
| **SeFM** | **CQ17** | 12.0 ± 0.6 | 3.50 ± 0.10 | 1.20 ± 0.01 | 41.0 ± 0.5 | 4.00 ± 1.0 | 0.08 ± 0.01 | 1.70 ± 0.04 | 0.09 ± 0.02 | 51.5 ± 2.5 | 6 |
| **SeFT** | **CQ2** | 3.90 ± 0.9 | 1.00 ± 0.40 | 0.60 ± 0.05 | 45.0 ± 1.7 | 6.20 ± 2.0 | 0.03 ± 0.01 | 0.60 ± 0.30 | 0.03 ± 0.00 | 8.30 ± 3.30 | 7 |
| | **CQ13** | 5.80 ± 3.9 | 1.80 ± 1.30 | 0.70 ± 0.40 | 47.6 ± 3.5 | 2.70 ± 1.3 | 0.04 ± 0.01 | 0.90 ± 0.50 | 0.02 ± 0.01 | 13.5 ± 9.70 | 9 |
| | **CQ25** | 4.70 ± 1.9 | 1.50 ± 0.70 | 0.60 ± 0.20 | 50.8 ± 2.0 | 1.30 ± 0.4 | 0.05 ± 0.01 | 0.60 ± 0.03 | 0.02 ± 0.00 | 4.70 ± 0.90 | 5 |
| | **CQ48** | 2.90 ± 0.5 | 0.90 ± 0.20 | 0.40 ± 0.08 | 51.3 ± 1.8 | 1.50 ± 0.3 | 0.04 ± 0.00 | 0.40 ± 0.09 | 0.04 ± 0.04 | 9.30 ± 1.50 | 13 |
| | **CQ64** | 14.6 ± 7.4 | 5.00 ± 2.50 | 1.70 ± 0.80 | 41.0 ± 6.9 | 1.50 ± 0.4 | 0.05 ± 0.02 | 2.00 ± 1.00 | 0.10 ± 0.02 | 38.8 ± 4.90 | 10 |

[a] Oxides measured by ICP-OES after Li-metaborate fusion digestion (Chapter 2.4.2) with values presented in wt% except for Zr, which is in ppm

[b] Uncertainty presented as standard deviation of the number of samples presented in column **n.** The total number of samples presented in the table is 169

[c] Depths of the sampling sites vary with the cores

[d]SFB = sloping farmlands bottom; SFM = sloping farmlands middle; SFT = sloping farmlands top; AFB = abandoned farmlands bottom; AFM = abandoned farmlands middle; AFT abandoned farmlands top; SeFB = secondary forest bottom; SeFM = secondary forest middle; SeFT = secondary forest top

**Table 3.2:** Ratios and sums of the mineral oxides in the bedrock

| Site | Sample | $SiO_2/Al_2O3$ | $SiO_2+Al_2O_3$ | Mg/Ca | CaO+MgO | $(SiO_2+Al_2O_3)/(CaO+MgO)$ | K/Rb | n |
|---|---|---|---|---|---|---|---|---|
| **SFB** | **CQ7** | 2.90 ± 0.20 | 9.00 ± 7.4 | 0.02 ± 0.01 | 49.6 ± 5.0 | 0.20 ± 0.20 | 0.03 ± 0.00 | 7 |
| | **CQ41** | 4.00 ± 1.00 | 1.90 ± 1.7 | 0.01 ± 0.00 | 54.0 ± 1.0 | 0.04 ± 0.03 | 0.20 ± 0.20 | 11 |
| | **CQ43** | 4.00 ± 0.80 | 11.0 ± 10 | 0.20 ± 0.20 | 35.9 ± 18.9 | 0.40 ± 0.30 | 0.08 ± 0.08 | 12 |
| | **CQ45** | 5.70 ± 1.00 | 1.0 ± 0.5 | 0.01 ± 0.00 | 55.0 ± 0.9 | 0.02 ± 0.00 | 0.05 ± 0.01 | 8 |
| | **CQ61** | 5.40 ± 0.80 | 0.80 ± 0.8 | 0.01 ± 0.00 | 55.4 ± 0.5 | 0.02 ± 0.01 | 0.05 ± 0.02 | 12 |
| **SFM** | **CQ37** | 4.00 ± 0.60 | 7.00 ± 2.5 | 0.09 ± 0.05 | 51.4 ± 1.5 | 0.10 ± 0.05 | 0.05 ± 0.01 | 6 |
| **AFB** | **CQ38** | 3.00 ± 0.01 | 11.3 ± 2.0 | 0.09 ± 0.01 | 49 ± 1.80 | 0.20 ± 0.06 | 0.04 ± 0.00 | 6 |
| **AFM** | **CQ1** | 3.00 ± 0.40 | 18.8 ± 6.6 | 0.20 ± 0.30 | 41.9 ± 5.3 | 0.50 ± 0.20 | 0.04 ± 0.01 | 10 |
| | **CQ40** | 4.30 ± 0.40 | 6.50 ± 0.4 | 0.03 ± 0.01 | 50.9 ± 0.4 | 0.10 ± 0.00 | 0.05 ± 0.01 | 8 |
| | **CQ46** | 3.00 ± 0.80 | 7.90 ± 4.0 | 0.10 ± 0.07 | 50.9 ± 2.9 | 0.20 ± 0.09 | 0.05 ± 0.01 | 9 |
| | **CQ55** | 3.60 ± 0.90 | 6.20 ± 4.4 | 0.40 ± 0.20 | 49.0 ± 3.0 | 0.10 ± 0.10 | 0.04 ± 0.01 | 11 |
| **AFT** | **CQ54** | 3.30 ± 0.10 | 12.5 ± 5.9 | 0.50 ± 0.30 | 45.0 ± 3.5 | 0.30 ± 0.20 | 0.04 ± 0.00 | 13 |
| **SeFB** | **CQ16** | 4.00 ± 0.80 | 3.30 ± 1.0 | 0.03 ± 0.02 | 54.0 ± 0.8 | 0.06 ± 0.02 | 0.02 ± 0.00 | 6 |
| **SeFM** | **CQ17** | 3.50 ± 0.30 | 15.6 ± 0.6 | 1.00 ± 0.30 | 45.0 ± 0.7 | 0.40 ± 0.01 | 0.04 ± 0.01 | 6 |
| **SeFT** | **CQ2** | 3.60 ± 0.40 | 5.00 ± 1.4 | 0.10 ± 0.05 | 51.6 ± 0.6 | 0.10 ± 0.03 | 0.06 ± 0.01 | 7 |
| | **CQ13** | 3.50 ± 0.50 | 7.60 ± 4.9 | 0.06 ± 0.03 | 50.2 ± 3.3 | 0.20 ± 0.10 | 0.05 ± 0.00 | 9 |
| | **CQ25** | 3.60 ± 1.00 | 6.00 ± 2.6 | 0.03 ± 0.01 | 52.0 ± 2.0 | 0.10 ± 0.05 | 0.04 ± 0.01 | 5 |
| | **CQ48** | 9.30 ± 10.8 | 3.90 ± 4.3 | 0.03 ± 0.03 | 52.8 ± 2.8 | 0.08 ± 0.08 | 0.04 ± 0.01 | 13 |
| | **CQ64** | 2.80 ± 0.09 | 19.7 ± 10 | 0.04 ± 0.01 | 42.6 ± 7.30 | 0.04 ± 0.01 | 0.04 ± 0.00 | 10 |

[a] Oxides measured by ICP-OES after Li-metaborate fusion digestion (Chapter 2.4.2) with values presented as ratios or sums of oxides in wt%

[b] Uncertainty presented as standard deviation of the number of samples presented in column **n.** The total number of samples presented in the table is 169

[c] depths of the sampling sites vary with the cores

[d]SFB = sloping farmlands bottom; SFM = sloping farmlands middle; SFT = sloping farmlands top; AFB = abandoned farmlands bottom; AFM = abandoned farmlands middle; AFT abandoned farmlands top; SeFB = secondary forest bottom; SeFM = secondary forest middle; SeFT = secondary forest top

While the Mg/Ca ratios (Table 3.7) in Tianlong soils are largely similar to both Chenqi and Chenjiazhai, $SiO_2/Al_2O_3$ is lower than in Chenjiazhai and Chenqi. The estimated abundances of carbonate minerals shown by CaO + MgO in Tianlong soils is similar to Chenqi but more than Chenjiazhai while the aluminosilicates shown by the sum $SiO_2$ + $Al_2O_3$, is similar with most of the sites in both Chenqi and Chenjiazhai.

The CaO + MgO in the Chenqi soils (Table 3.4) is relatively invariant and is significantly lower than in the bedrock. On the other hand, the $SiO_2$ + $Al_2O_3$ in the Chenqi soils varies within and between land uses and slope positions; is considerably higher in the soil of Chenqi than in the bedrock.

The sums of CaO and MgO (Table 3.4) which as mentioned earlier was used to estimate the abundance of the carbonate minerals in the soil is found to be significantly lower than the bedrock and are mostly within uncertainty with each other. On the other hand, the sums of $SiO_2$ and $Al_2O_3$ used to estimate the abundances of aluminosilicates in the soil and the bedrock, while showing variability within and between land uses and slope positions; and mostly within uncertainty with each other, are considerably higher in the soil of Chenqi than in the bedrock.

The $(SiO_2+Al_2O_3)/(CaO+MgO)$ ratios, used to estimate the abundances of the aluminosilicates relative to the carbonate minerals in the soil also mostly show variability but with some of the values within uncertainty of each other within and between land uses and slope positions. On the other hand, Mg/Ca ratios also followed similar pattern with the other parameters by largely showing variability while being within uncertainty within and between sites.

**Table 3.3:** Soil bulk chemistry in Chenqi watershed

| Sites | Sample | [a]$SiO_2$ | $Al_2O_3$ | $Fe_2O_3$ | CaO | MgO | $Na_2O$ | $K_2O$ | $P_2O_5$ | Zr | [b]n |
|---|---|---|---|---|---|---|---|---|---|---|---|
| [d]SFB | [c]CQ7 | 42.0 ± 3.3 | 15.4 ± 1.2 | 6.8 ± 0.40 | 8.0 ± 3.00 | 2.0 ± 0.10 | 0.10 ± 0.00 | 3.8 ± 0.30 | 0.09 ± 0.02 | 150 ± 12.3 | 7 |
| | CQ41 | 57.9 ± 6.1 | 16.0 ± 2.6 | 6.4 ± 1.00 | 0.7 ± 0.30 | 2.0 ± 0.60 | 0.10 ± 0.00 | 4.7 ± 0.60 | 0.10 ± 0.03 | 216 ± 40.0 | 11 |
| | CQ43 | 49.0 ± 2.0 | 19.0 ± 1.4 | 8.4 ± 0.70 | 1.0 ± 0.30 | 3.0± 0.40 | 0.10 ± 0.01 | 4.0 ± 0.10 | 0.10 ± 0.04 | 159 ± 18.0 | 12 |
| | CQ45 | 63.0 ± 1.3 | 13.0 ± 0.5 | 6.4 ± 0.20 | 0.5 ± 0.20 | 1.0 ± 0.10 | 0.10 ± 0.00 | 2.8 ± 0.05 | 0.10 ± 0.03 | 327 ± 28.8 | 8 |
| | CQ61 | 53.8 ± 2.8 | 16.6 ± 1.3 | 7.8 ± 0.50 | 0.5 ± 0.10 | 1.30 ± 0.20 | 0.10 ± 0.00 | 2.8 ± 0.20 | 0.08 ± 0.03 | 289 ± 25.2 | 12 |
| | S9 | 56.9 ± 0.5 | 13.8 ± 0.2 | 6.0± 0.10 | 1.0 ± 0.10 | 1.0 ± 0.02 | 0.10 ± 0.00 | 2.8 ± 0.10 | 0.20 ± 0.05 | 267 ± 6.80 | 9 |
| | S15 | 53.8 ± 0.2 | 16.5 ± 0.04 | 6.60 ± 0.07 | 0.9 ± 0.10 | 1.6 ± 0.01 | 0.10 ± 0.00 | 3.7 ± 0.03 | 0.10 ± 0.03 | 206 ± 6.40 | 6 |
| AFB | CQ38 | 51.3 ± 0.5 | 13.8 ± 0.20 | 5.9 ± 0.20 | 1.2 ± 0.05 | 1.3 ± 0.02 | 0.10 ± 0.00 | 3.3 ± 0.03 | 0.10 ± 0.02 | 192 ± 6.60 | 6 |
| | S25 | 56.5 ± 0.1 | 15.0 ± 0.05 | 6.5 ± 0.03 | 0.8 ± 0.09 | 1.2 ± 0.01 | 0.10 ± 0.04 | 3.0 ± 0.03 | 0.20 ± 0.01 | 244 ± 10.0 | 5 |
| SeFB | CQ16 | 57.0 ± 0.9 | 14.5 ± 0.40 | 6.0 ± 0.20 | 1.0 ± 0.10 | 1.3 ± 0.09 | 0.10 ± 0.00 | 3.5 ± 0.07 | 0.20 ± 0.04 | 217 ± 11.0 | 6 |
| | S3 | 53.9 ± 2.2 | 14.0 ± 1.00 | 6.3 ± 0.40 | 1.5 ± 0.50 | 1.0 ± 0.06 | 0.10 ± 0.01 | 2.9 ± 0.08 | 0.20 ± 0.02 | 240 ± 22.8 | 10 |
| SFM | CQ37 | 55.4 ± 2.8 | 17.5 ± 1.00 | 6.0 ± 1.80 | 0.7 ± 0.05 | 3.4 ± 0.60 | 0.10 ± 0.01 | 5.8 ± 1.00 | 0.08 ± 0.04 | 144 ± 43.4 | 6 |
| | PIPE | 55.9 ± 1.0 | 14.0 ± 1.00 | 6.6 ± 0.70 | 1.2 ± 0.20 | 1.0 ± 0.10 | 0.08 ± 0.01 | 2.4 ± 0.20 | 0.20 ± 0.02 | 278 ± 18.0 | 19 |
| | S8 | 58.9 ± 0.5 | 14.0 ± 0.20 | 6.7 ± 0.10 | 1.0 ± 0.10 | 1.2 ± 0.03 | 0.10 ± 0.00 | 2.5 ± 0.04 | 0.20 ± 0.02 | 284 ± 10.4 | 7 |
| | S14 | 54.0 ± 0.8 | 15.5 ± 0.40 | 5.9 ± 0.20 | 1.0 ± 0.10 | 1.5 ± 0.10 | 0.10 ± 0.00 | 3.9 ± 0.10 | 0.10 ± 0.04 | 220 ± 14.7 | 9 |
| AFM | CQ1 | 50.7 ± 2.0 | 15.4 ± 0.40 | 6.3 ± 0.20 | 1.7 ± 0.70 | 3.5 ± 0.60 | 0.10 ± 0.00 | 4.6 ± 0.10 | 0.10 ± 0.03 | 185 ± 18.3 | 10 |
| | CQ40 | 51.0 ± 0.9 | 15.8 ± 0.30 | 6.4 ± 0.10 | 1.0 ± 0.10 | 1.9 ± 0.05 | 0.10 ± 0.00 | 4.5 ± 0.10 | 0.10 ± 0.02 | 208 ± 11.7 | 8 |
| | CQ46 | 52.0 ± 0.7 | 16.0 ± 0.40 | 6.8 ± 0.20 | 1.0 ± 0.06 | 1.9 ± 0.06 | 0.10 ± 0.00 | 4.7 ± 0.20 | 0.10 ± 0.01 | 194 ± 6.00 | 9 |
| | CQ55 | 56.0 ± 2.0 | 14.3 ± 0.70 | 6.5 ± 0.30 | 0.8 ± 0.30 | 1.5 ± 0.20 | 0.10 ± 0.00 | 3.9 ± 0.10 | 0.10 ± 0.02 | 223 ± 13.6 | 11 |
| | S20 | 52.9 ± 0.6 | 17.4 ± 0.60 | 7.4 ± 0.20 | 0.8 ± 0.10 | 2.0 ± 0.10 | 0.10 ± 0.00 | 4.8 ± 0.30 | 0.20 ± 0.02 | 180 ± 8.00 | 6 |
| | S26 | 56.8 ± 0.4 | 15.0 ± 0.10 | 6.4 ± 0.05 | 1.0 ± 0.10 | 1.3 ± 0.01 | 0.10 ± 0.00 | 3.0 ± 0.01 | 0.20 ± 0.03 | 249 ± 5.70 | 6 |
| SeFM | CQ17 | 61.9 ± 1.9 | 14.0 ± 0.90 | 5.5 ± 0.40 | 0.4 ± 0.20 | 1.5 ± 0.20 | 0.10 ± 0.00 | 4.3 ± 0.10 | 0.02 ± 0.00 | 268 ± 14.2 | 6 |
| | CQ63 | 54.0 ± 3.3 | 17.0 ± 1.60 | 8.0 ± 0.70 | 0.5 ± 0.10 | 1.5 ± 0.50 | 0.10 ± 0.01 | 3.6 ± 0.70 | 0.10 ± 0.04 | 214 ± 39.5 | 13 |
| SFT | S6 | 54.6 ± 0.4 | 15.5 ± 0.30 | 6.6 ± 0.14 | 1.2 ± 0.10 | 1.5 ± 0.03 | 0.10 ± 0.00 | 3.3 ± 0.07 | 0.20 ± 0.02 | 232 ± 5.40 | 5 |
| | S7 | 55.3 ± 1.0 | 15.0 ± 1.10 | 6.3 ± 0.50 | 1.2 ± 0.10 | 1.2 ± 0.06 | 0.10 ± 0.00 | 3.0 ± 0.15 | 0.20 ± 0.03 | 243 ± 13.6 | 10 |

| | | | | | | | | | | | |
|---|---|---|---|---|---|---|---|---|---|---|---|
| | **S11** | 56.9 ± 0.5 | 14.6 ± 0.20 | 6.3 ± 0.10 | 0.8 ± 0.10 | 1.2 ± 0.02 | 0.10 ± 0.01 | 2.9 ± 0.05 | 0.30 ± 0.03 | 243 ± 8.90 | 6 |
| | **S12** | 57.8 ± 0.8 | 14.8 ± 0.20 | 6.3 ± 0.10 | 0.6 ± 0.13 | 1.2 ± 0.02 | 0.10 ± 0.00 | 3.0 ± 0.03 | 0.20 ± 0.02 | 273 ± 24.8 | 6 |
| **AFT** | **CQ48** | 49.0 ± 6.0 | 17.0 ± 2.00 | 7.0 ± 1.00 | 2.0 ± 3.00 | 4.0 ± 2.00 | 0.10 ± 0.10 | 4.8 ± 0.75 | 0.05 ± 0.03 | 180 ± 48.9 | 13 |
| | **CQ54** | 58.3 ± 3.0 | 16.0 ± 2.00 | 6.5 ± 0.20 | 0.3 ± 0.10 | 2.0 ± 0.40 | 0.10 ± 0.01 | 5.0 ± 0.40 | 0.05 ± 0.02 | 205 ± 25.6 | 13 |
| | **S24** | 50.6 ± 0.8 | 15.8 ± 0.50 | 6.0 ± 0.10 | 3.4 ± 0.70 | 2.0 ± 0.10 | 0.10 ± 0.00 | 4.5 ± 0.10 | 0.20 ± 0.03 | 190 ± 9.00 | 6 |
| | **S27** | 55.7 ± 0.9 | 15.0 ± 0.30 | 6.7 ± 0.50 | 1.0 ± 0.05 | 1.4 ± 0.05 | 0.10 ± 0.00 | 3.2 ± 0.30 | 0.20 ± 0.02 | 257 ± 17.0 | 10 |
| **SeFT** | **CQ2** | 48.8 ± 4.0 | 16.0 ± 0.90 | 6.7 ± 0.60 | 2.3 ± 1.60 | 4.0 ± 0.80 | 0.10 ± 0.00 | 5.0 ± 0.50 | 0.10 ± 0.03 | 188 ± 29.0 | 7 |
| | **CQ13** | 47.6 ± 8.6 | 11.6 ± 1.90 | 3.9 ± 0.50 | 2.4 ± 0.70 | 0.9 ± 0.10 | 0.10 ± 0.01 | 3.3 ± 0.60 | 0.10 ± 0.01 | 218. ± 37.0 | 9 |
| | **CQ25** | 41.9 ± 2.0 | 15.9 ± 0.40 | 6.0 ± 0.30 | 4.7 ± 3.60 | 2.3 ± 0.10 | 0.10 ± 0.00 | 4.0 ± 0.20 | 0.10 ± 0.02 | 127 ± 5.70 | 5 |
| | **CQ64** | 56.9 ± 2.6 | 15.0 ± 1.60 | 6.7 ± 0.80 | 0.7 ± 0.07 | 1.5 ± 0.20 | 0.10 ± 0.01 | 3.5 ± 0.10 | 0.10 ± 0.04 | 262 ± 17.7 | 10 |
| | **S2** | 48.8 ± 8.0 | 13.6 ± 1.00 | 5.6 ± 0.80 | 5.6 ± 7.60 | 1.6 ± 0.70 | 0.10 ± 0.01 | 3.4 ± 0.60 | 0.20 ± 0.03 | 197 ± 53.8 | 7 |

[a] Oxides measured by ICP-OES after Li-metaborate fusion digestion (Chapter 2.4.2) with values presented in wt% except for Zr, which is in ppm

[b] Uncertainty presented as standard deviation of the number of samples presented in column n. The total number of samples presented in the table is 169

[c] depths of the sampling sites vary with the cores

[d]SFB = sloping farmlands bottom; SFM = sloping farmlands middle; SFT = sloping farmlands top; AFB = abandoned farmlands bottom; AFM = abandoned farmlands middle; AFT abandoned farmlands top; SeFB = secondary forest bottom; SeFM = secondary forest middle; SeFT = secondary forest top

**Table 3.4:** Ratios and sums of the mineral oxides in Chenqi

| Sites | Sample | [a]$SiO_2/Al_2O_3$ | $SiO_2+Al_2O_3$ | Mg/Ca | CaO+MgO | $(SiO_2+Al_2O_3)/(CaO+MgO)$ | K/Rb | [b]n |
|---|---|---|---|---|---|---|---|---|
| [d]**SFB** | [c]**CQ7** | 2.7 ± 0.08 | 57.5 ± 4.5 | 0.30 ± 0.1 | 10.2 ± 2.9 | 6.20 ± 2.00 | 0.02 ± 0.00 | 7 |
| | **CQ41** | 3.7 ± 0.90 | 74.0 ± 3.7 | 3.00 ± 0.8 | 2.7 ± 0.80 | 30.4 ± 10.0 | 0.03 ± 0.00 | 11 |
| | **CQ43** | 2.6 ± 0.30 | 68.0 ± 1.0 | 2.90 ± 0.8 | 3.9 ± 0.30 | 17.5 ± 1.60 | 0.02 ± 0.00 | 12 |
| | **CQ45** | 4.8 ± 0.20 | 76.4 ± 1.0 | 2.00 ± 0.4 | 1.6 ± 0.20 | 50.0 ± 7.00 | 0.02 ± 0.00 | 8 |
| | **CQ61** | 3.3 ± 0.40 | 70.4 ± 2.0 | 2.50 ± 0.1 | 1.8 ± 0.20 | 72.0 ± 2.00 | 0.02 ± 0.00 | 12 |
| | **S9** | 4.0 ± 0.05 | 70.6 ± 0.6 | 0.90 ± 0.1 | 2.4 ± 0.07 | 29.6 ± 0.90 | 0.02 ± 0.00 | 9 |
| | **S15** | 3.3 ± 0.01 | 70.3 ± 0.2 | 1.70 ± 0.1 | 2.5 ± 0.09 | 28.3 ± 1.00 | 0.02 ± 0.00 | 6 |
| **SFM** | **CQ37** | 3.0 ± 0.30 | 72.8 ± 2.3 | 4.84 ± 1.0 | 4.0 ± 0.56 | 18.3 ± 2.11 | 0.03 ± 0.01 | 6 |
| | **PIPE** | 4.0 ± 0.30 | 69.9 ± 2.0 | 0.90 ± 0.2 | 2.3 ± 0.20 | 30.4 ± 3.40 | 0.02 ± 0.00 | 5 |
| | **S8** | 4.0 ± 0.07 | 72.9 ± 0.5 | 1.00 ± 0.1 | 2.0 ± 0.10 | 33.3 ± 1.70 | 0.02 ± 0.00 | 6 |
| | **S14** | 3.5 ± 0.10 | 69.7 ± 0.8 | 1.40 ± 0.2 | 2.6 ± 0.09 | 26.8 ± 1.20 | 0.02 ± 0.00 | 10 |
| | **S11** | 3.9 ± 0.05 | 71.5 ± 0.6 | 1.60 ± 0.2 | 2.0 ± 0.10 | 35.9 ± 0.80 | 0.02 ± 0.00 | 6 |
| **SFT** | **S6** | 3.5 ± 0.06 | 70.0 ± 0.7 | 1.30 ± 0.1 | 2.7 ± 0.09 | 26.5 ± 0.70 | 0.02 ± 0.00 | 19 |
| | **S12** | 3.9 ± 0.02 | 72.6 ± 0.9 | 2.00 ± 0.4 | 1.8 ± 0.10 | 40.0 ± 2.80 | 0.02 ± 0.00 | 7 |
| | **S7** | 3.7 ± 0.30 | 70.3 ± 1.0 | 1.00 ± 0.1 | 2.4 ± 0.08 | 28.8 ± 1.30 | 0.02 ± 0.00 | 9 |
| **AFB** | **CQ38** | 2.7 ± 0.03 | 65.1 ± 0.7 | 1.12 ± 0.05 | 2.5 ± 0.07 | 25.8 ± 0.80 | 0.03 ± 0.01 | 10 |
| | **S25** | 3.7 ± 0.01 | 71.6 ± 0.2 | 1.60 ± 0.2 | 2.0 ± 0.09 | 35.4 ± 1.60 | 0.02 ± 0.00 | 8 |
| **AFM** | **CQ1** | 3.3 ± 0.10 | 66.1 ± 2.3 | 2.23 ± 0.5 | 5.2 ± 1.20 | 13.3 ± 2.43 | 0.03 ± 0.00 | 9 |
| | **CQ40** | 3.3 ± 0.03 | 67.0 ± 1.0 | 1.80 ± 0.2 | 3.0 ± 0.10 | 22.7 ± 1.00 | 0.03 ± 0.00 | 11 |
| | **CQ46** | 3.3 ± 0.06 | 68.4 ± 0.9 | 1.90 ± 0.2 | 2.9 ± 0.03 | 23.0 ± 0.30 | 0.03 ± 0.00 | 6 |
| | **CQ55** | 4.0 ± 0.30 | 70.7 ± 1.9 | 2.00 ± 0.3 | 2.3 ± 0.50 | 31.5 ± 5.00 | 0.03 ± 0.00 | 6 |
| | **S26** | 3.8 ± 0.02 | 71.7 ± 0.5 | 1.40 ± 0.1 | 2.00 ± 0.09 | 32.0 ± 1.00 | 0.03 ± 0.00 | 6 |
| | **S20** | 3.0 ± 0.08 | 70.3 ± 1.0 | 2.70 ± 0.3 | 2.9 ± 0.20 | 24.5 ± 2.00 | 0.02 ± 0.00 | 13 |
| **AFT** | **CQ48** | 2.9 ± 0.55 | 66.3 ± 6.9 | 3.74 ± 1.9 | 6.1 ± 5.23 | 16.6 ± 8.40 | 0.03 ± 0.01 | 5 |
| | **CQ54** | 3.8 ± 0.50 | 73.9 ± 1.3 | 5.90 ± 1.0 | 2.3± 0.40 | 33.4 ± 6.30 | 0.03 ± 0.00 | 5 |
| | **S24** | 3.0 ± 0.10 | 66.5 ± 0.9 | 0.60 ± 0.1 | 5.3 ± 0.80 | 12.7 ± 1.60 | 0.03 ± 0.00 | 10 |

| | | | | | | | | |
|---|---|---|---|---|---|---|---|---|
| | **S27** | 3.6 ± 0.10 | 71.0 ± 0.9 | 1.50 ± 0.1 | 2.3 ± 0.07 | 31.0 ± 1.00 | 0.02 ± 0.00 | 6 |
| **SeFB** | **CQ16** | 4.0 ± 0.20 | 71.5 ± 0.6 | 1.30 ± 0.04 | 2.4 ± 0.20 | 30.3 ± 2.00 | 0.02 ± 0.00 | 6 |
| | **S3** | 3.8 ± 0.20 | 68.0 ± 2.9 | 0.90 ± 0.3 | 2.8 ± 0.50 | 25.3 ±4.50 | 0.02 ± 0.00 | 13 |
| **SeFM** | **CQ17** | 4.4 ± 0.30 | 75.8 ± 2.1 | 4.67 ± 2.2 | 1.9 ± 0.35 | 42.3 ± 8.60 | 0.04 ± 0.00 | 13 |
| | **CQ63** | 3.0 ± 0.50 | 71.5 ± 2.0 | 2.90 ± 0.5 | 2.0 ± 0.50 | 36.7 ± 7.00 | 0.02 ± 0.00 | 6 |
| **SeFT** | **CQ2** | 3.0 ± 0.20 | 64.9 ± 4.7 | 2.88 ± 1.7 | 6.3 ± 2.35 | 12.1 ± 5.20 | 0.03 ± 0.00 | 10 |
| | **CQ13** | 4.0 ± 0.08 | 59.0 ± 11 | 0.40 ± 0.2 | 3.3 ± 0.60 | 19.4 ± 6.80 | 0.06 ± 0.01 | 7 |
| | **CQ25** | 2.6 ± 0.10 | 57.5 ± 2.3 | 0.90 ± 0.5 | 7.0 ± 3.60 | 10.7 ± 4.90 | 0.03 ± 0.00 | 9 |
| | **CQ64** | 3.8 ± 0.50 | 72.0 ± 1.7 | 2.00 ± 0.3 | 2.0 ± 0.30 | 33.0 ± 4.40 | 0.03 ± 0.00 | 10 |
| | **S2** | 3.6 ± 0.50 | 62.4 ± 8.5 | 0.80 ± 0.4 | 7.3 ± 8.00 | 20.4 ± 11.0 | 0.03 ± 0.00 | 7 |

[a] Oxides measured by ICP-OES after Li-metaborate fusion digestion (Chapter 2.4.2) with values presented as ratios or sums of oxides in wt%

[b] Uncertainty presented as standard deviation of the number of samples presented in column **n.** The total number of samples presented in the table is 169

[c] depths of the sampling sites vary with the cores

[d]SFB = sloping farmlands bottom; SFM = sloping farmlands middle; SFT = sloping farmlands top; AFB = abandoned farmlands bottom; AFM = abandoned farmlands middle; AFT abandoned farmlands top; SeFB = secondary forest bottom; SeFM = secondary forest middle; SeFT = secondary forest top

Chenjiazhai is a sloping farmland that is recovering from perturbation and is classified based on different slope positions and the distribution and sizes of outcrops (Chapter 2.2.1). The bulk chemistry of the soils (Table 3.5) shows that abundances of Si and Fe are similar to Chenqi soils, although Al shows higher abundances in some sites in Chenjiazhai than in Chen qi. In contrast, abundances of Ca, Mg and K in Chenjiazhai are lower than those of Chenqi while Fe is higher, and P is lower in Chenjiazhai than in Chenqi. The CaO + MgO is similar within the sites and slope positions in Chenjiazhai but within uncertainty of each other but is mostly lower than Chenqi. The Mg/Ca ratios vary within and between slope positions in Chenjiazhai and are mostly higher than in Chenqi, although some sites (with no trend with respect to land use and slope positions) in Chenqi show similar values to Chenjiazhai. Also, the $SiO_2/Al_2O_3$ ratios and $SiO_2 + Al_2O_3$ show similar abundances with Chenqi.

### 3.2.3 Mass Transfer Analysis of the Soil Profiles

Mass transfer analysis (Chapter 2.5) was used to determine the mobilisation (gain or loss) of elements in the soil by normalising their concentrations to an assumed immobile element (Zr in this case) and the net gain or loss of mass of the immobile element was determined relative to the bedrock (deepest sample, in this study) (Anderson et al., 2002; Brimhall and Dietrich, 1987; Chadwick et al., 1990).

#### 3.2.3.1 Low Mobility Elements

The mobilisation of the less mobile elements Si, Al, and Fe in the sloping farmlands in Chenqi reveal conservation of these elements (Figure 3.3) although there were moderate depletions of the elements in sites CQ61 (20 cm) and CQ37 (30 cm) in the bottom and middle slopes of the sloping farmlands, respectively. In the secondary forest (Figure 3.4), there were slight depletions of Al and Fe at sites S3, CQ17 and CQ64 (in the bottom, middle and the top slopes, respectively) while sites CQ63 (middle slope, secondary forest) and CQ13 (top slope, secondary forest) showed significant depletion of these elements in comparison to other sites in the same land use. The abandoned farmlands (Fig. 3.4) also show mostly conservation of these

elements, but with sites CQ1 demonstrating slight depletion-enrichment and CQ54 showing moderate depletion.

**Table 3.5:** Soil bulk chemistry at Chenjiazhai

| Site | Sample | [a]$SiO_2$ | $Al_2O_3$ | $Fe_2O_3$ | CaO | MgO | $Na_2O$ | $K_2O$ | $P_2O_5$ | Zr | [b]n |
|---|---|---|---|---|---|---|---|---|---|---|---|
| [d]**SFB** | [c]**RP130** | 55.0 ± 0.7 | 15.9 ± 0.4 | 10.5 ± 0.2 | 0.50 ± 0.06 | 1.00 ± 0.01 | 0.08 ± 0.01 | 1.70 ± 0.02 | 0.20 ± 0.02 | 402.6 ± 17.4 | 10 |
| | **RP171** | 58.5 ± 5.9 | 15.6 ± 1.2 | 8.00 ± 1.9 | 0.50 ± 0.03 | 1.30 ± 0.04 | 0.10 ± 0.01 | 2.00 ± 0.05 | 0.10 ± 0.10 | 375.7 ± 52.0 | 14 |
| | **RP196** | 54.5 ± 1.9 | 16.6 ± 0.3 | 10.4 ± 0.2 | 0.30 ± 0.08 | 1.00 ± 0.02 | 0.08 ± 0.00 | 1.70 ± 0.03 | 0.20 ± 0.03 | 405.8 ± 22.0 | 12 |
| **SFM** | **RP230** | 57.7 ± 1.0 | 14.7 ± 0.2 | 9.80 ± 0.2 | 0.50 ± 0.05 | 1.00 ± 0.01 | 0.08 ± 0.00 | 1.60 ± 0.03 | 0.20 ± 0.02 | 409.2 ± 16.4 | 12 |
| | **RP293** | 54.6 ± 1.0 | 15.9 ± 0.3 | 9.90 ± 0.2 | 0.40 ± 0.03 | 1.00 ± 0.01 | 0.08 ± 0.00 | 1.80 ± 0.03 | 0.20 ± 0.02 | 381.2 ± 13.9 | 10 |
| | **RP2170** | 48.0 ± 2.0 | 19.5 ± 1.2 | 11.3 ± 0.5 | 0.50 ± 0.05 | 1.30 ± 0.10 | 0.08 ± 0.00 | 2.00 ± 0.10 | 0.20 ± 0.02 | 311.0 ± 26.8 | 11 |
| **SFT** | **RP324** | 56.9 ± 0.7 | 14.8 ± 0.2 | 10.3 ± 0.4 | 0.50 ± 0.03 | 1.00 ± 0.01 | 0.08 ± 0.00 | 1.60 ± 0.03 | 0.20 ± 0.03 | 398.7 ± 20.9 | 12 |
| | **RP378** | 57.3 ± 1.7 | 15.6 ± 0.2 | 10.0 ± 0.2 | 0.40 ± 0.09 | 1.00 ± 0.04 | 0.08 ± 0.00 | 1.70 ± 0.03 | 0.20 ± 0.02 | 430.6 ± 32.0 | 8 |
| | **RP3135** | 49.0 ± 0.8 | 19.0 ± 1.0 | 11.0 ± 0.1 | 0.60 ± 0.10 | 1.40 ± 0.05 | 0.08 ± 0.00 | 2.00 ± 0.10 | 0.20 ± 0.02 | 320.0 ± 9.90 | 10 |

[a] Oxides measured by ICP-OES after Li-metaborate fusion digestion (Chapter 2.4.2) with values presented in wt% except for Zr, which is in ppm

[b] Uncertainty presented as standard deviation of the number of samples presented in column **n.** The total number of samples presented in the table is 99

[c] Depths of pits at the sampling sites vary

[d]SFB = sloping farmlands bottom; SFM = sloping farmlands middle; SFT = sloping farmlands top

**Table 3.6:** Ratios and sums of the mineral oxides in Chenjiazhai

| Site | Sample | [a]$SiO_2/Al_2O_3$ | $SiO_2+Al_2O_3$ | Mg/Ca | CaO+MgO | $(SiO_2+Al_2O_3)/(CaO+MgO)$ | K/Rb | [b]n |
|---|---|---|---|---|---|---|---|---|
| [d]SFB | [c]RP130 | 3.5 ± 0.09 | 71.0 ± 0.70 | 2.0 ± 0.30 | 1.5 ± 0.07 | 47.0 ± 2.30 | 0.01 ± 0.00 | 10 |
| | RP171 | 3.8 ± 0.60 | 74.0 ± 4.70 | 2.8 ± 0.30 | 1.8 ± 0.05 | 41.8 ± 3.30 | 0.02 ± 0.00 | 14 |
| | RP196 | 3.3 ± 0.08 | 71.0 ± 2.00 | 3.7 ± 0.80 | 1.3 ± 0.09 | 53.0 ± 4.30 | 0.01 ± 0.00 | 12 |
| SFM | RP230 | 3.9 ± 0.08 | 72.4 ± 1.00 | 2.0 ± 0.20 | 1.5 ± 0.06 | 49.5 ± 2.30 | 0.01 ± 0.00 | 12 |
| | RP293 | 3.4 ± 0.04 | 70.5 ± 1.30 | 2.5 ± 0.20 | 1.5 ± 0.03 | 46.5 ± 1.00 | 0.01 ± 0.00 | 10 |
| | RP2170 | 2.5 ± 0.30 | 67.6 ± 0.90 | 3.0 ± 0.20 | 1.8 ± 0.10 | 38.9 ± 3.50 | 0.01 ± 0.00 | 11 |
| SFT | RP324 | 3.9 ± 0.05 | 71.7 ± 0.80 | 2.0 ± 0.10 | 1.5 ± 0.03 | 49.5 ± 1.00 | 0.01 ± 0.00 | 12 |
| | RP378 | 3.7 ± 0.20 | 72.9 ± 1.60 | 2.5 ± 0.40 | 1.4 ± 0.10 | 52.8 ± 5.50 | 0.01 ± 0.00 | 8 |
| | RP3135 | 2.6 ± 0.10 | 68.0 ± 1.70 | 2.3 ± 0.50 | 2.0 ± 0.06 | 34.8 ± 2.00 | 0.01 ± 0.00 | 10 |

[a] Oxides measured by ICP-OES after Li-metaborate fusion digestion (Chapter 2.4.2) with values presented in wt% except for Zr, which is in ppm

[b] Uncertainty presented as standard deviation of the number of samples presented in column **n.** The total number of samples presented in the table is 99

[c] Depths of pits at the sampling sites vary

[d]SFB = sloping farmlands bottom; SFM = sloping farmlands middle; SFT = sloping farmlands top

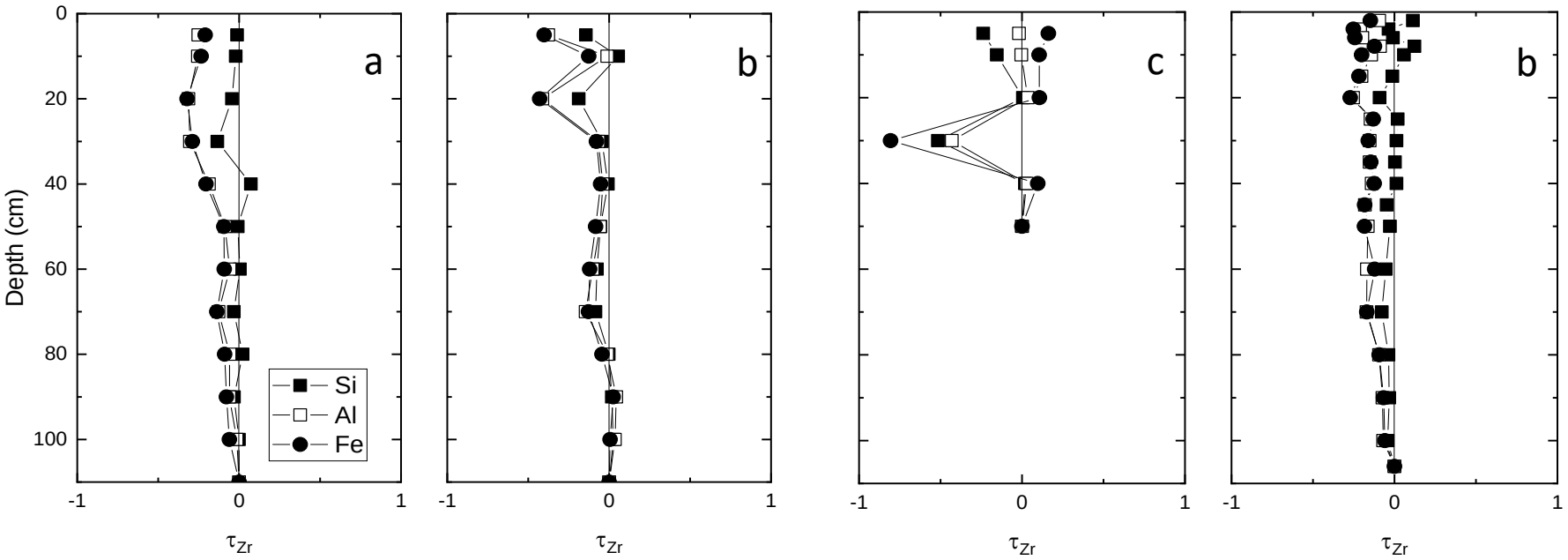


**Figure 3.3:** Mass transfer profiles of the less mobile elements Si, Al, and Fe in the sloping farmlands in Chenqi watershed. a) CQ43 b) CQ61 c) CQ37 d) PIPE showing the mobilisations of the less mobile elements. Sites a) and b) are from the bottom slopes while c) and d) are from the middle slopes. Tau plots from the top slopes were not included in this figure because the pits were too shallow to be readable when the depths of the sites have been normalised in the figure.

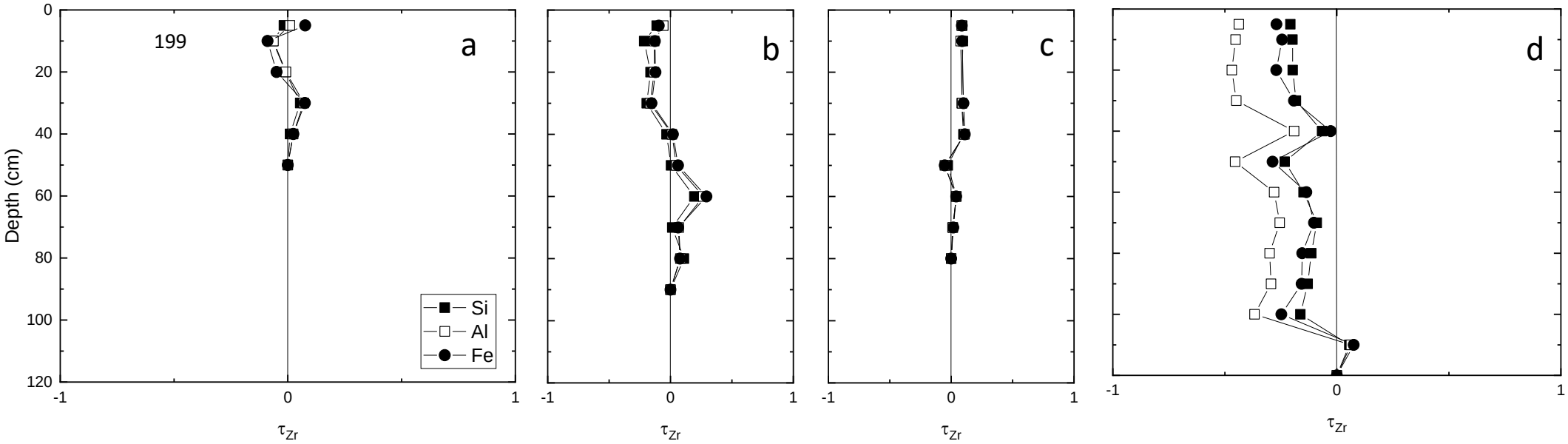


**Figure 3.4:** Mass transfer profiles showing the mobilisations of the less mobile elements Si, Al, and Fe soil cores of the abandoned farmlands in Chenqi watershed. a) CQ38 b) CQ1 c) CQ40 d) CQ54. Sites a) is from the bottom slope, b) and c) are from the middle slopes, while d) is the bottom slope.

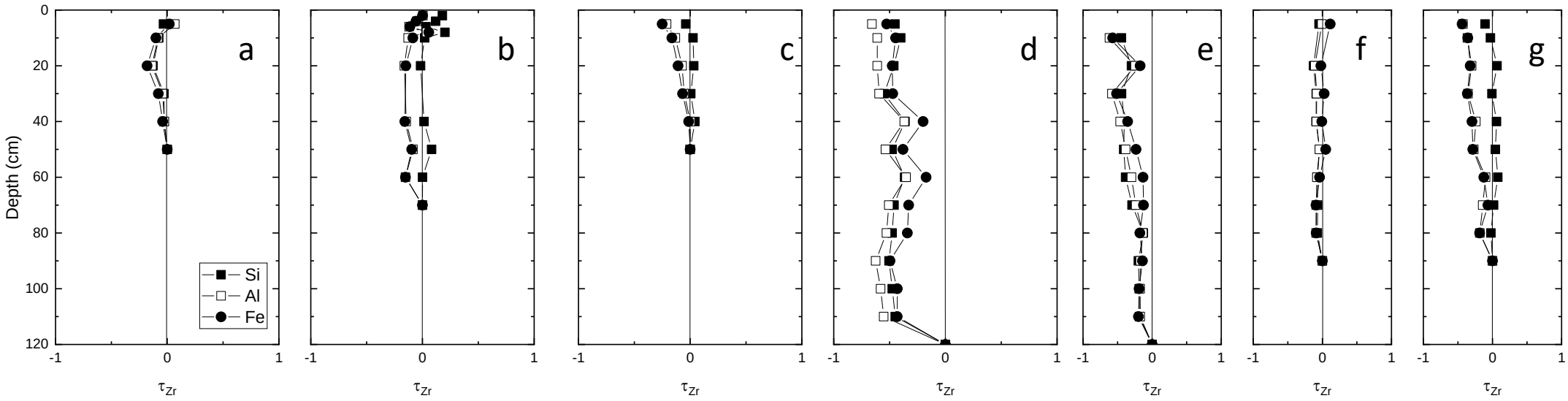


**Figure 3.5:** Mass transfer profiles showing the mobilisations of the less mobile elements Si, Al, and Fe in secondary forest in Chenqi watershed. a) CQ16 b) S3 c) CQ17 d) CQ63 e) CQ13 e) CQ48 f) CQ64. Sites a) and b) are from the bottom slope, c) and d) are from the middle slopes, while e), f) and g) are from the top slope.

In Chenjiazhai (Figs 3.9, 3.10 and 3.11), the less mobile elements are mostly conserved except in site RP1-71 in the bottom slope of the sloping farmland which showed significant enrichment of Fe above 15 cm depth. On the other hand, Al showed depletion-enrichment (slight enrichment in the top 10 cm) at the same site while Si was depleted. In the pristine forest of Tianlong (Fig. 3.15, 3.16 and 3.17), the less mobile elements are mostly conserved with slight depletions in sites TL1 (10 cm), TL2 (above 10 cm) and TL3-4 (above 16 cm).

#### 3.2.3.2 Mobile Elements

Mobile elements Ca, Mg, Na, K and P also show different mass transfer profiles in the different land uses and slope positions analysed. In the sloping farmlands of Chenqi (Fig 3.6), Mg and K are conserved in the bottom slope of the sloping farmland with slight depletions in the top 30 cm of sites CQ43 and CQ61. Also, in the same slope, Ca and Na are also conserved below 10 cm (CQ43) and 40 cm (CQ61) while P is significantly enriched throughout most of the CQ43 profile and has a depletion-enrichment profile at site CQ61 (enriched in the top 20 cm and depleted below).

In the abandoned farmlands (Fig 3.7), Mg, Na and K are mostly conserved in the bottom and the middle slopes (Mg shows depletion above 60 cm in site CQ1). However, Ca (conserved in the bottom slope, Fig 3.7a) and P are depleted (Fig 3.7a) in site CQ38 while Ca, Mg, Na and P all are depleted (site CQ40, Fig. 3.7b) with only P being enriched at the top and depleted at the bottom of the top slope (site CQ 54, Fig. 3.7d).

The bottom slope of the secondary forest (Fig 3.8) the mass transfer show conservation of Mg, Na and K with Ca and P being slightly enriched (P enriched above 100% in the top 10 cm) in site S3 while in site CQ16, only P is depleted while the other elements are all conserved. The middle slope also shows enrichment of P and conservation of all the other elements while site CQ17 reveals depletion of Ca and Mg. Site CQ48 in the top slope of the secondary forest (Fig. 3.8) showed complete depletion of Ca and Mg while Na, K and P were moderately depleted.

Other sites (CQ13 and CQ64) in the top slope of the secondary forest (Fig. 3.8) reveal conservation of Ca, Mg, Na and K with P enriched above 100%.

In the recovering farmlands of Chenjiazhai, site RP1-30 (bottom slope with rock outcrops less than 30 cm, Fig. 3.12) Mg and K are conserved in the bottom slope while Ca and P are depleted, and Na is slightly enriched in the top 10 cm. On the other hand, sites RP1-71 and RP1-96 (Fig. 3.12), with outcrops bigger than 50 cm but less than 100 cm, P is enriched above while Ca is depleted below 10 cm while Mg and K are conserved (Na slightly enriched in the top 10 cm). The middle slope, site RP2-30, with distributed outcrops less than 50 cm, Mg, K and Na were conserved while P and Ca were moderately enriched while in site RP2-93, with outcrops bigger than 50 cm but less than 100 cm shows slight enrichment of all the elements analysed. However, in site RP2-170, with outcrops bigger than 100 cm, Ca, Mg, K and Na are depleted in the top 13 cm before being conserved up to the deepest sample while P was slightly enriched in the top 10 cm and conserved below the 10 cm depth. In the top slope, site RP3-24, Mg, K, Na and Ca (enriched in the top 5 cm) were conserved while P was moderately enriched. Sites RP3-78 and RP3-135 show enrichment of Ca and P but conservation of Mg, K and Na RP3-78 showed enrichment of Mg, Na and K in the top 7 cm before returning to the concentrations of the deepest sample.

In the pristine forests of Tianlong, the mass transfer profiles in the bottom slope (Fig. 3.18) show depletion of K and conservation of Mg, Na and Ca (enriched in the top 7 cm of site TL1) while P is enriched. In the middle slope (Fig. 3.19), enrichments in P (more than 100%), Na (slight) and Ca (in the top 5 cm) are evident in site TL1-2 while K and Mg were slightly depleted in site TL3 and in site TL2, only K is conserved with Ca, Mg, Na, and P depleted. In the top slope of the pristine forest in Tianlong (Fig. 3.17) Na (depleted in site TL4) is conserved in TL3-4. However, Ca, Mg, K (enriched in the 10 cm of site TL4) were depleted while P is enriched above 100%.

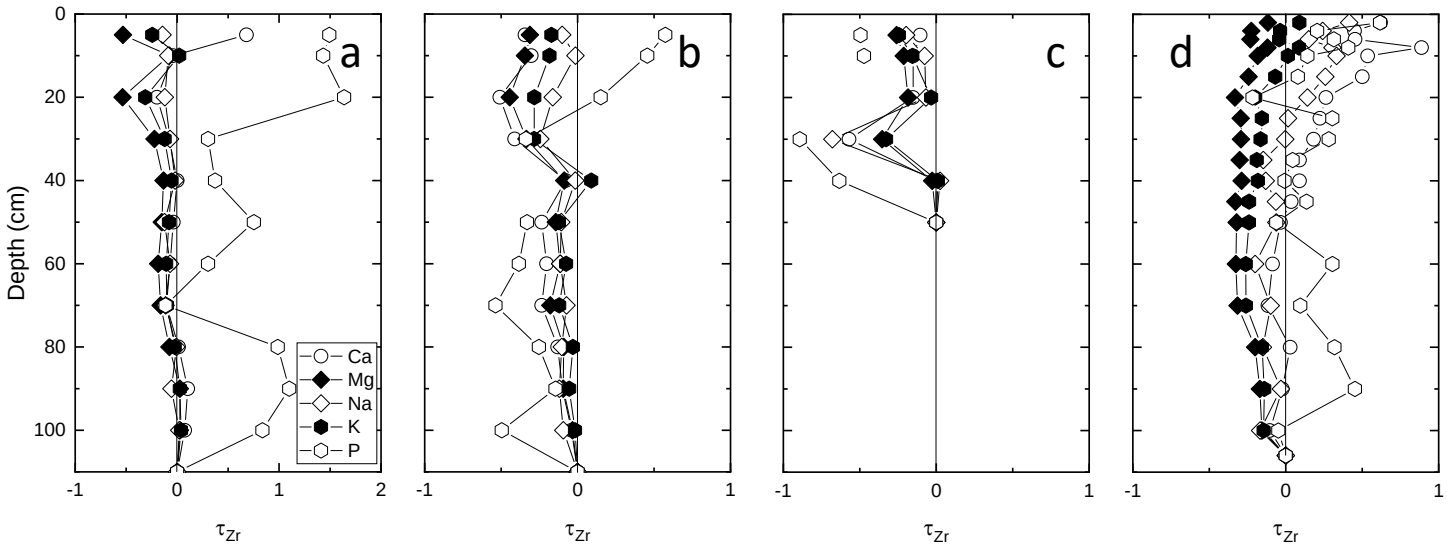


**Figure 3.6:** Mass transfer profiles showing the mobilisations of the mobile elements Ca, Mg, Na, K and P in the sloping farmlands a) CQ43 b) CQ61 c) CQ37 d) PIPE showing the mobilisations of the mobile elements. Sites a) and b) are from the bottom slopes while c) and d) are from the middle slopes. Tau plots from the top slopes were not included in this figure because the pits were too shallow to be readable when the depths of the sites have been normalised in the figure. The pits in the top slope will be shown in the appendix.

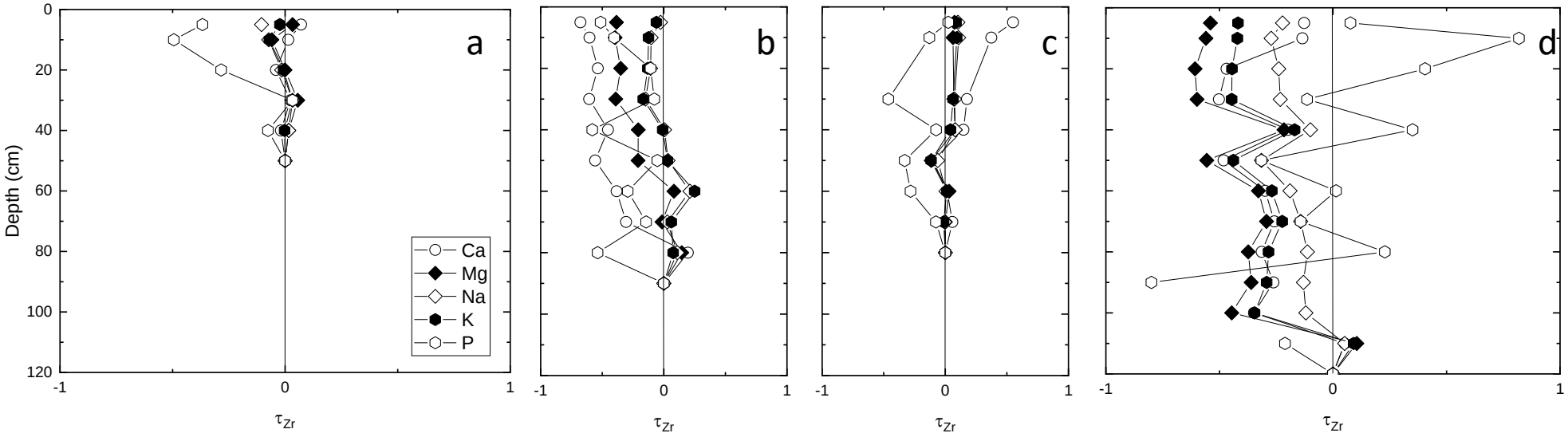


**Figure 3.7:** Mass transfer profiles showing the mobilisations of the mobile elements Ca, Mg, Na, K and P in the abandoned farmlands in Chenqi watershed. a) CQ38 b) CQ1 c) CQ40 d) CQ54. Sites a) is from the bottom slope, b) and c) are from the middle slopes, while d) is the bottom slope. All samples were from the soil cores.

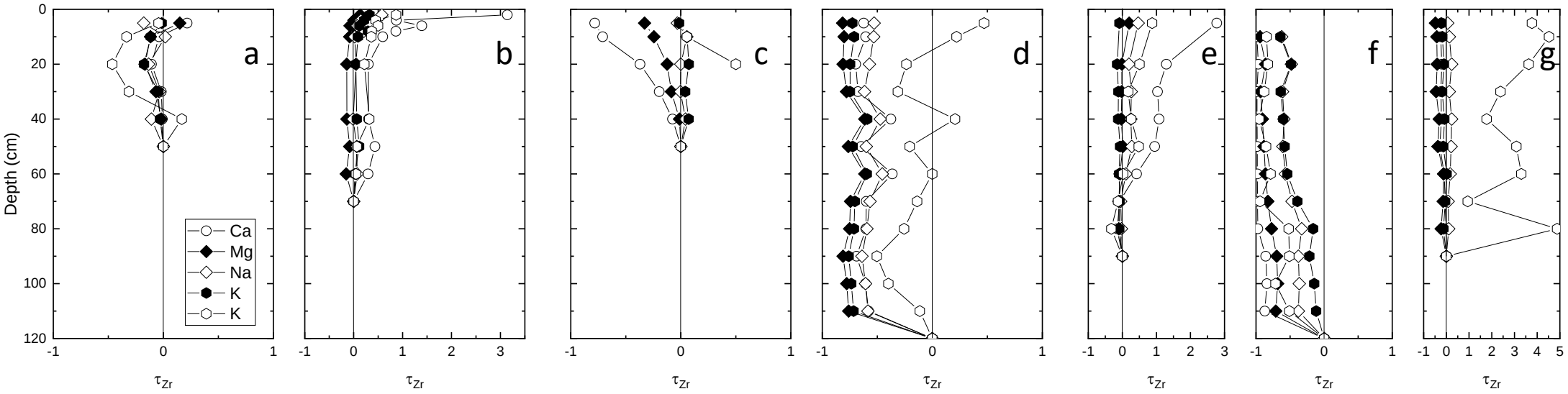


**Figure 3.8:** Mass transfer profiles showing the mobilisations of the mobile elements Ca, Mg, Na, K and P in secondary forest in Chenqi watershed. a) CQ16 b) S3 c) CQ17 d) CQ63 e) CQ13 f) CQ48 g) CQ64. Sites a) and b) are from the bottom slope, c) and d) are from the middle slopes, while e), f) and g) are the top slope. Samples were from both soil cores and pits.

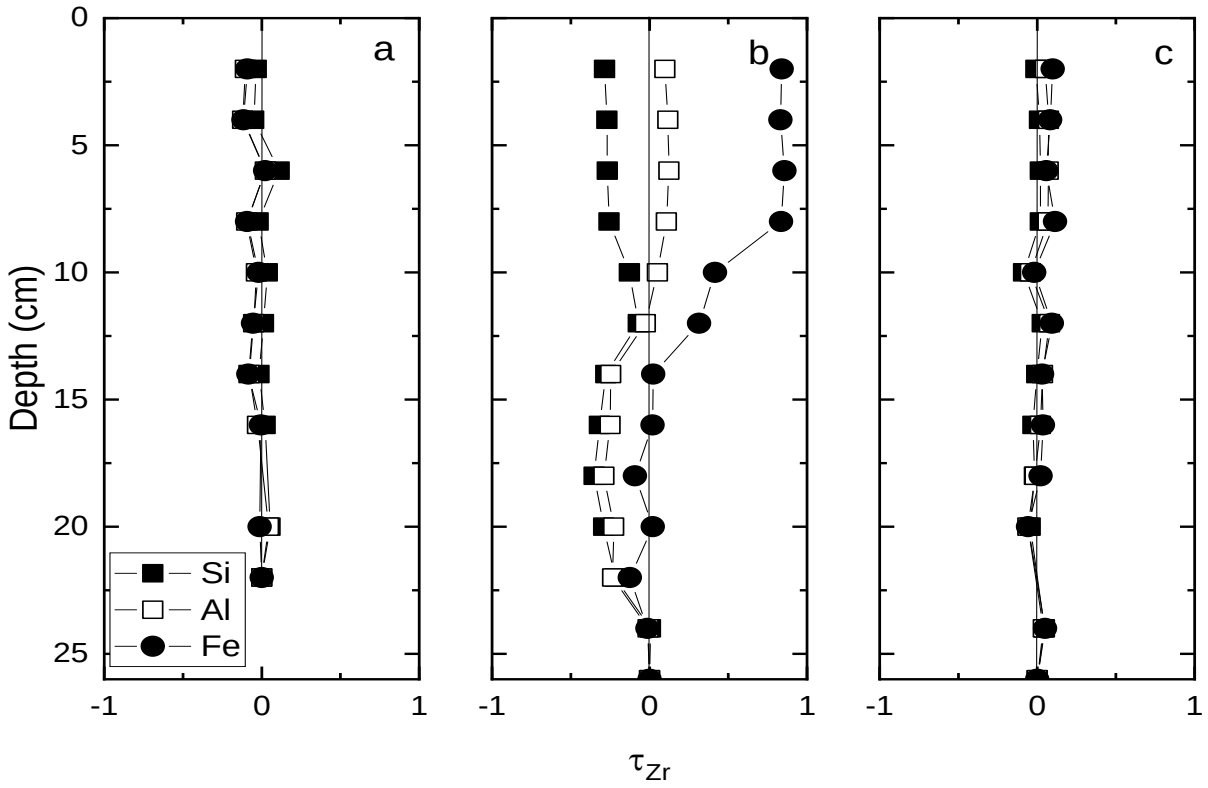


**Figure 3.9:** Mass transfer profiles showing the mobilisations of the less mobile elements Si, Al, and Fe in the bottom slope of the sloping farmlands in Chenjiazhai watershed. a) RP 1-30 b) RP 1-71 c) RP 1-96. All samples were from soil pits.

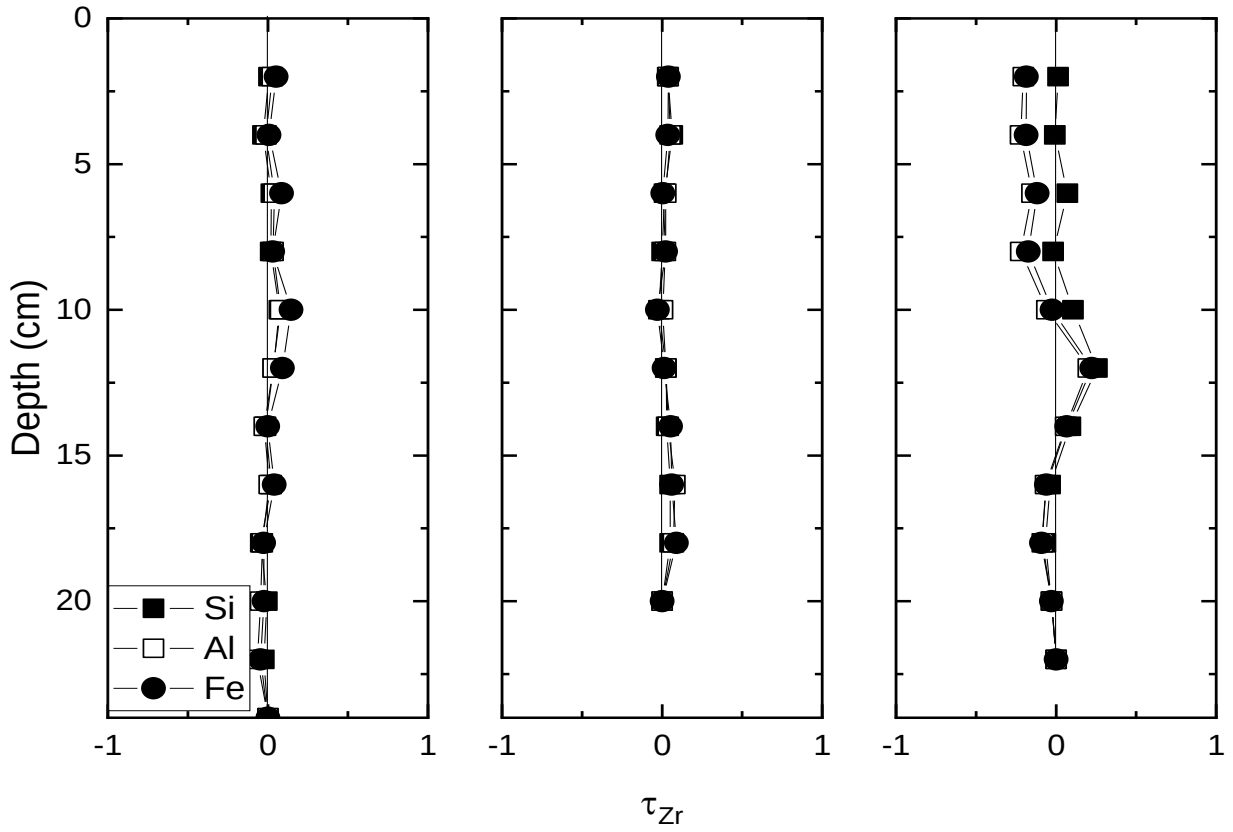


**Figure 3.10:** Mass transfer profiles showing the mobilisations of the less mobile elements Si, Al, and Fe in the middle slope of the abandoned farmlands in Chenjiazhai watershed. a) RP 2-30 b) RP 2-93 c) RP 2-170. Samples were from soil pits. Samples collected from soil pits.

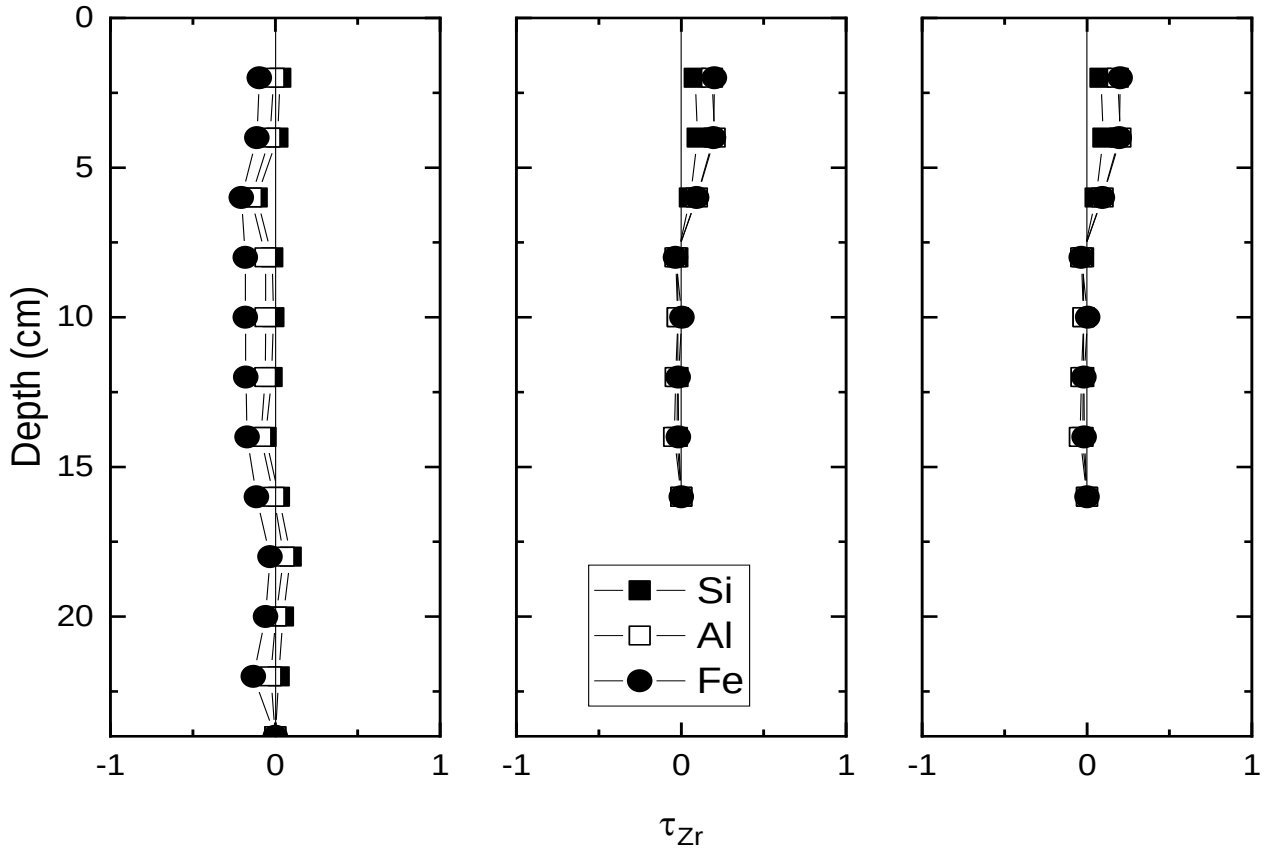


**Figure 3.11:** Mass transfer profiles showing the mobilisations of the less mobile elements Si, Al, and Fe in the middle slope of the secondary forest in Chenjiazhai watershed. a) RP 3-24 b) RP 3-78 c) RP 3-175. Samples were from the soil pits. Samples were from soil pits.

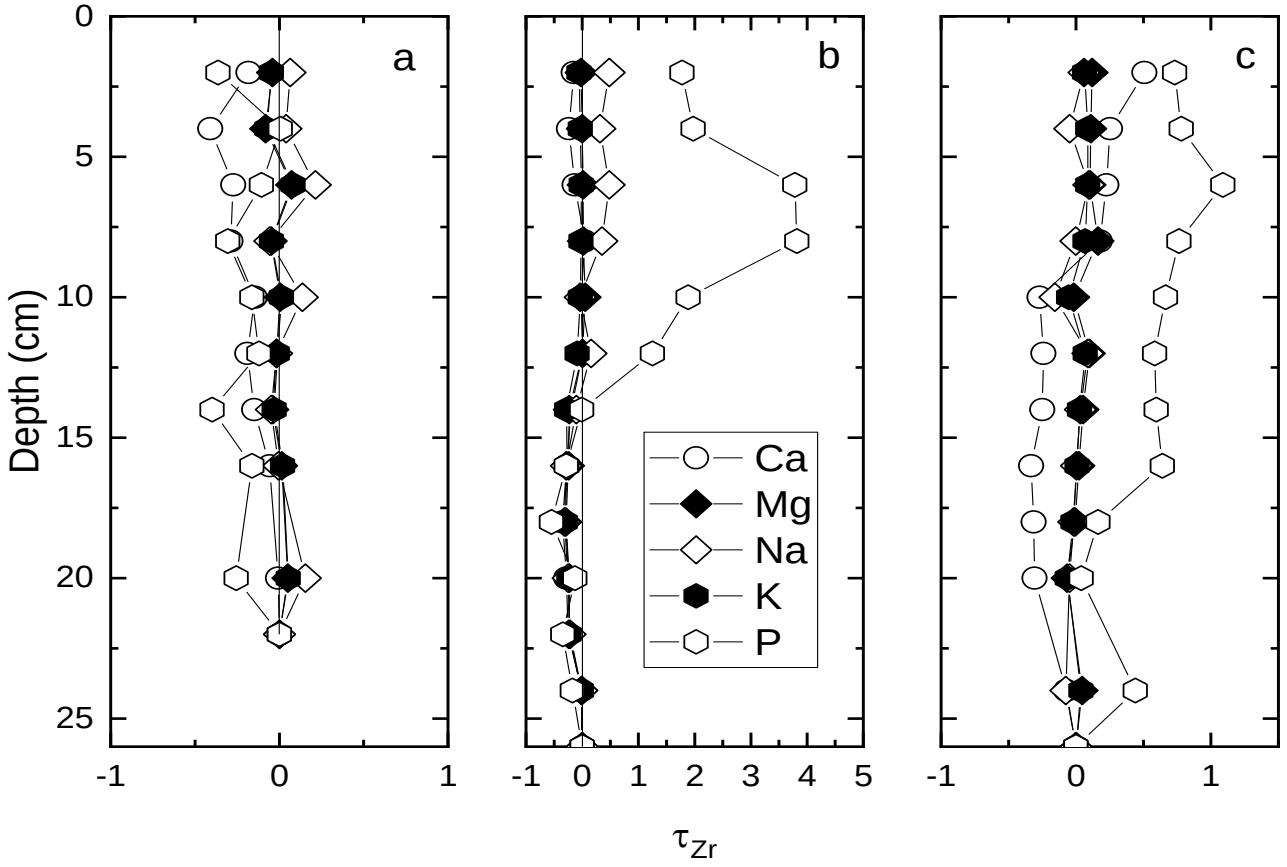


**Figure 3.12:** Mass transfer profiles analysis of the mobile elements Ca, Mg, Na, K and P in the bottom slopes of the sloping farmlands in the Chenjiazhai watershed a) RP1-30 b) RP1-71 c) RP1-96. The difference in scale on x-axis is due to the high enrichment of some of the elements in the soil. Samples collected from soil pits.

**Table 3.7:** Soil bulk chemistry at Tianlong

| Sites | Sample | $SiO_2$[a] | $Al_2O_3$ | $Fe_2O_3$ | CaO | MgO | $Na_2O$ | $K_2O$ | $P_2O_5$ | Zr | n[b] |
|---|---|---|---|---|---|---|---|---|---|---|---|
| FB[d] | TL1[c] | 49.60 ± 1.50 | 18.80 ± 1.00 | 7.90 ± 0.40 | 0.90 ± 0.20 | 1.80 ± 0.10 | 0.10 ± 0.02 | 1.30 ± 0.20 | 0.10 ± 0.02 | 299.00 ± 19.60 | 9 |
| | TL1-2 | 48.40 ± 1.70 | 18.80 ± 1.00 | 7.90 ± 0.40 | 1.00 ± 0.10 | 1.80 ± 0.07 | 0.10 ± 0.01 | 1.40 ± 0.20 | 0.20 ± 0.03 | 286.00 ± 12.20 | 9 |
| FM | TL2 | 28.30 ± 3.40 | 12.00 ± 1.50 | 5.00 ± 0.60 | 11.30 ± 3.30 | 8.80 ± 2.00 | 0.10 ± 0.02 | 0.40 ± 0.08 | 0.20 ± 0.02 | 151.00 ± 27.00 | 5 |
| | TL3 | 48.00 ± 1.50 | 19.00 ± 1.00 | 8.00 ± 0.50 | 0.80 ± 0.20 | 2.00 ± 0.10 | 0.10 ± 0.00 | 1.00 ± 0.10 | 0.20 ± 0.04 | 302.50 ± 15.90 | 8 |
| FT | TL3-4 | 47.40 ± 3.00 | 19.00 ± 1.60 | 8.00 ± 0.70 | 1.00 ± 0.50 | 2.00 ± 0.30 | 0.10 ± 0.00 | 1.00 ± 0.10 | 0.10 ± 0.03 | 301.80 ± 21.00 | 9 |
| | TL4 | 11.00 ± 1.00 | 4.90 ± 0.60 | 2.00 ± 0.20 | 18.90 ± 2.50 | 12.90 ± 2.00 | 0.10 ± 0.02 | 0.20 ± 0.07 | 0.20 ± 0.10 | 64.70 ± 6.60 | 7 |

[a] Oxides measured by ICP-OES after Li-metaborate fusion digestion (Chapter 2.4.2) with values presented in wt% except for Zr, which is in ppm

[b] Uncertainty presented as standard deviation of the number of samples presented in column **n.** The total number of samples presented in the table is 47

[c] depths of pits at the sampling sites vary.

[d]FB = pristine forest bottom; FM = pristine forest middle; FT = pristine forest top

**Table 3.8:** Ratios and sums of the mineral oxides in Tianlong

| Sites | Sample | $SiO_2/Al_2O_3$[d] | $SiO_2+Al_2O_3$ | Mg/Ca | CaO+MgO | $(SiO_2+Al_2O_3)/(CaO+MgO)$ | n[b] |
|---|---|---|---|---|---|---|---|
| **FB**[d] | **TL1**[c] | 2.60 ± 0.10 | 68.40 ± 2.50 | 2.00 ± 0.40 | 2.70 ± 0.20 | 25.30 ± 1.90 | 9 |
| | **TL1-2** | 2.60 ± 0.06 | 67.00 ± 2.70 | 1.70 ± 0.20 | 2.90 ± 0.10 | 23.30 ± 1.40 | 9 |
| **FM** | **TL2** | 2.30 ± 0.03 | 40.40 ± 5.00 | 0.80 ± 0.06 | 20.00 ± 5.30 | 60.40 ± 0.70 | 5 |
| | **TL3** | 2.50 ± 0.06 | 67.30 ± 2.50 | 2.70 ± 0.50 | 2.90 ± 0.10 | 23.00 ± 1.40 | 8 |
| **FT** | **TL3-4** | 2.50 ± 0.07 | 66.40 ± 4.60 | 2.40 ± 0.70 | 3.00 ± 0.70 | 21.50 ± 4.00 | 9 |
| | **TL4** | 2.30 ± 0.10 | 16.00 ± 1.80 | 0.68 ± 0.03 | 31.80 ± 4.60 | 0.50 ± 0.10 | 7 |

[a] Oxides measured by ICP-OES after Li-metaborate fusion digestion (Chapter 2.4.2) with values presented in wt% except for Zr, which is in ppm

[b] Uncertainty presented as standard deviation of the number of samples presented in column **n.** The total number of samples presented in the table is 47

[c] depths of pits at the sampling sites vary

[d]FB = pristine forest bottom; FM = pristine forest middle; FT = pristine forest top

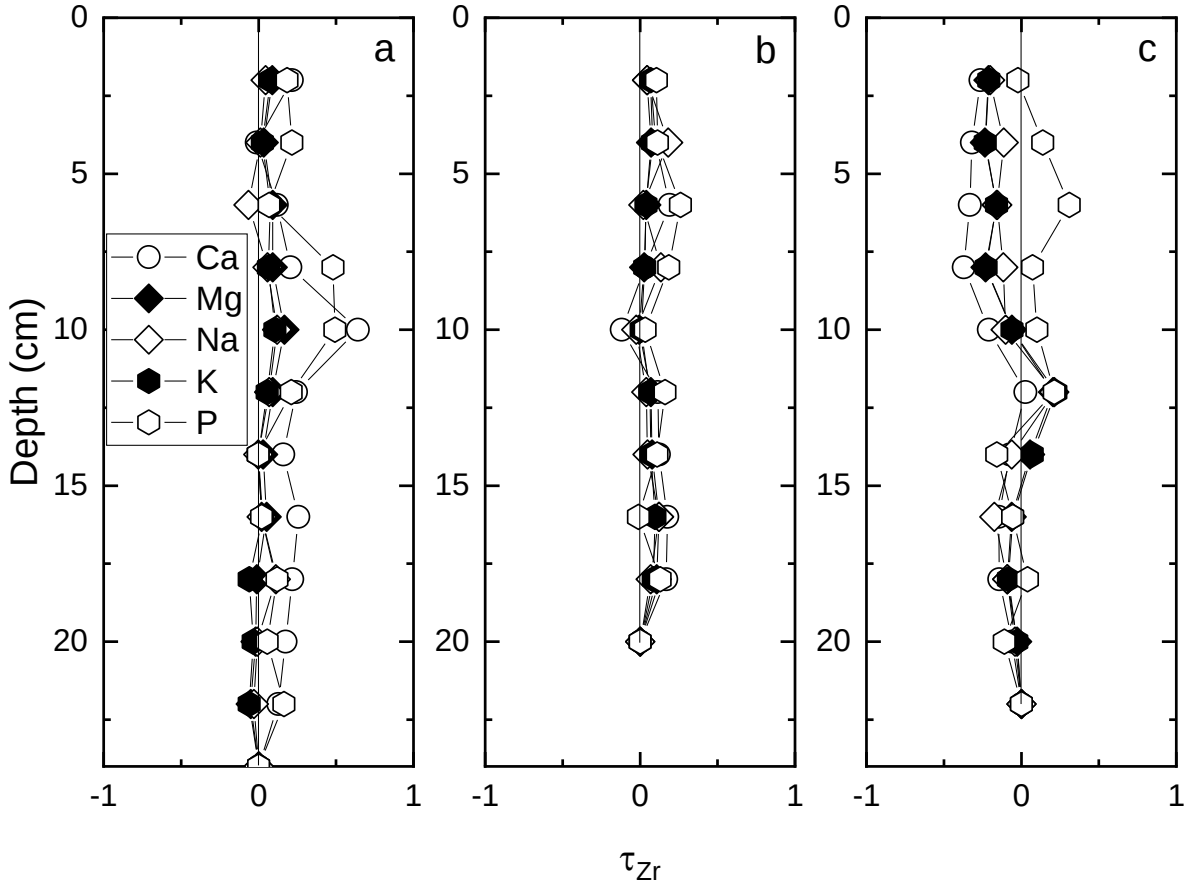


**Figure 3.13:** Mass transfer profiles analysis of the mobile elements Ca, Mg, Na, K and P in the middle slopes of the abandoned farmlands in the Chenjiazhai watershed a) RP 2-30 b) RP 2-93 c) RP 2-170. The difference in scale on x-axis is due to the high enrichment of some of the elements in the soil. Samples collected from soil pits.

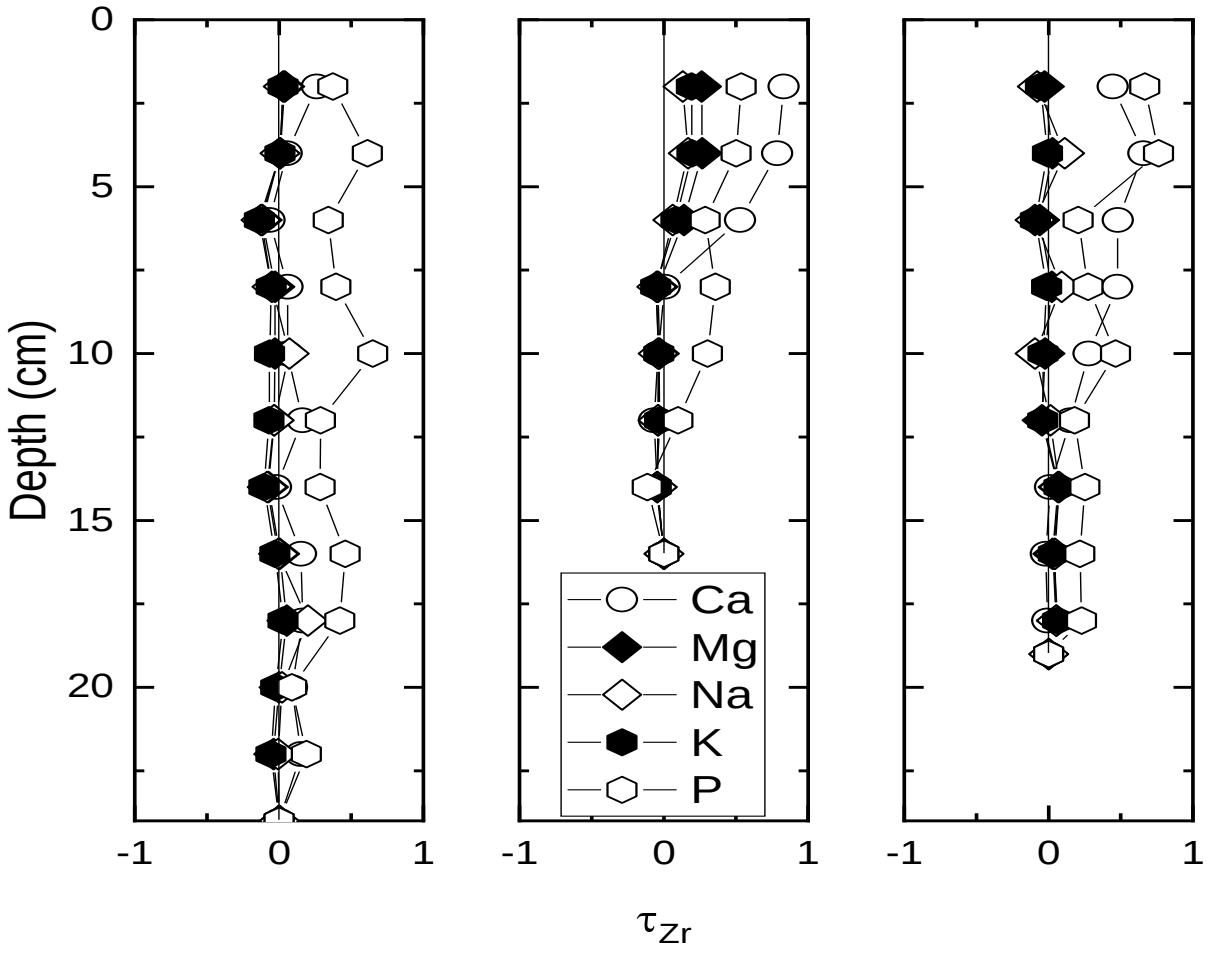


**Figure 3.14:** Mass transfer profiles analysis of the mobile elements Ca, Mg, Na, K and P in the top slopes of the secondary forest in the Chenjiazhai watershed a) RP 3-24 b) RP 3-78 c) RP 3-175. The difference in scale on x-axis is due to the high enrichment of some of the elements in the soil.

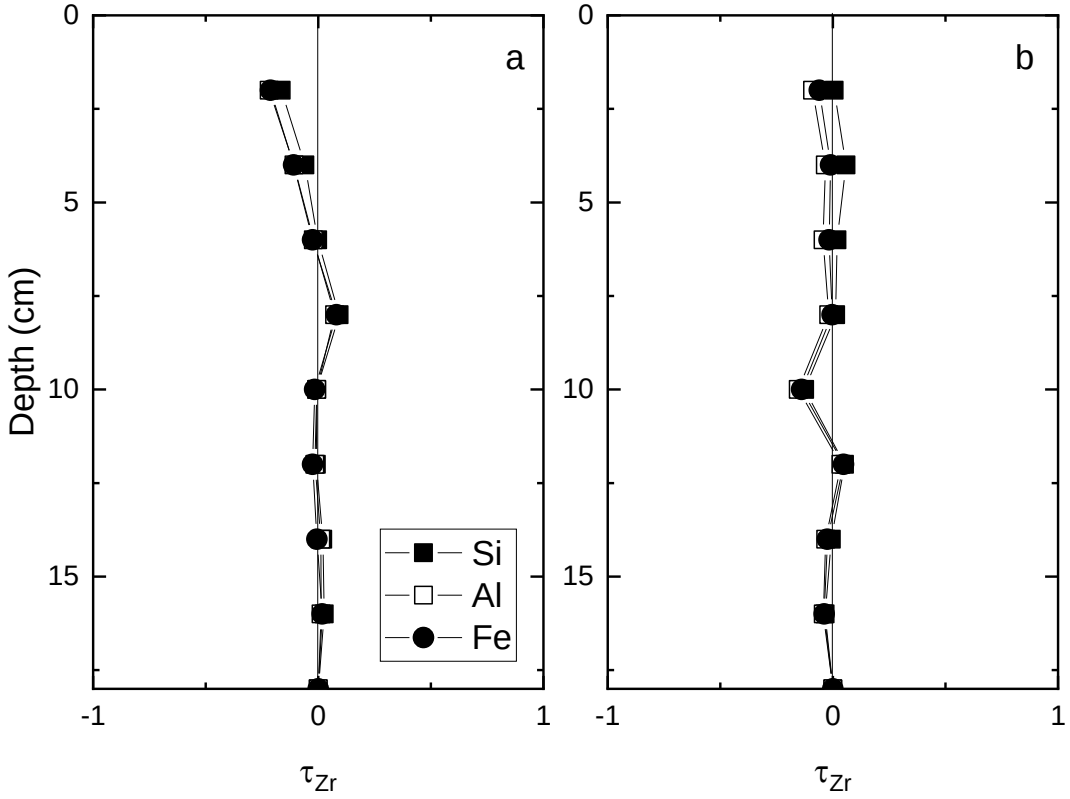


**Figure 3.15:** Mass transfer profiles analysis of the less mobile elements Si, Al and Fe in the bottom slopes of the forest in Tianlong watershed a) TL1-2 b) TL1. Samples were collected from soil pits.

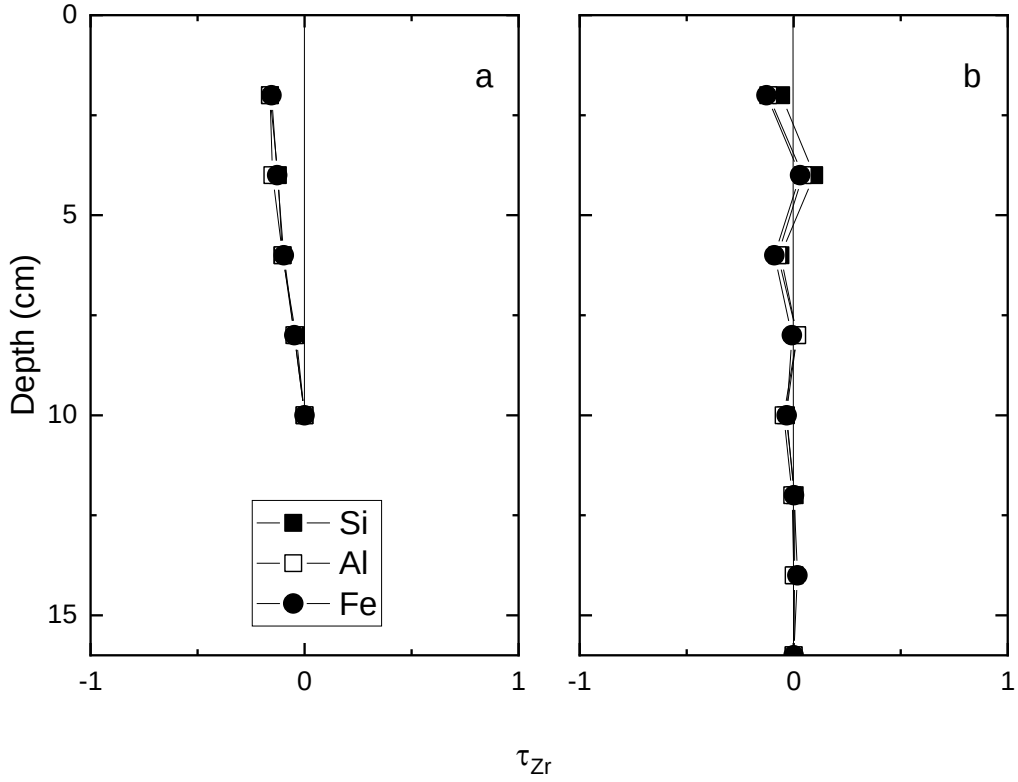


**Figure 3.16:** Mass transfer profiles analysis of the less mobile elements Si, Al and Fe in the middle slopes of the forest in Tianlong watershed a) TL2 b) TL3. Samples were collected from soil pits.

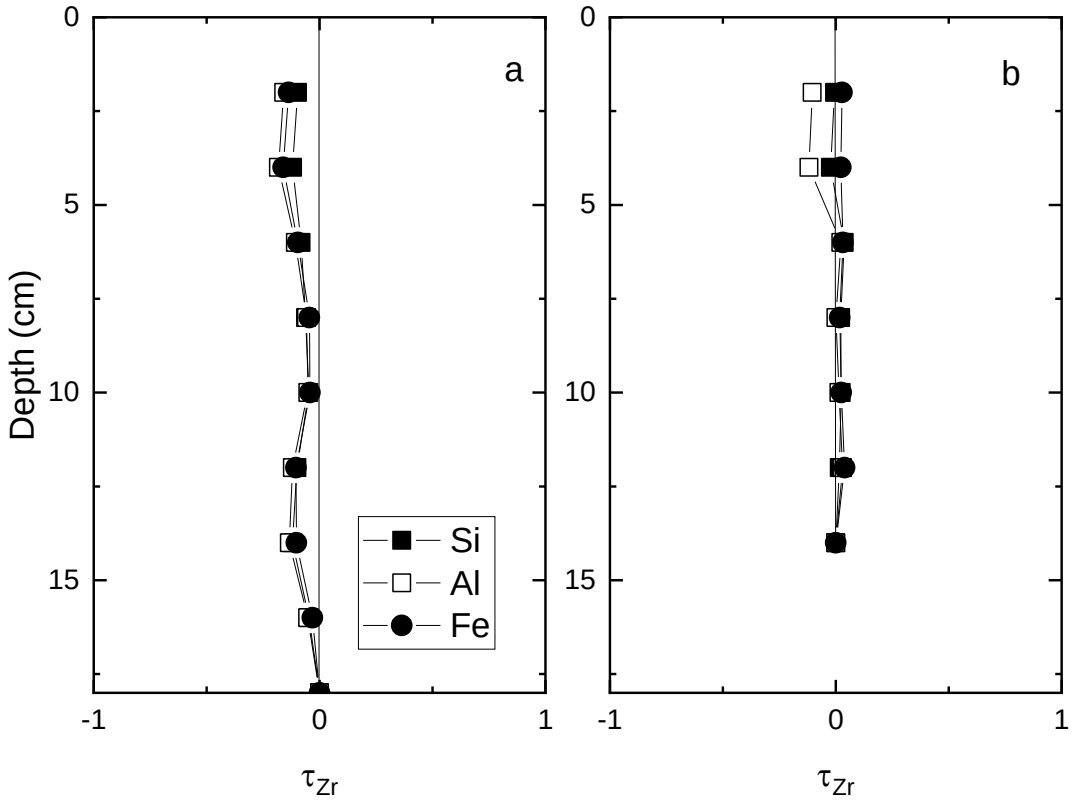


**Figure 3.17:** Mass transfer profiles analysis of the less mobile elements Si, Al and Fe in the top slopes of the forest in Tianlong watershed a) TL3-4 b) TL4. Samples were collected from soil pits.

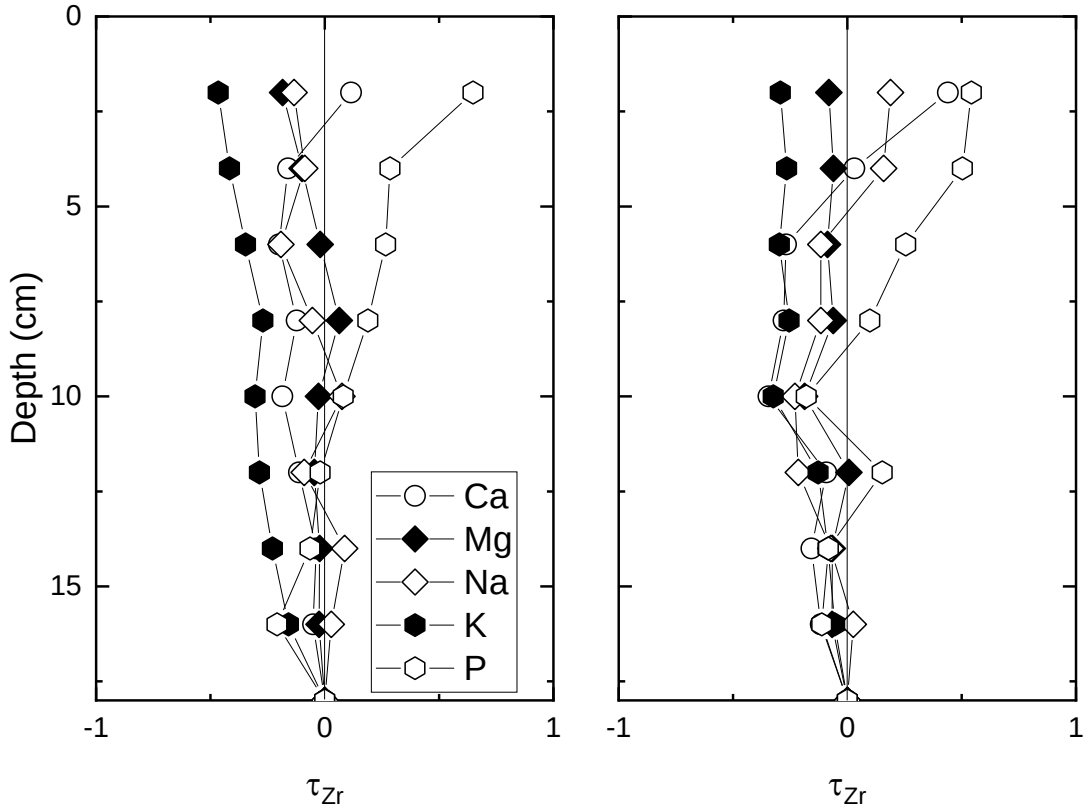


**Figure 3.18:** Mass transfer profiles analysis of the mobile elements Ca, Mg, Na, K and P in the bottom slopes of the forest in Tianlong watershed a) TL1-2 b) TL1. Samples were collected from soil pits.

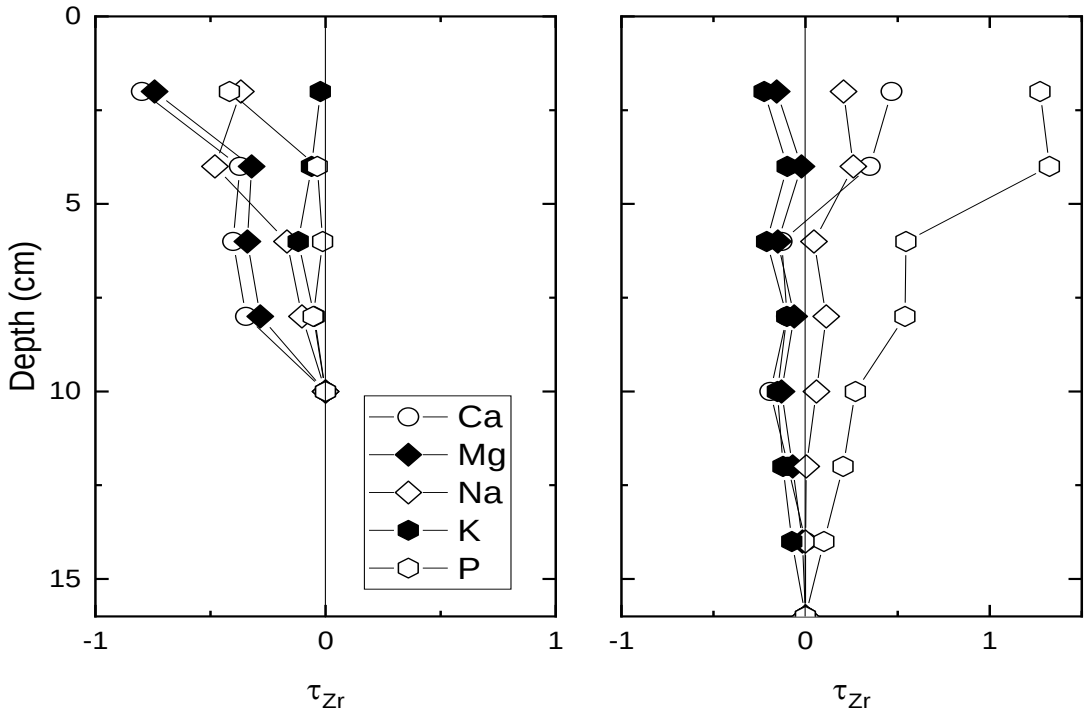


**Figure 3.19:** Mass transfer profiles analysis of the mobile elements Ca, Mg, Na, K and P in the middle slopes of the forest in Tianlong watershed a) TL2 b) TL3. Samples were collected from soil pits.

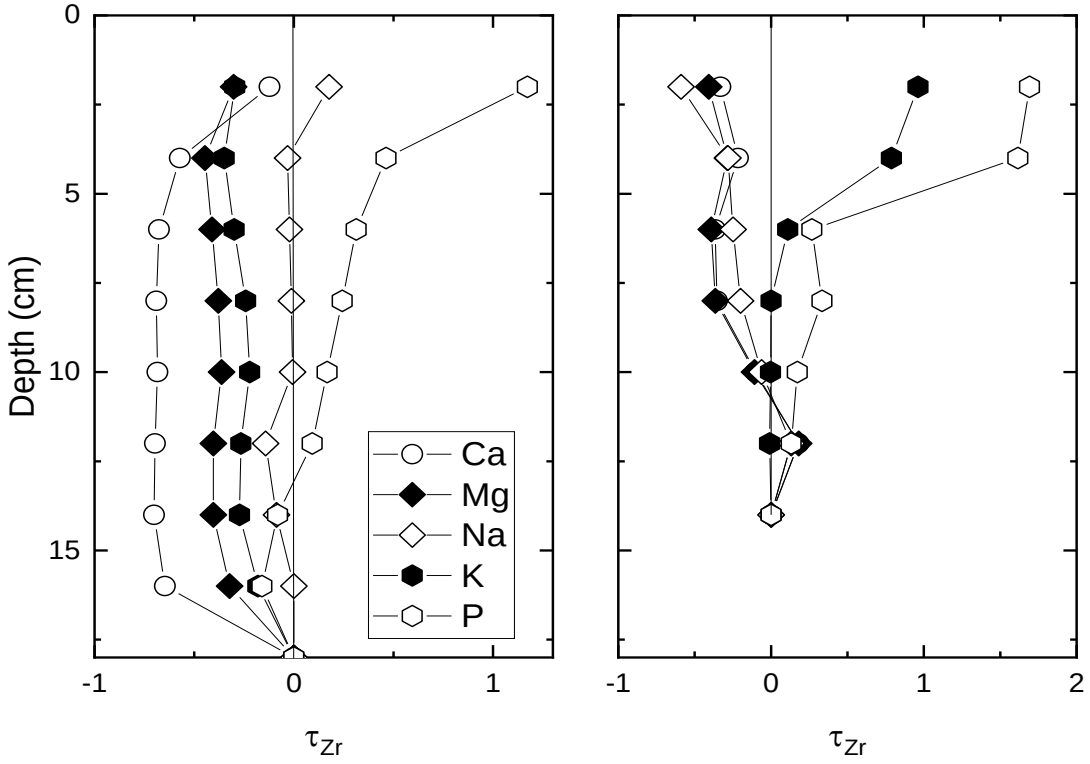


**Figure 3.20:** Mass transfer profiles analysis of the mobile elements Ca, Mg, Na, K and P in the middle slopes of the forest in Tianlong watershed a) TL3-4 b) TL4. Samples were collected from soil pits.

## 3.3 Discussion

### 3.3.1 Bedrock Chemistry and Mineralogy

Abundance of mineral nutrient elements in the soils in carbonate environments is reported to result from the enrichment of the soil matrix after the dissolution of dominant minerals (calcite and dolomite) in the bedrock or through atmospheric (aeolian) dust deposition from nearby or distant places (Avila et al., 1997; Durn, 2003; Durn et al., 1999; Herwitz and Muhs, 1995; Muhs and Budahn, 2009; Muhs et al., 2007). In Guizhou, SEM images of the bedrock (Figs. 3.1) confirm the presence of carbonate (calcite and dolomite) minerals, aluminosilicates such as quartz, kaolinite, orthoclase and illite; and other metal hydr(oxides) and sulphides such as accessory hematite and pyrite. The SEM images (Figs 3.1) and the Mg/Ca ratios (Table 3.2) confirm the predominance of the carbonate minerals in the bedrock, consistent with a regional geological map by Ma (2002) and earlier studies of the regional bedrock (Chen and Bi, 2011; Jiang et al., 2014; Moore et al., 2017; Wang et al., 2004b). Ratios of Mg/Ca in the bulk chemistry of the bedrock (Table 3.2) further confirm that calcite is dominant in the bedrock-forming mineral throughout the Chenqi watershed. The predominance of calcite in the bedrock corresponds to low porosity in the (qualitatively observed in SEM images), consistent with a preliminary study (Moore et al., 2017) that reported 1.1 ± 0.8% porosity in calcite-dominated Chenqi bedrock and Wang et al. (2004b) which reported average porosities of 2% for limestone and 4% for dolostone in the region.

Low Mg/Ca ratios in some sites, however, may be as a result of faster dolomite dissolution rather than calcite dominance in the bedrock. The more even distribution of rock fragmentation in the bedrock (observed in the SEM images, Fig. 3.1 and reported by Wang et al. (2004b)), in the dolomite dominated sites forms small crystal interstices and small cavities; provides suitable condition for water retention and promotes higher rock-mineral contact time and higher dolomite dissolution than calcite. Minerals found in recrystallized dolomites have large grain sizes with well-developed porosity which led to the development of even fractures along the crystal interstices. This even distribution of fractures promotes even dissolution and longer

mineral-water contact time in dolomite. Low abundance of Na (Table 3.1) in the bedrock indicates the absence of Na-bearing minerals such as plagioclase or hornblende. Although the abundance of K in the bedrock is also low, its presence indicates K-bearing minerals such as orthoclase and illite as confirmed by the SEM data (Figs 3.1 and 3.2).

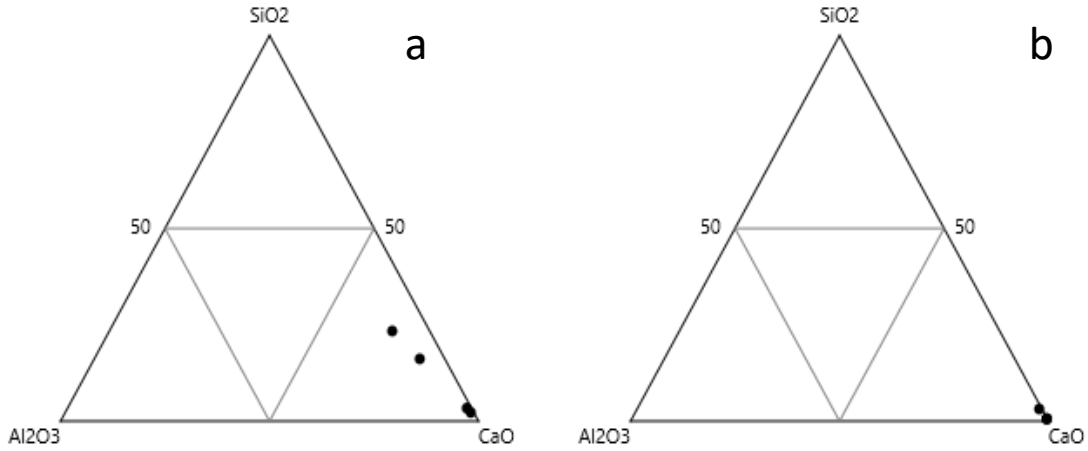


**Figure 3.21:** $SiO_2$-$Al_2O_3$-CaO (SAC) ternary plot of the bedrock a) CQ7 from the bottom slope and b) CQ37 from the middle slope of the sloping farmlands. There are no bedrock samples from the top slope of the sloping farmlands.

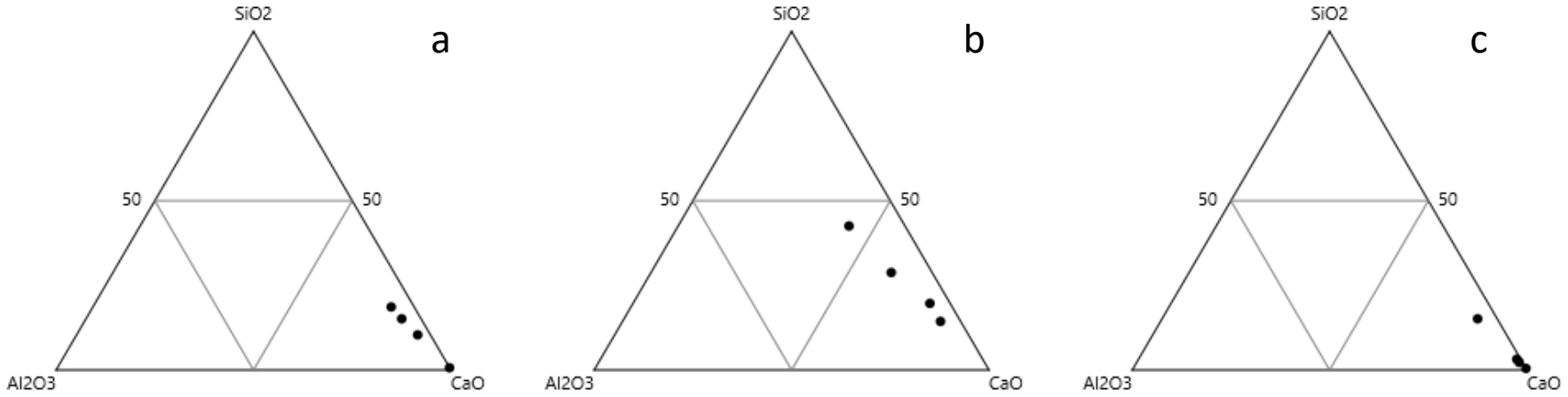


**Figure 3.22:** $SiO_2$-$Al_2O_3$-CaO (SAC) ternary plot of the bedrock a) CQ38 from the bottom slope, b) CQ1 from the middle slope and c) CQ54 from the top slope of the abandoned farmlands.

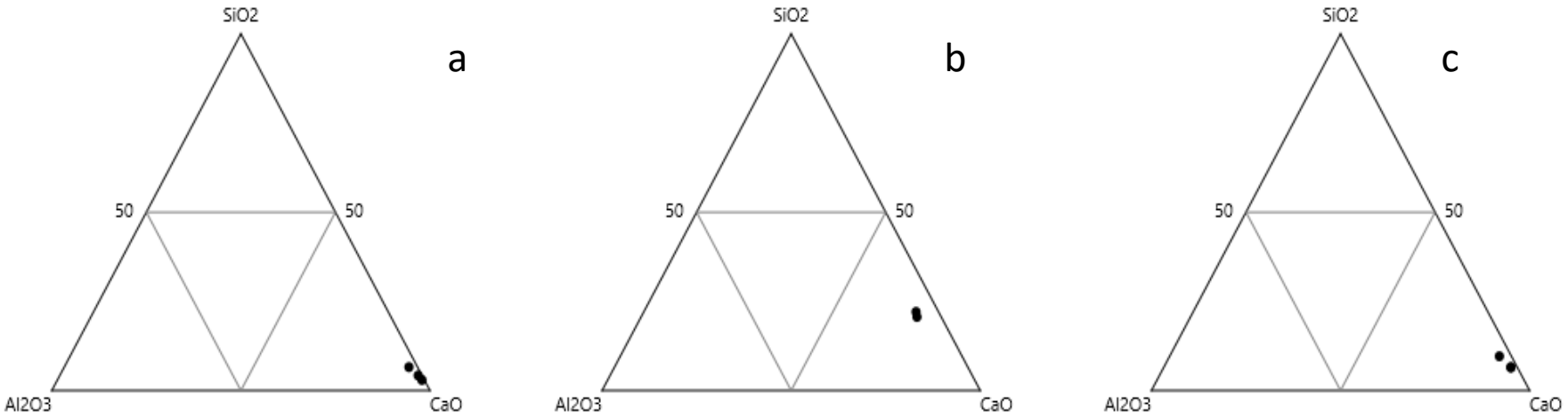


**Figure 3.23:** $SiO_2$-$Al_2O_3$-CaO (SAC) ternary plot of the bedrock a) CQ16 from the bottom slope, b) CQ17 from the middle slope and c) CQ2 from the top slope of the secondary forest.

Abundances of Si and Al in the bedrock (Table 3.1) also confirms the presence of clay minerals (aluminosilicates) identified by the SEM (Figs. 3.1). The relatively high $SiO_2/Al_2O_3$ ratios (Table 3.2) are consistent with higher quartz, relative to other aluminosilicates such as illite and kaolinite which also confirms the SEM observations that aside calcite and dolomite, quartz is the most widely distributed non-carbonate mineral in the bedrock. This interpretation is supported by the Si-Al-Ca ternary plots (Figs 3.21 – 3.23) of selected sites in different land uses and slope positions that show conservation of $SiO_2$ in the bedrock in relation to other aluminosilicates.

Fe-bearing minerals in carbonate soils exist in the form of hematite, goethite and/or pyrite (Muhs and Budahn, 2009; Zhu et al., 2008). In Guizhou, the SEM data (Figs 3.1) confirms that the Fe-bearing minerals are hematite and pyrite. However, hematite is more widely distributed than pyrite in the bedrock (Fig. 3.1) consistent with soil provenance studies on carbonate soils in the Caribbean Islands (Foos, 1991; Muhs et al., 1987), the USA (Arthur Bettis, 2003; Muhs et al., 2008; Muhs et al., 2007) and Mediterranean regions such as Spain, Italy and Greece (Avila et al., 1997; Durn, 2003; Moraetis et al., 2015; Muhs et al., 2010). On the other hand, abundances of P in the bedrock (Table 3.1) may result from percolation and possible mineralisation of P from the surface due to aeolian deposition of P from the nearby mines. Yang et al. (2015) and Tang et al. (2016) established that dust from the nearby mines contribute to the local soil provenance in Guizhou. The lack of trend in the distributions and abundances of nutrient elements with respect to land uses and slope positions suggests that P percolates deep into the soil to the bedrock instead of moving downslope. Tang et al. (2016) reported that local Mn and P mining activities are sources of significant P and Mn (Moore et al., 2017) enrichment in Guizhou. Furthermore, local farmers were observed to liberally apply chemical fertiliser on the cultivated plots in Chenqi (Pers. Comm. H.L. Buss). If the fertiliser application observed is representative of the long term, fertiliser input may account for a significant proportion of P in the Chenqi soils and shallow bedrock.

### 3.3.2 Sources and Mobilisation of Mineral Nutrient Elements in the Soil

#### 3.3.2.1 Mineral Nutrients in Chenqi

In Chenqi, the bedrock (Table 3.1) and soil (Table 3.3) bulk chemistry indicate the dissolution of calcite and dolomite from the bedrock and the depletion of these minerals from the soil matrix, consistent with studies on the formation of soils in carbonate environments (Durn, 2003; Durn et al., 1999; Muhs and Budahn, 2009; Muhs et al., 2007; Pye, 1992). The different land uses – sloping farmlands, abandoned farmlands and secondary forest – and slope positions (Chapter 2.5) in Chenqi, show no particular trend in the mass mobilisation of Ca and Mg, elements that are mobile and easily leached out of weathering environments (Brantley et al., 2007; Chapela Lara et al., 2018; Dere et al., 2016; Zhu et al., 2008). The partial depletion and conservation of these elements (Figs 3.6, 3.7 and 3.8) in the soil is consistent with *in situ* weathering of the carbonate minerals and indicates that the bedrock contributes to the abundance of these elements (Ca and Mg) in the soil. However, in some of the sites (e.g. S3, bottom slope of the secondary forest, Fig. 3.8) enrichment of some elements, especially Ca, suggests an external source, most likely aeolian dust deposition, contributing to the Ca budget in Chenqi.

Atmospheric dust deposition likely contributes the majority of the Na found in the soils as the Na content of the bedrock is low (Table 3.1) indicating absence of Na-conatining minerals. An atmospheric Na source is consistent with previous work by Muhs et al. (2007) who studied the provenance of carbonate soils in Barbados and western Florida. Similarly, although the abundances of K are low in the soil (but generally higher than Na), its presence indicates the presence of K-bearing minerals such as orthoclase and illite identified in the bedrock (Fig. 3.1) suggesting that the bedrock is likely the major contributor to the abundance of K in the soil. Durn (2003), also reported that clay minerals such as illite and orthoclase in carbonate bedrocks of Croatia contribute to the abundances of K in the soil. It is also likely that K is contributed through fertiliser addition to the soil especially in the sloping farmlands and the (recently) abandoned farmlands. Although, according to Aciego et al. (2017),

Muhs et al. (2008) and Kurtz et al. (2001) atmospheric dust deposition contributes to K abundances in carbonate soils, the conservation (mostly) of K shown by mass transfer analysis of Chenqi soils (Figs 3.6, 3.7 and 3.8) indicates a likely conservation of clay minerals in the soil consistent with the findings of a study Hahm et al. (2014) on Sierra Nevadan batholiths and that bedrock contributes to the K budget in the Chenqi soils. It is also likely the enrichment of K is likely contributed to the Chenqi soil through fertiliser addition.

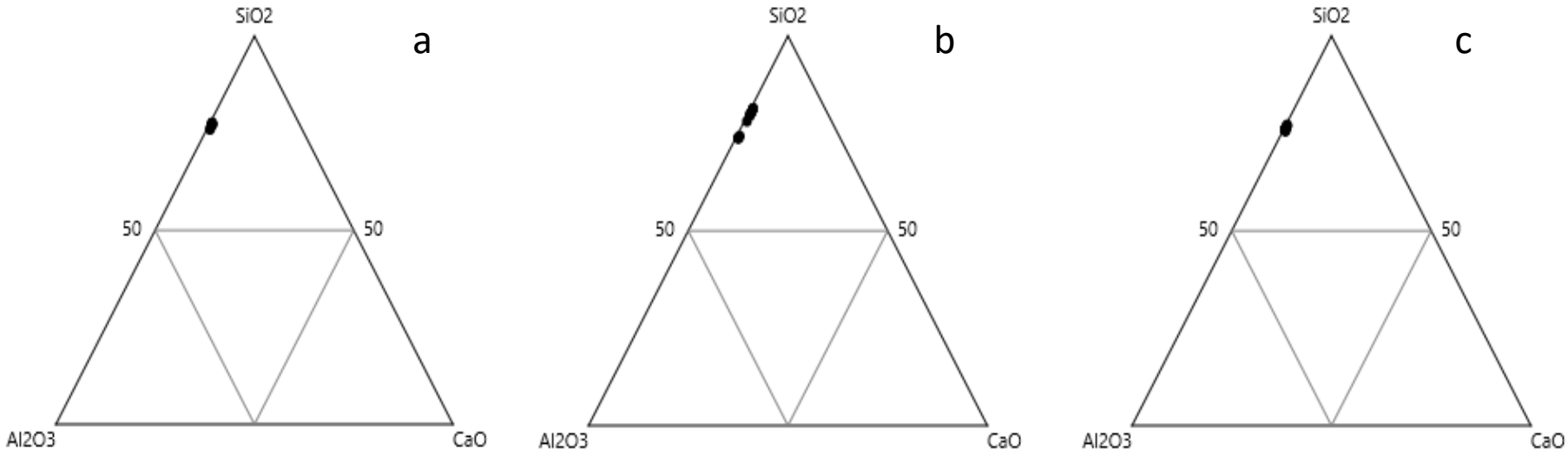


**Figure 3.24:** $SiO_2$-$Al_2O_3$-CaO (SAC) ternary plot of the bedrock a) RP1 30 from the bottom slope, b) RP1 71 from the middle slope and c) RP1 96 from the bottom slope of the sloping farmlands in Chenjiazhai.

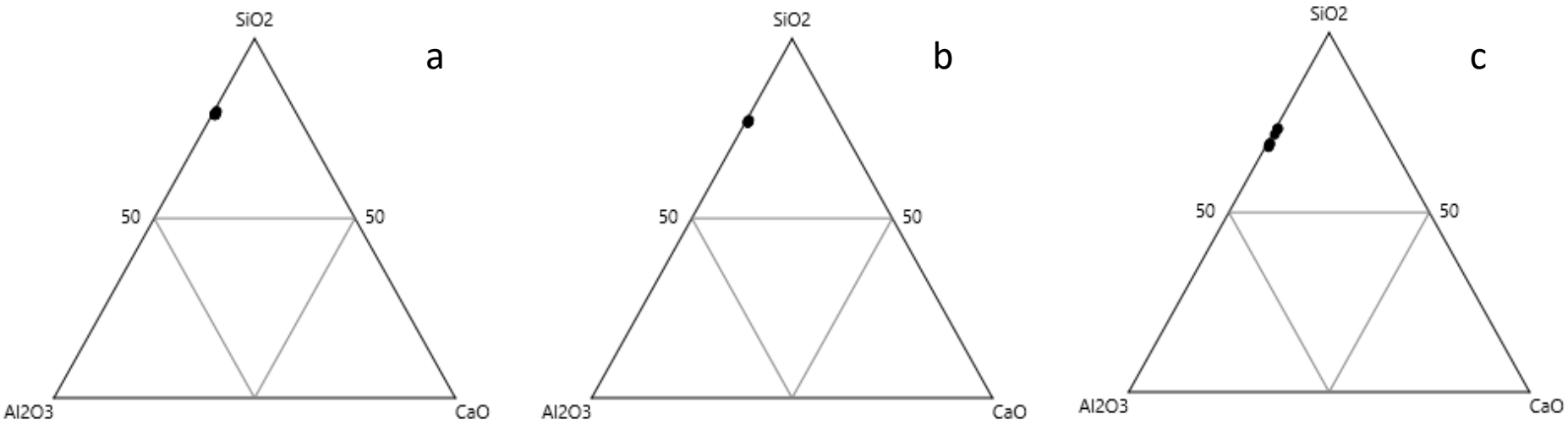


**Figure 3.25:** $SiO_2$-$Al_2O_3$-CaO (SAC) ternary plot of the bedrock a) RP1 30 from the middle slope, b) RP1 71 from the middle slope and c) RP1 96 from the middle slope of the sloping farmlands in Chenjiazhai

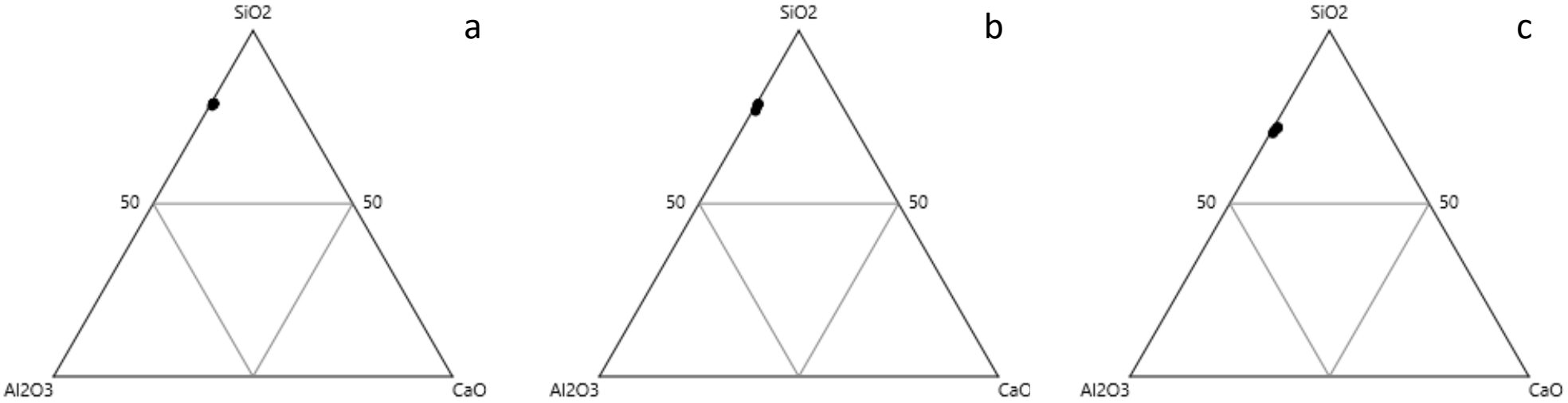


**Figure 3.26:** $SiO_2$-$Al_2O_3$-CaO (SAC) ternary plot of the bedrock a) RP1 30 from the top slope, b) RP1 71 from the middle slope and c) RP1 96 from the top slope of the sloping farmlands in Chenjiazhai

To further understand the abundance of K (and, by extension, P) in the soils of Chenqi due to fertiliser addition, K/Rb ratios (Tables 3.2, 3.4, 3.6 and 3.8) in both the bedrock and the soils were analysed. Similar chemistry between K and Rb such as their ability to compete for the same carriers in plant uptake and their fixation of cavities in clay minerals was used by Drobner and Tyler (1998) to justify the use of Rb as a tracer for K in rocks, soils and plants. Given that Rb is not a nutrient element and is more tightly bound to mineral surfaces than K (Peltola et al., 2008), it is expected that its abundance in the soil to be higher than the bedrock resulting from the weathering of source minerals and/or recycling of K through plant litter (Rb uptake by plants is largely dependent on the abundance of K in the soil). Both K and Rb pools in the soil are hosted by minerals such as muscovite, biotite, rubicline and K-feldspars (Peltola et al., 2008). However, in the bedrock in Chenqi, only K-feldspar (orthoclase) was identified through the SEM (Fig. 3.1). The K/Rb ratios in the soils of Chenqi (Table 3.4) are largely similar with the variations mostly within uncertainty and show no trend between and within land uses and slope positions. Also, the bedrock ratios (Table 3.2) are similar to those in the soil (Tables 3.2, 3.4, 3.6 and 3.8), also showing no trend with respect to land use and slope position. This lack of difference, coupled with high $(SiO_2+Al_2O_3)/(CaO+MgO)$ ratios, which is a characteristic of soils formed on carbonate rocks composed of mainly quartz and aluminosilicates (illite, kaolinite and orthoclase) in the Chenqi soil explain the abundance of K in the soil as being contributed by the bedrock (Avila et al., 1997; Foos, 1991; Hahm et al., 2014). The high Si indicates that some (alumino)silicates were retained (Figs. 3.3, 3.4 and 3.5) during soil formation (Foos, 1991; Muhs et al., 1987), and are likely contributing to the K content of the soil. Therefore, the K mass transfer profiles (Figs 3.6 – 3.8), the K/Rb ratios (Table 3.4) and $(SiO_2+Al_2O_3)/(CaO+MgO)$ (Table 3.4) suggest that fertiliser application has no significant role in the bulk abundance of K and P in the soil. It is possible that P from fertiliser is not retained long enough in the soil and is rapidly leached out, consistent with the findings of Porder et al. (2007b), or percolated directly into the bedrock and mineralised by forming Ca-phosphates as shown by the abundance of P in the bedrock (Table 3.1). This interpretation agrees with the findings of Jiang et al. (2020) who reported abundance of P in soils with high Ca content.

Higher abundances of Si in the soil (Table 3.3) than in the bedrock (Table 3.1) is also consistent with *in situ* weathering and dissolution of carbonate minerals (Dere et al., 2016; Moore et al., 2017) leaving the soil matrix enriched with quartz and aluminosilicates (here mostly kaolinite and illite, with some orthoclase), which suggests that the Si content in the soil is mostly contributed by the bedrock. Higher Si content in Chenqi soils than other carbonate soils of, for example, Jamaica, Barbados, the Bahamas, Florida, Croatia, and Spain (Durn, 2003; Durn et al., 1999; Muhs and Budahn, 2009; Muhs et al., 2007) suggests that the carbonate rocks of Guizhou contain more non-carbonate 'impurities' than reported in the other carbonate environments mentioned earlier. While Muhs and Budahn (2009) and Foos (1991) reported the bedrock of Jamaica, the Bahamas and the neighbouring Caribbean islands being up to 96% pure carbonate, the carbonate minerals abundance in the bedrock (Table 3.5), including marls (Moore et al., 2017), in Chenqi shows that there is a significant quantity of non-carbonate minerals in Guizhou compared to other carbonate environments (such as Jamaica and the USA) which makes the bedrock a major contributor to the abundance of mineral nutrient elements associated with these minerals in the soil. This interpretation is consistent with the findings of Wang et al. (2004b) who reported that bedrock composition in Guizhou reflects regional soil composition and depth. Similarly, Al abundances (Table 3.3), which reflect the conservation of Al in the soil (Figs. 3.3, 3.4 and 3.5), with no trend in terms of land use or slope position, indicate that the clay minerals in the soil are the main host of Al in the soil.

As with Si and Al, abundances of Fe are higher in the soil (Table 3.4) than in the bedrock (Table 3.1) and mass transfer profiles reveal conservation of Fe (Figs 3.3 – 3.5), which indicate that Fe is contributed to the soil by the bedrock. The SEM images and EDS spectra showed that Fe in the bedrock of Chenqi is mainly hosted by hematite, consistent with other studies on the mineralogy of carbonate environments in the Caribbean islands, Croatia, Spain and Italy (Avila et al., 1997; Boero et al., 1992; Boero and Schwertmann, 1989; Foos, 1991; Muhs et al., 2010).

In contrast to the conserved elements Al, Si, and Fe, P abundances (Table 3.3) in the soil do not appear to be derived from the bedrock. The P abundances show similarity

with the abundances of the same element in shale soils (Dere et al., 2016) and other carbonate soils especially in Mallorca, Spain (Muhs et al., 2010) which was attributed to aeolian deposition. The enrichment of P in Chenqi soils (often above 100%, Figs 3.6, 3.7 and 3.8) as shown by the mass transfer, reveals no trend in terms of land uses and slope positions, also indicating an external source for P in the soil (Moore et al., 2017; Tang et al., 2016; Yang et al., 2015). Tang et al. (2016) and Yang et al. (2015) reported that neighbouring mines are major contributors to aeolian dust and P enrichments in the soils of Guizhou. It is also possible that P is enriched in the soil through biolifting (Bullen and Chadwick, 2015), a process through which plant roots scavenge for nutrients at depth and concentrate them on the surface or fertiliser application. However, the lack of trend in P abundances in the soil with respect to land use as well as absence of legacy P content due to past agricultural practices (Hussey, 2018) suggests that fertiliser application is not a contributor to the P content in the soil.

#### 3.3.2.2 Mineral Nutrients in Chenjiazhai

Chenjiazhai is a recovering catchment abandoned for a longer time than Chenqi (Chapter 2.4.2). The sloping farmlands in this recovering catchment have lower Ca and Mg abundances (Table 3.5) in the soil than Chenqi. As with Chenqi, the Ca and Mg in the soil is likely to have derived from the bedrock due to the incomplete dissolution of the dominant calcite and dolomite as shown by the mass transfer profiles of Ca and Mg in the soil (Fig. 3.12), which indicate *in situ* weathering. In carbonate environments, leaching of Ca and Mg is largely dependent on the time and the intensity of the weathering regime (Zhu et al., 2008) and incomplete mass transfer profiles are an indicator that the elements in consideration are at least partially retained in the soil or the bedrock (Chapela Lara et al., 2018). Also, as with Chenqi, the abundance of Na (Table 3.7) in the soils of Chenjiazhai indicates lack of Na-bearing minerals which suggests that the Na in the soil is likely contributed by aeolian deposition, consistent with the findings of Muhs and Budahn (2009) which reported atmospheric dust as the source of Na in the carbonate soils of Jamaica, the Bahamas and western Florida in the United States (Muhs et al., 2007). On the other hand, abundance of K (Table 3.5) in Chenjiazhai is mostly lower than Chenqi (Table

3.3) which, while indicating the presence of clay minerals such as illite and orthoclase, could indicate that the bedrock in Chenjiazhai has lower aluminosilicates than Chenqi**.** The bedrock in Chenjiazhai has not been analysed in this study and as a result, The soil in Chenjiazhai also has high ($SiO_2$+$Al_2O_3$)/(CaO+MgO) ratios similar to the soil in Chenqi suggesting clay minerals production in the soil are the likely host of K in the soil of Chenjiazhai. Hahm et al. (2014) reported increases in the bedrock and soil Si abundances of the Sierra Nevada batholith as evidence of increasing quartz, K-feldspar, and other clay minerals contents in the soil. This interpretation is supported by the mass transfer profiles (Figs. 3.12, 3.13 and 3.14) of the soil in Chenjiazhai which show that K is mostly conserved in the soil. As with Chenqi, the high $SiO_2/Al_2O_3$ ratios and conservative mass transfer profiles of Si (Figs 3.9 – 3.11) show that Si is not being leached out and that the clay minerals are not being weathered. Foos (1991) reported that loss of Si in the carbonate soils in the Bahamas is driven largely by the weathering of clay minerals to goethite and results in low $SiO_2/Al_2O_3$ ratios. While the abundances of Fe in the soils of Chenjiazhai are higher than those in the soil of Chenqi (Tables 3.3 and 3.5), the largely conservative behaviour of Fe in the soil of Chenjiazhai (Figs 3.9 – 3.11) suggests that bedrock is the major source of Fe to the soil, consistent with the findings of Durn et al. (1999) who analysed the mineralogy of the terra rossa in the Mediterranean region.

The impact of fertiliser addition to the soil could not be established in Chenjiazhai. The similar abundances of both K and Rb (Table 3.6) in the soil suggests that both elements are contributed to the soil from the bedrock. It is also likely that any fertiliser-derived K may have been leached out of the soil. Fertiliser applications were reported (Chaudhuri et al., 2007) to contribute about 7% of global K export to the rivers. However, the contribution of carbonate bedrock weathering to the global K export to the rivers is unknown and I interpret the similarity in the abundance of K and Rb in the soil of Chenjiazhai to suggest bedrock influence in K abundance.

Abundance of P in the soil was interpreted as having been transported from the upper slopes (where P revealed slight to moderate enrichment) or enriched at the surface by biolifting wherein plants scavenge for P from depth and concentrate it to the surface. Biolifting was established as one of the processes through which

enrichments of P in topsoil of montane forests were observed (Uhliq and Blanckenburg, 2020). It is also likely that calcite content in the soil controls the P abundance in the soil by forming a less soluble Ca-phosphates, consistent with the findings of Jiang et al. (2020) who reported calcite influence in P abundance in karst soils. Although K/Rb ratios of ≈ 1 were interpreted as lack of fertiliser-derived K in the soil of Chenjiazhai, enrichment of P in the soil is likely contributed by fertiliser, thereby suggesting that K additions to the soil from fertiliser and/or decayed plant litter was removed from the soil through leaching, consistent with the findings of Chaudhuri et al. (2007) who reported loss of K from the decomposition of litterfalls in soils. On the other hand, P enrichment in the soil suggests that P is likely to have been contributed to the soil through aeolian dust deposition. A study of dust in a town about 140 km away from Chenqi and Chenjiazhai confirms that local P mining was responsible for the elevation of P in the soil (Yang et al., 2015).

#### 3.3.2.3 Mineral Nutrients in Tianlong

In the pristine forest at Tianlong, the CaO+MgO sums (Tables 3.5, 3.6 and 3.8) are like those and of Chenqi but higher than Chenjiazhai except for sites TL2 and TL4 in the middle and the top slopes, respectively which showed considerably higher abundances of Ca and Mg than the other sites in the three catchments. Therefore, Chenjiazhai likely has lower carbonate mineral content in the soils than Tianlong and Chenqi. However, the mass transfer analyses of both Ca and Mg in the soil of Tianlong largely showed partial depletion of these elements consistent with *in situ* dissolution of carbonate minerals (Dere et al., 2016; Jin et al., 2010b; Moore et al., 2017) suggesting that these mineral elements were contributed to the soil from the bedrock.

As with Chenqi and Chenjiazhai, the mass transfer analyses of Si, Al, and Fe in Tianlong soils (Fig 3.15 – 3.17) indicate conservation in the soil from the bedrock while Na, similar in abundance (Table 3.7) to both Chenqi and Chenjiazhai, is likely contributed from aeolian dust deposition. On the other hand, K abundances are similar to Chenjiazhai than Chenqi and shows conservation or slight depletion in mass transfer profiles (Fig. 3.18, 3.19 and 3.20), which indicates retention of most of

the K in the soil matrix (Jin et al., 2010b; Muhs et al., 2010) after weathering from the bedrock . However, the abundances of P, largely enriched in the soil (Fig. 3.18, 3.19 and 3.20), are consistent with the amounts deposited from aeolian dust (Garrett and Lalor, 2005; Muhs et al., 2007) in Caribbean carbonate soils suggesting that P in Tianlong soils is also contributed by aeolian deposition.

Absence and/or low abundances of primary soil forming minerals such as mica and feldspars in carbonate soils (Muhs and Budahn, 2009) in the bedrock in Guizhou is consistent with other carbonate soils in the Caribbean islands (Muhs and Budahn, 2009; Muhs et al., 2007), Croatia (Durn, 2003; Durn et al., 1999) and Spain (Muhs et al., 2010). Therefore, presence of the elements such as Na and K hosted by these minerals in the soils of the three catchments is commonly attributed to atmospheric dust deposition. However, K is higher in abundance in the soils of the three catchments than Na due to the presence of K-bearing minerals such as illite and orthoclase, identified by the SEM, in the bedrock and the soil which suggests that in addition to the aeolian deposition, bedrock contributes to the abundance of the nutrient elements in the soil. While fertiliser application potentially contributes to the abundance of K and P in the soil especially in the sloping farmlands, we have seen no evidence of fertiliser contributing to the abundance of these elements especially given that there is no trend in the elemental abundance in the different land uses and slope positions and because K exhibits mass transfer profiles characteristic of *in situ* weathering of bedrock. However, P is mostly added to the soil through aeolian deposition and, likely, vegetation cycling where plants absorb the element from the soil and then recycle it to the soil through litterfall and throughfall (Muhs et al., 2008; Uhlig et al., 2017). In all the three catchments, the bedrock as well as atmospheric dust deposition are the major the sources of mineral nutrient elements in the soils.

### 3.3.3 Lithological Control on Weathering and Mineral Nutrient Production in S-CZO

Elements from primary minerals in soil profiles are either removed through leaching or retained in solid phases as weathering advances (Chapela Lara et al., 2018). As

most of the mass transfer profiles (Figs 3.3 – 3.20) in all the three catchments Chenqi, Chenjiazhai and Tianlong, are incompletely developed, the weathering front, defined by Buss et al. (2017), as the zone where the weathering reaction occurs, extended from depth (deepest samples in this study) to the surface. In Guizhou, mobilisation of mobile and less mobile elements in the soil in all the three catchments is an indicator of considerable weathering of the bedrock over time and supported my hypothesis that the mineral nutrient production in Guizhou, in addition to other processes such as aeolian deposition), is dependent on the abundances of the silicate and other metal (hydr)oxide (non-carbonate) mineral 'impurities' in the bedrock, consistent with studies on soil provenance on carbonate soils in Jamaica, USA, and the Mediterranean region (Caquineau, 2002; Durn, 2003; Durn et al., 1999; Garrett and Lalor, 2005; Muhs and Budahn, 2009; Muhs et al., 2008). Although Muhs and Budahn (2009) reported that soils overlying the carbonate bedrock of northern Jamaica are formed largely as a result of aeolian dust deposition, rather than from bedrock weathering.

The abundance of the non-carbonate minerals (Tables 3.3, 3.5 3.7) in the soil showed that the bedrock has sufficient abundance of these minerals (retained after dissolution of carbonate minerals) in the bedrock to support mineral nutrient production and soil formation. Weathering of carbonate minerals has been described as a profile initiation reaction that drives the disaggregation of rocks into soil as well as the deepest weathering reactions in various lithologies (Brantley et al., 2013; Dere et al., 2016; Jin et al., 2010a). *In situ* dissolution of calcite and dolomite in the bedrock leaves the soils of the three catchments enriched in the mineral nutrient elements found in the soils (Tables 3.3, 3.5 and 3.7). The abundance of Si in the soil in the three catchments as explained previously (Section 3.2.1) comes from the Si-bearing minerals identified in the bedrock and the soil such as illite, kaolinite, orthoclase and quartz, consistent with clay mineralogy as shown by Hahm et al. (2014) and Muhs and Budahn (2009). Hahm et al. (2014) posited that increase in Si abundances in the soil usually corresponds with increasing abundances of quartz and loss of feldspars and plagioclase. As we have not identified plagioclase or any other Na-bearing mineral in the bedrock, and as K is largely conserved in the soil, I then

attribute the increase in the Si abundance in the soil to the dissolution and removal of carbonate minerals from the soil and the concomitant enrichment of clay minerals across the catchments, which I interpret to be responsible for soil formation and the source of soil mineral nutrients.

The soils in the three catchments have high $SiO_2/Al_2O_3$ ratios (Tables 3.4, 3.6 and 3.8) which show no trend with respect to slope positions within land uses. The secondary forest in Chenqi (Table 3.4) has higher $SiO_2/Al_2O_3$ ratios than the pristine forest of Tianlong (Table 3.8), suggesting that the Si is likely being lost in the pristine forest due to clay mineral weathering, consistent with the findings of Hahm et al. (2014), or that the soil in Chenqi is younger than the soil in Tianlong. Muhs and Budahn (2009) reported that more extensive weathering in older carbonate soils in Jamaica leads to lower $SiO_2/Al_2O_3$ ratios than in younger soils.

The Si-Al-Ca ternary plots (Figs 3.21 – 3.26) showed that compared to the soil in the other catchments (especially the secondary forest of Chenqi), the Si abundance is lower in the soils of Tianlong, and I attribute this to either reduced anthropogenic activities in the Tianlong forest compared to the secondary forest in Chenqi or a more extensive weathering regime in Tianlong. Low Si in carbonate soils in the Bahamas has been reported by Foos (1991) to be driven by clay mineral weathering leading to low $SiO_2/Al_2O_3$ ratios in the soils. In the same vein, Muhs and Budahn (2009) also reported that loss of Si in the older carbonate soils in Jamaica is driven by clay mineral weathering and leads to the formation of gibbsite in the soils. Hahm et al. (2014) also attributed the loss of Si in the Sierran batholiths in the USA to the weathering of clay minerals in the soil.

In addition to low Si abundances in older carbonate soils of northern Jamaica, (Garrett and Lalor, 2005) reported that older carbonate soils reveal high Fe abundances (mostly in the form of hematite) in the soil largely due to loss of primary minerals (Birkeland, 1999). The Fe abundances in Jamaican carbonate soils (Muhs and Budahn, 2009) were attributed to hematite content in the soil. Although the SEM images of the bedrock (e.g., Fig. 3.1) in Chenqi and bulk chemistry (Tables 3.3, 3.5 and 3.7) confirm the presence of Fe-bearing minerals (pyrite and hematite in the case of Chenqi, Fig. 3.1, and Appendix 1A) as reported in soil providence studies

(Birkeland, 1999; Durn, 2003; Moraetis et al., 2015; Muhs and Budahn, 2009; Muhs et al., 2008) in different carbonate environments, hematite was more evenly distributed in the bedrock than pyrite which suggests that Fe in the soils of Chenqi, Chenjiazhai and Tianlong is largely hosted by hematite in the soil, consistent with the findings of Muhs and Budahn (2009). Although the bedrock does not contain many clay-forming primary minerals such as plagioclase, clay minerals were identified in the bedrock and there is high abundance of elements usually hosted by clay minerals such as Si and Al in the three catchments. Abundances of Fe in Chenjiazhai, which suggests that the soils in Chenjiazhai are younger and may have a less intense weathering regime than Chenqi and Tianlong, consistent with the findings of Muhs and Budahn (2009).

The relatively high $SiO_2/Al_2O_3$ ratios (Tables 3.4, 3.6 and 3.8), used by Muhs and Budahn (2009) to indicate the degree of weathering and high Si content in the soils of western Jamaica, suggests the influence of lithology on the production of mineral nutrients in the soil. Soils with high Si content are usually characterised as having high clay contents, which increases water retention capacity of the soil and thus, longer mineral-water interaction that results in the production of more nutrients in the soil through weathering. Jiang et al. (2020) established that high clay content in the soils of Guizhou results in high water holding capacity in the soil. This view is further reinforced by the higher $SiO_2/Al_2O_3$ ratios (Tables 3.4, 3.6 and 3.8) than similar ratios in the soils reported by Muhs and Budahn (2009) and Garrett and Lalor (2005) to be formed by aeolian deposition in western Jamaica indicating that the bedrock in Chenqi, Chenjiazhai and Tianlong has sufficient abundance of Si- and Al-bearing minerals to control the production of mineral nutrients in the soils which agrees with my hypothesis that non-carbonate minerals in the soils drive mineral nutrient production.

Apart from quartz, soil forming primary minerals were not observed in the bedrock (Fig. 3.1) and the soil, consistent with the mineralogy of carbonate soils in the Caribbean islands (Garrett and Lalor, 2005; Muhs et al., 2007) and the Mediterranean region (Durn, 2003; Muhs et al., 2010). The abundances of K and Al in the three catchments suggest that the soils reflect the clay mineralogy identified by

SEM (Figs 3.1 and 3.2) indicating that the presence of these nutrient elements in the soil is controlled by the bedrock lithology. The incomplete depletion of Ca and Mg (Figs 3.3, 3.7, 3.8; 3.15, 3.16, 3.17; 3.18, 3.19 and 3.20) in the soils of all the three catchments reflects the presence of calcite and dolomite in the soil which stems from incomplete dissolution of calcite and dolomite in the bedrock. Bedrock contribution to the abundance of Ca and Mg in carbonate soils has been reported in several soil provenance studies (Durn et al., 1999; Moraetis et al., 2015; Muhs et al., 2008). The SEM data also revealed near absence of P-containing minerals and the enrichment of P in the soil has been attributed to either biolifting or dust deposition. However, calcite content in the soil, confirmed by the partial conservation of Ca and Mg the soil, may likely control P abundance by producing Ca-phosphates which reduce P solubility. Phosphorous abundance in Guizhou was established to be widespread in soils with high calcite content (Jiang et al., 2020).

## 3.4 Conclusions

In this Chapter, I investigated the mineral nutrient production in the three catchments of the S-CZO in the province of Guizhou in southwestern China. The findings have confirmed that production of the mineral nutrient elements in the soil are more reliant on the lithology of the bedrock than anthropogenic perturbation. I found that bedrock plays important role in the abundance of these mineral nutrient elements in addition to aeolian dust deposition. I established that weathering of the dominant minerals (calcite and dolomite) in the catchments is the major process through which these mineral elements are enriched in the soil matrix. As reported by Muhs and Budahn (2009), Hahm et al. (2014) and Jiang et al. (2020), presence of clay minerals in the soil is the primary control in the retention of these mineral nutrient elements in the soil. I have also not established any effect of land use and slope positions in the production of the mineral elements.

# Chapter 4

# Mechanism of Mineral Weathering and Mass Transfer in the Koiliaris Critical Zone Observatory (K-CZO)

**Author contribution declaration:** Parts of this work have been presented at Goldschmidt (Lawal et al, 2020; Appendix B) and sections of the work will be presented at the OSZCAR-TERENO conference (Lawal et al., 2021; Appendix C). Rock cutting and thin sections were conducted by Aminu Lawal under the guidance of Evangelos Mouchos. SEM analysis was also conducted by ALS Geochemistry Loughrea.

## 4.1 Introduction

In Chapter 3, the role of lithology on mineral nutrient distribution, production, and retention in soils was investigated in the subtropical SPECTRA Critical Zone Observatory (S-CZO) in southwestern China. Silicate mineral 'impurities' in the dominantly carbonate bedrock, as well as aeolian dust deposition, were found to provide the matrix for soil formation and to control the production and distribution of mineral nutrient elements in the soil. This chapter extends that work to a Mediterranean environment, the Koiliaris Critical Zone Observatory (K-CZO) near Chania on the Island of Crete, to investigate the role of lithology on the production of mineral nutrients in the soil in the Mediterranean climate, with dry summers and wet winters, opposite that of S-CZO, which has wet summers and dry winters (Chapter 2.5.2).

A previous study on sediment provenance and soil development at five sites differing in land use, geomorphic positions, and lithology in the K-CZO found relatively young soils with soil development processes such as weathering and/or erosion primarily related to land use and geomorphic position (Moraetis et al., 2015). In the present chapter, two of their sites are investigated: K4 and K5, a manmade terrace growing olive trees and a mountainous site mainly used for grazing, respectively (Chapter 2.5.2). Moraetis et al. (2015) found that the soil at site K4 is older and developed partly from bedrock weathering while, at site K5, aeolian dust deposition exhibited greater control on soil development than bedrock weathering/lithology. Their study, however, did not examine the distribution and weathering of minerals in the bedrock, which may affect mineral nutrient production and distribution in the area. With this study, I seek to understand the relationship between mineral nutrient production in the soil and the distribution of mineral 'impurities' (non-carbonate minerals such as quartz, hematite, and mica) in the dominant carbonate (limestone and dolostone) bedrock. I hypothesize that the distribution of non-carbonate minerals in the soil and the bedrock controls the mineral nutrient production while climate variability (wet winters and dry summers) influences the abundances of mineral nutrient elements in the soil. Here, bulk elemental chemistry and SEM-EDS analysis (Sections 2.4.2-2.4.3) of bedrock at sites K4 and K5 are compared to the bulk

elemental chemistry and mass transfer (Chapter 2.5, Eqn 2.1) in the overlying soils. Although the deepest sample is not the parent material, in this study, the deepest sample is regarded as the parent material.

## 4.2 Results

### 4.2.1 Bedrock Mineralogy in the K-CZO

The area is composed of mainly carbonate bedrock with the karstic system of the island mainly comprising limestones and dolostones from the Mesozoic period and the calcaric marls of the Neogene formation (Papanikolaou and Vassilakis, 2010). The bedrock at site K4, as shown by our SEM results (Fig. 4.1) is composed of non-carbonate minerals such as illite, orthoclase, quartz, accessory hematite, pyrite, and amphibole in addition to the dominant calcite and dolomite. Hematite, and clay (mostly kaolinite and illite) are associated with pores and weathering veins (Fig. 4.1). The SEM images also confirm the predominance of carbonate minerals (calcite and dolomite) in the bedrock. As with S-CZO (Chapter 3.2.1) after calcite and dolomite, quartz is the most abundant and evenly distributed mineral (Tables 4.1 and 4.2) in the bedrocks of the two sites. Dolomite in the bedrock was visibly observed by SEM to be more porous than calcite, consistent with this study (Chapter 3) as well as the findings of Wang et al. (2004b) in a study in southwestern China.

Bedrock bulk chemistry at site K4 (Table 4.1) revealed that Si abundances are lower than those of site K5 except for K5-OR3 which shows lower abundance than K4. The abundances of Al and Fe are different between sites K4 and K5 except for K5-OR3 (similar Al abundance with K4-OR5 in site K4).

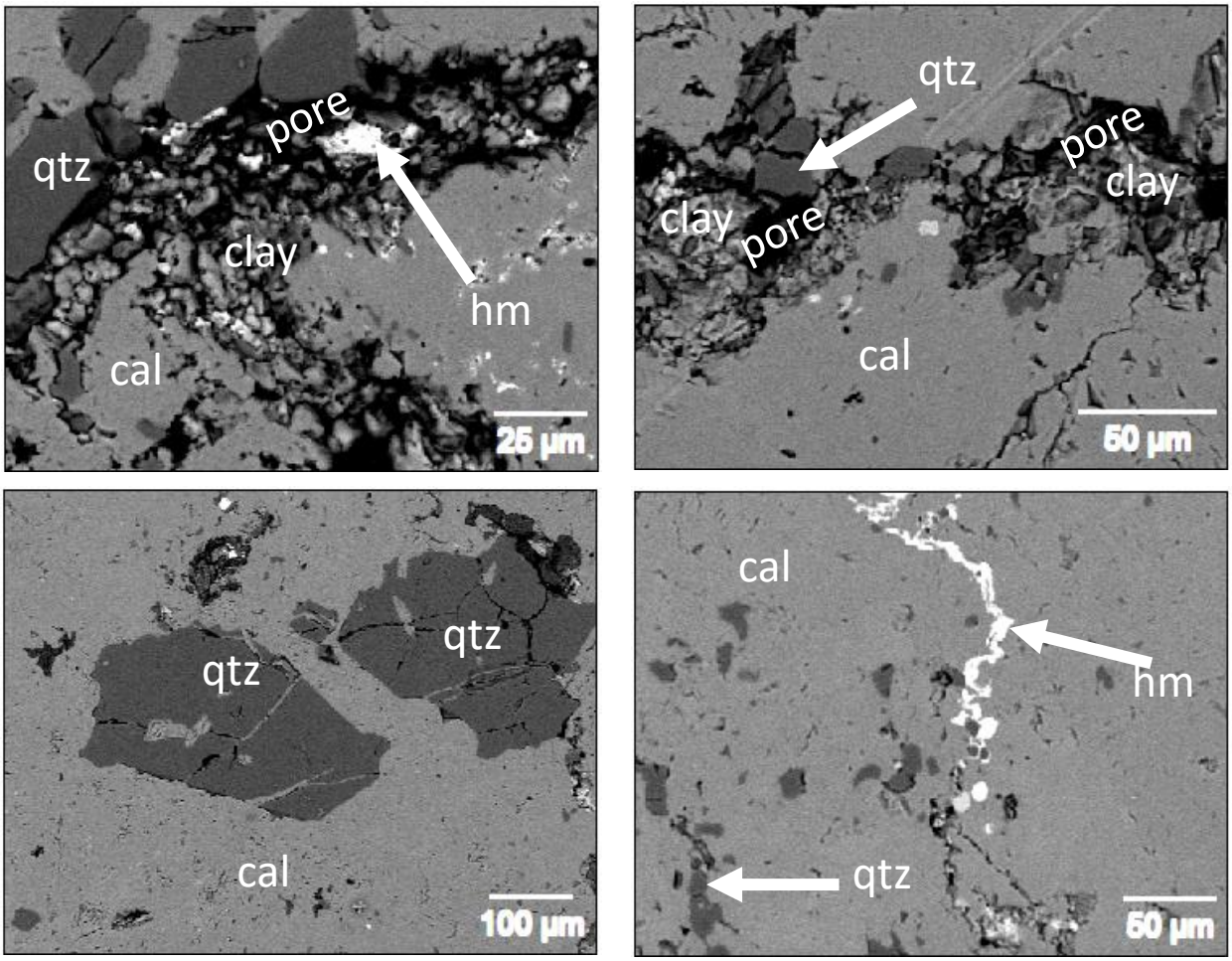


**Figure 4.1:** SEM image of the bedrock at the K5 site showing hematite (hm) and clay (mostly kaolinite and illite) associated with weathering veins and pores with quartz (qtz) significantly distributed on a calcite bedrock.

At each site, Ca, and Mg abundances in the bedrock (Table 4.1) vary amongst the samples, but bedrock at site K5 has higher Ca abundances than K4. On the other hand, site K5 has lower Mg abundances than K4 (K4-OR5 showed similar abundance with the bedrock in site K5). Although there were variabilities in the abundances of Na, K and P within sites, they were all within uncertainty with each other. However, K4-OR4 has higher abundance of Na in the bedrock that K4-OR5 and higher than the bedrock at K5 but both K and P have similar abundances between the sites.

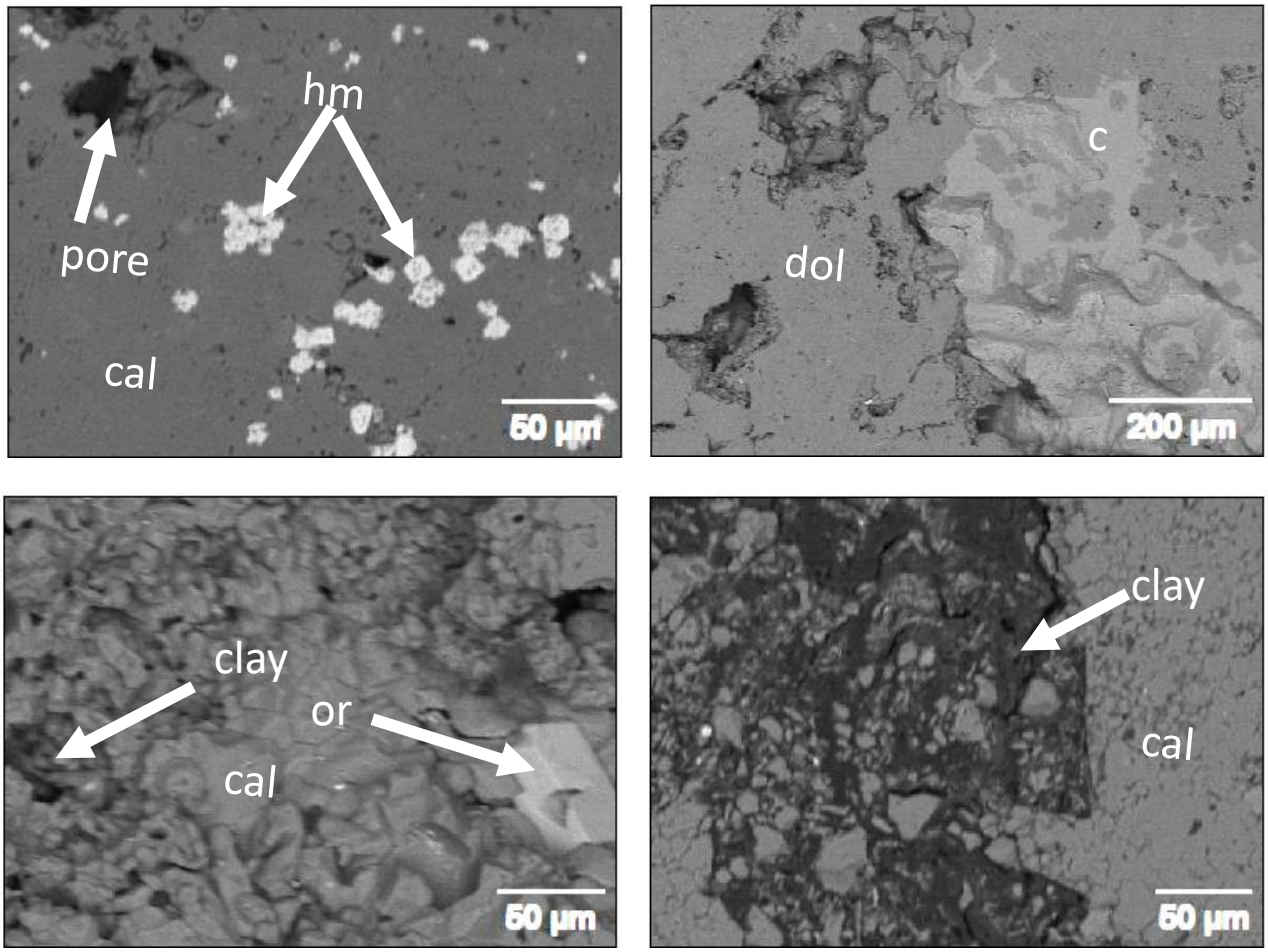


**Figure 4.2:** SEM image of the bedrock at the K4 site showing dolomite (dol), hematite (hm) and clay associated with weathering veins and pores with quartz (qtz) significantly distributed on a calcite (cal) bedrock.

The Mg/Ca (Table 4.2), used to determine the dominant mineral in the bedrock is similar at both sites. Total carbonate mineral content shown by the summing CaO and MgO (Table 4.2), also showed that the two sites have similar carbonate mineral content although K5-OR4 and KR-OR5 show lower abundances of carbonate minerals than other sites. The $SiO_2/Al_2O_3$ ratios (Table 4.2), used to show the abundance of quartz in the bedrock relative to other aluminosilicates show significant variability within – and between – sites.

**Table 4.1:** Bedrock bulk chemistry of sites K4 and K5 at the K-CZO

| Sites | Sample | $SiO_2$ | $Al_2O_3$ | $Fe_2O_3$ | CaO | MgO | $Na_2O$ | $K_2O$ | $P_2O_5$ | Zr |
|---|---|---|---|---|---|---|---|---|---|---|
| **K4** | **K4-OR4** | 2.80 ± 0.01 | 0.60 ± 0.01 | 0.30 ± 0.01 | 31.70 ± 0.01 | 18.80 ± 0.01 | 0.20 ± 0.01 | 0.06 ± 0.01 | 0.08 ± 0.01 | 8.0 ± 2.00 |
| | **K4-OR5** | 0.80 ± 0.01 | 0.07 ± 0.01 | 0.04 ± 0.01 | 55.00 ± 0.01 | 0.70 ± 0.01 | 0.01 ± 0.01 | 0.03 ± 0.01 | 0.04 ± 0.01 | 16 ± 2.00 |
| | **Average** | 1.80 ± 0.01 | 0.30 ± 0.01 | 0.20 ± 0.01 | 43.50 ± 0.01 | 9.80 ± 0.01 | 0.10 ± 0.01 | 0.05 ± 0.01 | 0.06 ± 0.01 | 12 ± 2.00 |
| **K5** | **K5-OR1** | 3.50 ± 0.01 | 0.30 ± 0.01 | 0.20 ± 0.01 | 52.00 ± 0.01 | 0.70 ± 0.01 | 0.03 ± 0.01 | 0.03 ± 0.01 | 0.04 ± 0.01 | 5.0 ± 2.00 |
| | **K5-OR2** | 4.00 ± 0.01 | 0.30 ± 0.01 | 0.20 ± 0.01 | 52.00 ± 0.01 | 0.30 ± 0.01 | 0.02 ± 0.01 | 0.03 ± 0.01 | 0.03 ± 0.01 | 9.0 ± 2.00 |
| | **K5-OR3** | 0.50 ± 0.01 | 0.07 ± 0.01 | 0.08 ± 0.01 | 54.70 ± 0.01 | 0.09 ± 0.01 | 0.01 ± 0.01 | <0.01 | 0.03 ± 0.01 | 2.0 ± 2.00 |
| | **Average** | 2.70 ± 0.01 | 0.20 ± 0.01 | 0.20 ± 0.01 | 53.00 ± 0.01 | 0.40 ± 0.01 | 0.02 ± 0.01 | 0.03 ± 0.01 | 0.03 ± 0.01 | 5.3 ± 2.00 |

[a] Oxides measured by ICP-OES after Li-metaborate fusion digestion (Chapter 2.4.2) with values presented in wt% except for Zr, which is in ppm

[b] Uncertainty presented as analytical uncertainty.

[c] bedrock samples collected as outcrops.

**Table 4.2:** Ratios and sums of the bedrock bulk chemistry of sites K4 and K5 at the K-CZO

| Sites | Sample | $SiO_2/Al_2O_3$ | $SiO_2+Al_2O_3$ | MgO+CaO | Mg/Ca | $SiO_2+Al_2O_3$/CaO+MgO |
|---|---|---|---|---|---|---|
| **K4** | **K4-OR4** | 4.60 ± 0.01 | 3.40 ± 0.01 | 50.5 ± 0.01 | 0.60 ± 0.01 | 0.07 ± 0.01 |
| | **K4-OR5** | 11.7 ± 0.01 | 0.90 ± 0.01 | 56.0 ± 0.01 | 0.01 ± 0.01 | 0.02 ± 0.01 |
| | **Average** | 8.00 ± 0.01 | 2.00 ± 0.01 | 53.2 ± 0.01 | 0.30 ± 0.01 | 0.04 ± 0.01 |
| **K5** | **K5-OR1** | 6.40 ± 0.01 | 0.50 ± 0.01 | 54.8 ± 0.01 | 0.00 ± 0.00 | 0.01 ± 0.01 |
| | **K5-OR2** | 42.6 ± 0.01 | 22.0 ± 0.01 | 42.6 ± 0.01 | 0.01 ± 0.01 | 0.50 ± 0.01 |
| | **K5-OR3** | 67.5 ± 0.01 | 30.0 ± 0.01 | 38.4 ± 0.01 | 0.01 ± 0.01 | 0.80 ± 0.01 |
| | **Average** | 10.7 ± 0.01 | 3.00 ± 0.01 | 53.3 ± 0.01 | 0.01 ± 0.01 | 0.06 ± 0.01 |

[a] Oxides measured by ICP-OES after Li-metaborate fusion digestion (Chapter 2.4.2) with values presented in wt%

[b] Uncertainty presented as analytical uncertainty.

[c] bedrock samples collected as outcrops

**Table 4.3**: Soil bulk chemistry of sites K4 and K5 at the K-CZO

| Site | Sample | [a]$SiO_2$ | $Al_2O_3$ | $Fe_2O_3$ | CaO | MgO | $Na_2O$ | $K_2O$ | $P_2O_5$ | Zr |
|---|---|---|---|---|---|---|---|---|---|---|
| **K4** | **5** | 71.30 ± 0.01 | 10.70 ± 0.01 | 4.80 ± 0.01 | 0.60 ± 0.01 | 0.70 ± 0.01 | 0.06 ± 0.01 | 0.80 ± 0.01 | 0.20 ± 0.01 | 119.0 ± 9.00 |
| | **10** | 70.00 ± 0.01 | 12.50 ± 0.01 | 5.60 ± 0.01 | 0.50 ± 0.01 | 0.80 ± 0.01 | 0.05 ± 0.01 | 0.90 ± 0.01 | 0.20 ± 0.01 | 126.0 ± 9.00 |
| | **20** | 66.50 ± 0.01 | 14.30 ± 0.01 | 6.40 ± 0.01 | 0.50 ± 0.01 | 0.80 ± 0.01 | 0.05 ± 0.01 | 0.90 ± 0.01 | 0.20 ± 0.01 | 137.7 ± 9.00 |
| | **26** | 69.40 ± 0.01 | 13.40 ± 0.01 | 6.00 ± 0.01 | 0.40 ± 0.01 | 0.80 ± 0.01 | 0.05 ± 0.01 | 0.90 ± 0.01 | 0.20 ± 0.01 | 142.3 ± 9.00 |
| | **Average** | 69.30 ± 0.01 | 12.70 ± 0.01 | 5.70 ± 0.01 | 0.50 ± 0.01 | 0.80 ± 0.01 | 0.06 ± 0.01 | 0.90 ± 0.01 | 0.20 ± 0.01 | 131.3 ± 9.00 |
| **K5** | **5** | 57.40 ± 0.01 | 14.30 ± 0.01 | 6.50 ± 0.01 | 0.60 ± 0.01 | 2.00 ± 0.01 | 0.40 ± 0.01 | 2.00 ± 0.01 | 0.30 ± 0.01 | 255.7 ± 6.90 |
| | **12** | 57.50 ± 0.01 | 15.50 ± 0.01 | 7.00 ± 0.01 | 0.60 ± 0.01 | 2.09 ± 0.01 | 0.40 ± 0.01 | 2.00 ± 0.01 | 0.30 ± 0.01 | 252.7 ± 6.90 |
| | **20** | 57.00 ± 0.01 | 15.40 ± 0.01 | 7.00 ± 0.01 | 0.60 ± 0.01 | 2.00 ± 0.01 | 0.40 ± 0.01 | 2.00 ± 0.01 | 0.30 ± 0.01 | 242.0 ± 6.90 |
| | **30** | 58.30 ± 0.01 | 15.50 ± 0.01 | 6.90 ± 0.01 | 0.60 ± 0.01 | 1.98 ± 0.01 | 0.30 ± 0.01 | 2.00 ± 0.01 | 0.30 ± 0.01 | 239.0 ± 6.90 |
| | **Average** | 57.60 ± 0.01 | 15.00 ± 0.01 | 6.90 ± 0.01 | 0.60 ± 0.01 | 2.00 ± 0.01 | 0.40 ± 0.01 | 2.00 ± 0.01 | 0.30 ± 0.01 | 247.4 ± 6.90 |

[a] Oxides measured by ICP-OES after Li-metaborate fusion digestion (Chapter 2.4.2) with values presented in wt% except for Zr, which is in ppm

[b] Uncertainty presented as standard deviation of the number of samples analysed.

**Table 4.4:** Ratios and sums of the mineral oxides in the soils at sites K4 and K5 at the K-CZO

| Sites | Sample | $SiO_2/Al_2O_3$ | $SiO_2+Al_2O_3$ | Mg/Ca | CaO+MgO | $(SiO_2+Al_2O_3)/(CaO+MgO)$ |
|---|---|---|---|---|---|---|
| **K4** | **5** | 6.70 ± 0.01 | 82.0 ± 0.01 | 1.00 ± 0.01 | 1.30 ± 0.01 | 70.0 ± 0.01 |
| | **10** | 5.60 ± 0.01 | 82.6 ± 0.01 | 1.50 ± 0.01 | 1.30 ± 0.01 | 55.8 ± 0.01 |
| | **20** | 4.60 ± 0.01 | 80.8 ± 0.01 | 1.80 ± 0.01 | 1.30 ± 0.01 | 43.8 ± 0.01 |
| | **26** | 5.00 ± 0.01 | 82.8 ± 0.01 | 1.80 ± 0.01 | 1.00 ± 0.01 | 47.0 ± 0.01 |
| | **Average** | 5.50 ± 0.01 | 82.0 ± 0.01 | 1.60 ± 0.01 | 1.30 ± 0.01 | 54.0 ± 0.01 |
| **K5** | **5** | 4.00 ± 0.01 | 71.7 ± 0.01 | 3.40 ± 0.01 | 2.60 ± 0.01 | 27.0 ± 0.01 |
| | **12** | 3.70 ± 0.01 | 73.0 ± 0.01 | 3.60 ± 0.01 | 2.70 ± 0.01 | 27.0 ± 0.01 |
| | **20** | 3.70 ± 0.01 | 72.6 ± 0.01 | 3.40 ± 0.01 | 2.70 ± 0.01 | 26.9 ± 0.01 |
| | **30** | 3.80 ± 0.01 | 73.6 ± 0.01 | 3.00 ± 0.01 | 2.60 ± 0.01 | 28.0 ± 0.01 |
| | **Average** | 3.80 ± 0.01 | 72.7 ± 0.01 | 3.40 ± 0.01 | 2.70 ± 0.01 | 27.4 ± 0.01 |

[a] Oxides measured by ICP-OES after Li-metaborate fusion digestion (Chapter 2.4.2) with values presented in wt%

[b] Uncertainty presented as standard deviation of the number of samples analysed.

### 4.2.2 Soil Mineralogy in the K-CZO

The Si abundances at both sites K4 and K5 (Table 4.3) are significantly higher than the bedrock. However, site K4 has higher Si abundances than K5. On the other hand, the abundances of Al, Fe and Na all have shown variability within the sites, but Al and Na are higher in site K5 than K4 while Fe and Ca are similar in abundance in both sites. On the other hand, K, Mg and P have higher abundances in site K5 than K4.

The Mg/Ca ratios (Table 4.4) used to estimate the relative abundance of calcite and dolomite are higher in site K5 than in site K4. Within the sites, at site K4 there is a variability in the Mg/Ca ratios in the top 10 cm which were within uncertainty of each other. Also, the $SiO_2/Al_2O_3$ ratios, are higher in site K4 than K5 although they vary with depth across both sites. At site K4, the ratios decreased with depth to 20 cm, then increased at the deepest sample. At site K5, the ratios were higher at the soil surface but also decreased with depth to 20 cm and increased at 30 cm (deepest sample) depth. The carbonate mineral abundance in the soil shown by CaO+MgO is higher at site K5 than K4 which also corresponds to site K4 having higher aluminosilicates compared to carbonate minerals (determined by the $(SiO_2+Al_2O_3)/(CaO+MgO)$) than K5, with the highest abundance of aluminosilicates being on the top 5 cm of site K4 which decreased with depth to 20 cm, then increasing at the deepest sample. At site K5, the highest abundances of the aluminosilicates compared to the carbonate minerals in the soil were at the deepest sample (30 cm depth).

### 4.2.3 Mass Transfer Analysis of the Soil Profiles

Mass transfer analysis (Section 2.5) was used to determine the mobilisation (gain or loss) of elements in the soil by normalising their concentrations to an assumed immobile element (Zr in this case) and the net gain or loss of mass of the immobile element was determined relative to the bedrock (deepest sample, in this study) (Anderson et al., 2002; Brimhall and Dietrich, 1987; Chadwick et al., 1990).

The mass transfer analysis of the less mobile elements, Si, Al, and Fe in the soils at both sites K4 and K5 (Fig. 4.3) shows, largely, conservation of these elements relative to the immobile element Zr and the deepest sample. At site K4 (Fig. 4.4a), typically

the more mobile elements showed moderate to significant enrichment with respect to the deepest soil sample, with Ca the most enriched, especially in the top 10 cm followed by Na, with Mg and K showing similar (lower) enrichment (Fig. 4.4). The typically mobile elements Ca, Mg, Na at site K5 (Fig. 4.4b), were largely conserved with very slight depletion of Ca and enrichment of Na. The less mobile elements Si, Al, and Fe as well as K and P show slight depletion in the shallowest sample but are largely conserved (Fig. 4.3b and 4.4b).

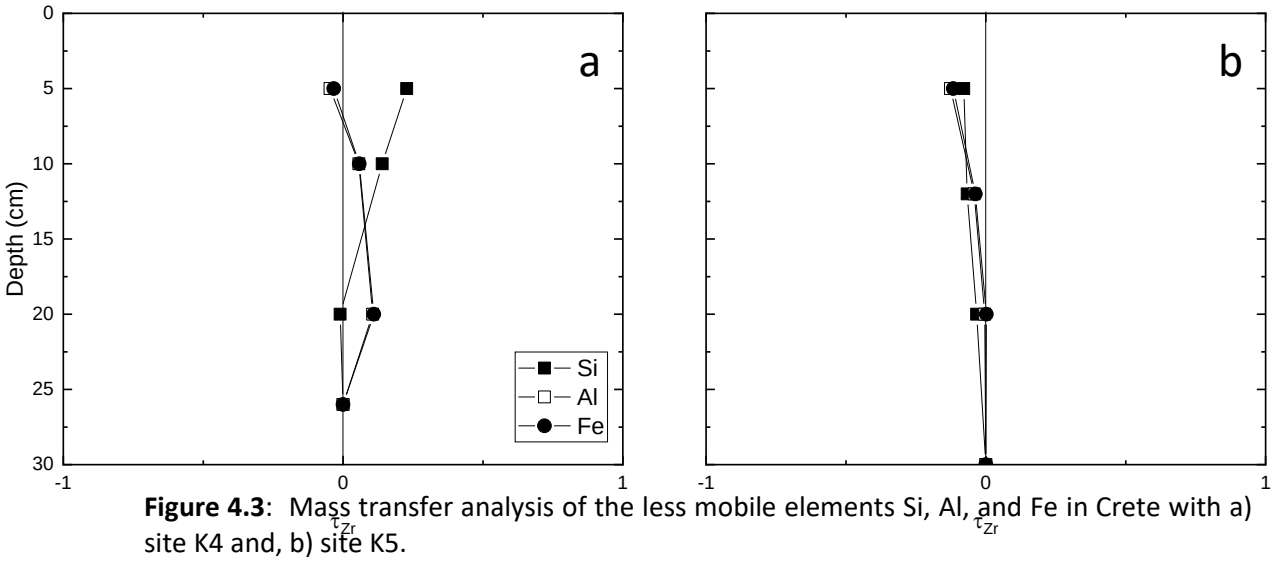


**Figure 4.3**: Mass transfer analysis of the less mobile elements Si, Al, and Fe in Crete with a) site K4 and, b) site K5.

### 4.3 Discussion

Studies on the soil formation and sources of mineral nutrients on carbonate bedrock typically assume one of two major hypotheses: soils are formed by the residual impurities that remained after the dissolution of the major minerals in the bedrock or that they are formed by the deposition of aeolian dust from nearby or distant places (Durn, 2003; Durn et al., 1999; Muhs et al., 2007). In most carbonate environments, there are few impurities in the bedrock to promote soil formation (Muhs and Budahn, 2009; Muhs et al., 2007; Pye, 1992), requiring a significant quantity of carbonates to produce the soils observed in some karst environments. Birkeland (1999) reported that the entire island of Rhoda has to dissolve to produce the quantity of the soil profiles observed in the island if the soils were formed

primarily from the dissolution of carbonate minerals which, according to Muhs and Budahn (2009), is physically impossible. It is therefore, believed that mineral nutrient production in such environments is also driven by weathering of mineral elements transported from other places (Bauer and Velde, 2014; Moraetis et al., 2015; Wang et al., 2019).

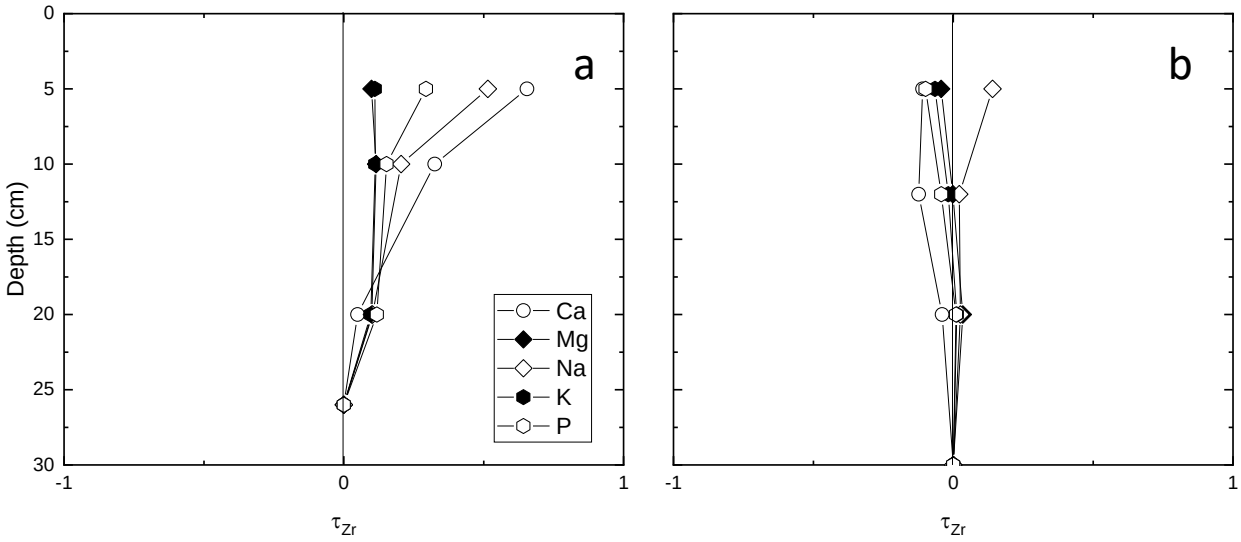


**Figure 4.4:** Mass transfer analysis of mineral elements Ca, Mg, Na, K and P in a) K4 and b) K5 revealing retention of the elements in K5 but enrichment in the K4 relative to the deepest sample.

### 4.3.1 Sources and Mobilisation of Mineral Nutrient Elements in the Soil

The mass transfer analysis of the soils at site K4 (Figs. 4.3 and 4.4) indicated the enrichment of the mobile elements Ca, Mg, K and Na (added here because of its importance in interpreting mineral weathering in the rock and soils, which can elucidate the sources of mineral-sourced nutrient elements like Ca, K, and Fe). The enrichment of these mineral elements in the soil profile is attributed to the likelihood of external addition to the soil, consistent with earlier studies (e.g., Brantley et al., 2007; Chapela Lara et al., 2018) which reported that elemental mass transfer profiles that show enrichment at the top are indicative of an external source to the elemental budgets. Moraetis et al. (2015) suggested that the external source of these elements in the soils of K4 is likely the Saharan dust from Africa. This view is also consistent with the sources of elemental enrichment on carbonate rocks in other Mediterranean environments reported in earlier studies (Durn, 2003; Muhs et

al., 2010; Yaalon, 1997) and other places (Aciego et al., 2017; Muhs et al., 2007). Presence of these elements (Ca, Mg, K and Na) in both the bedrock and the soil (Tables 4.1 and 4.3) indicates a likely bedrock source of the elements consistent with the interpretations of earlier studies in the region (Durn, 2003; Pye, 1992).

The mass transfer of the less mobile elements Si, Al, and Fe (Fig 4.3) also indicates slight enrichment of Si in the top 10 cm and Al and Fe from 10 cm to the deepest sample. Because these elements, especially Al and Si, are usually retained in the soil as they have low mobility (e.g., Chapela Lara et al., 2018; Dere et al., 2016), their enrichment in the soil more than the bedrock at both sites (Tables 4.1 and 4.3) is interpreted as, in addition to atmospheric dust, an evidence of *in situ* weathering and the dissolution of the dominant calcite and, to a lesser extent, dolomite in the bedrock. The enrichment of Al and Fe at depth is likely due to mobilisation by organic ligands and transported downwards (Jin et al., 2017). Also, enrichment of Si in the soil of K4 in the top 10 cm (Figs 4.3 and 4.4) of the soil more than the parent material (deepest sample in this case) suggesting that the element is likely added to the soil from external sources such as aeolian dust deposition. On the other hand, the abundances of Al and Fe increase with depth which we interpret as the likelihood of the deeper soil being older than the soil at the surface consistent with an earlier study of soils formed by dust deposition in Bermuda (Herwitz and Muhs, 1995). Also, the abundance of Fe in the soil of site K4 is likely as a result of chelation by organic ligands and transported downwards (Jin et al., 2017). This interpretation is also consistent with other studies on carbonate soils in Mediterranean environments in Croatia (Durn, 2003), Greece (Macleod, 1980; Pye, 1992) and Spain (Muhs et al., 2010); and other carbonate environments such as Barbados (Muhs et al., 2007). Also, increase in the abundance of Al with depth is likely as a result of bedrock contribution. Herwitz and Muhs (1995) reported low abundances of Al in the carbonate soils of Bermuda formed exclusively from dust deposition. Also, although the decrease of $SiO_2/Al_2O_3$ ratios (Table 4.4) with depth shows a relative increase in Al abundance with depth, the relatively higher ratios at site K4 compared to soils formed from dust deposition in Bermuda (Herwitz and Muhs, 1995) and Jamaica (Muhs and Budahn, 2009) can be interpreted as the contribution of bedrock

to the abundance of Al in the soil. On the other hand, P was slightly enriched in the soil most likely as a result of an external source such as aeolian deposition or redistribution such as biolifting (a process in which plant roots scavenge for nutrients at depth and concentrate them at the surface). Muhs et al. (2007) reported that P enrichment in the soils of Barbados and Bahamas, carbonate environments which contain no P-bearing minerals in the bedrock, as resulting from aeolian deposition.

Based on REE analysis, Moraetis et al. (2015) established that site K5 receives a larger influx of mineral nutrient elements from Saharan dust than site K4. However, only the mass transfer of Na showed slight enrichment in the top 10 cm of the soil at site K5 (Fig. 4.4) suggesting that only Na is contributed to the soil though aeolian dust deposition since Na is not usually incorporated into secondary minerals (Buss et al., 2017). Although this interpretation is supported by the higher abundance of Na in the soil of site K5 than K4 (Table 3.3) and the bedrock (Table 3.1), Moraetis et al. (2015) reported no Na abundance at the same depth in site K5. However, the proximity of the sites to the ocean also suggests the likelihood of input from the ocean.

The mass transfer of Ca shows slight depletion (Fig. 4.4) and though Ca abundances are the same with the parent material (deepest sample), the higher abundance of Ca in the bedrock (Table 4.1) than the soil (Table 4.3) is likely an indication of *in situ* weathering suggesting that Ca is contributed to the soil by the bedrock as expected. Mass transfer and abundances of Mg in the soil show no variation with the parent material (deepest sample) but is higher than in site K4 (Table 4.3) and the bedrock (Table 4.1). The high Mg/Ca ratios indicating higher dolomite content in K5 than K4 (assuming all the Mg in the soil comes from dolomite) suggests that Mg is contributed to the soil by the bedrock. Zhu et al. (2008) reported that higher Mg abundances in soils are indicative that the weathering profile is at the initial or semi-weathering stage characterised by having high Mg content as well as residual carbonate (dolomite in this case) minerals. Increase in the abundance of Fe with depth is also interpreted as external contribution of the element to the soil consistent with earlier studies in soils formed through atmospheric deposition in Bermuda (Herwitz and Muhs, 1995). On the other hand, high abundances of Al

(Table 4.3) also show that bedrock contributes to the Al budget in the soil consistent with the findings of Muhs and Budahn (2009) who attributed higher abundance of Al in relation to aluminosilicates in the carbonate soils of Jamaica as evidence of bedrock weathering.

Although Moraetis et al. (2015) reported higher kaolinite content at site K4 than site K5, higher K abundance at site K5 may be indicative of the abundance of other clay minerals in the soil. Clay minerals were identified in the bedrock (Fig. 4.2) which is likely the contributor of K to the soil. Enrichment of P in the soil is also attributed to the atmospheric dust deposition or biolifting consistent with earlier studies on carbonate soils (Muhs et al., 2007).

### 4.3.2 Lithological Control on Mineral Nutrient Sources in K-CZO

Weathering as a means of mineral nutrient production and soil formation is controlled by several factors, including climate, vegetation, and lithology. Production of mineral nutrients and soil (terra rossa) on carbonate bedrocks in different parts of the Mediterranean environment such as Croatia, Spain and Greece was reported to be dependent on the bedrock lithology and/or aeolian dust deposition (Avila et al., 1997; Durn et al., 1999; Macleod, 1980; Muhs et al., 2010; Pye, 1992). In both sites K4 and K5, the considerably lower Ca and Mg contents in the parent material (deepest sample in this case) (Table 4.3) than the bedrock (Table 4.1) suggests that the dissolution of carbonate minerals in the bedrock is the main weathering reaction taking place in the bedrock. Carbonate dissolution reactions have been described (Brantley et al., 2013) as both the reactions that initiate regolith formation and the deepest (i.e. first) weathering reactions in shale and igneous rocks (Brantley et al., 2006a; Jin et al., 2010b; White et al., 2005).

At site K5, however, the soil has higher Mg abundances than K4 (Table 4.3), despite K4 having notably higher Mg abundances in the bedrock (Table 4.1). The unexpected difference in Mg content between the sites might be explained by the higher illite content (Fig. 4.2, Moraetis et al., 2015) at the site than K4. Alternatively, Mg difference between the sites may be explained by Mg-substitution for Al in the octahedral clay layers as reported by Robertson et al. (1954) which showed 0.15 –

0.28% octahedral substitutions by Mg. Assuming that all the Mg in K-CZO comes from clay, the maximum Mg in the soil attributable to the kaolinite and illite (clay data obtained from Moraetis et al., 2015) was calculated. The difference in the Mg-substitution was not found to be too high to account for the difference in Mg abundance in the sites. However, Cuadros et al. (2013) reported Fe and Mg exchange in

| Site | Depth | Clay | 0.28% | % unaccounted |
|---|---|---|---|---|
| **K4** | **0-5** | 24.1 | 5.2 | 97.1 |
| | **5 - 10** | 29.1 | 6.3 | 96.7 |
| | **15 - 50** | 35.9 | 7.8 | 96.2 |
| | **Average** | 29.7 | 6.4 | 96.7 |
| **K5** | **0 – 5** | 24.3 | 5.3 | 99.0 |
| | **07-12** | 25.3 | 5.5 | 98.9 |
| | **40-45** | 27.1 | 5.9 | 98.9 |
| | **Average** | 25.6 | 5.5 | 98.9 |

octahedral systems in clay in hydrothermal vents in seafloor. Site K5 (Table 4.3) has higher MgO + $Fe_2O_3$ than K4 likely explains higher Mg abundance in site K5 than K4.

**Table 4.5:** Calculated Mg-substitution in the octahedral layers of clay in the soils at K-CZO

At site K5, however, higher Mg abundances than K4 may be explained by the higher illite content (Moraetis et al., 2015) (Fig. 4.2) at the site than K4. Magnesium was found to be hosted by illite in shale rocks (Dere et al., 2016). Although the soils at site K5 were reported (Moraetis et al., 2015) to have significant input from aeolian dust deposition, abundances of Ca and Mg in the soil are largely controlled by the bedrock lithology. The aluminosilicates largely have shown no variation with the parent materials (deepest samples) at both sites (Table 4.3) but are enriched in the soil after the dissolution of the carbonate minerals in the bedrock (Tables 4.1 and 4.3) and host nutrient elements K (illite and orthoclase) and Mg (illite) (Dere et al., 2016).

Conservation of Si and Al in the soils (Fig. 4.4) is an indication of retention of Si and Al in the soils at both sites which also indicates the presence of aluminosilicates such as quartz, kaolinite, illite and orthoclase reported by Moraetis et al. (2015) and confirmed by our SEM data (Figs. 4.1 and 4.2). Additionally, relatively higher

abundance of Si than Al at both sites shown by $SiO_2/Al_2O_3$ ratios (Table 4.4) indicates the relative early stages of the weathering regime at both sites or that the soil has been moved by other means to the present sites during the construction of terraces as reported by Moraetis et al. (2015). The aluminosilicates ($SiO_2+Al_2O_3$) largely have shown enrichment in the deepest sample at both sites but are enriched in the soil after the dissolution of the carbonate minerals in the bedrock (Tables 4.1 and 4.3) and host nutrient elements K (illite and orthoclase) and Mg (illite) (Dere et al., 2016). The moderate enrichment of Na in the upper parts of the soil revealed low weathering intensity in the soil profile, consistent with geochemical characteristics of Na in carbonate weathering profiles (enrichment in middle and lower parts of sites with high weathering intensity Muhs and Budahn, 2009; Zhu et al., 2008) and which is explained by aeolian deposition aeolian deposition (Muhs et al., 2007; Pye, 1992). On the other hand, K is usually depleted in the middle and the lower parts of a carbonate weathering profile which Zhu et al. (2008) attributed to the presence of K-bearing minerals illite and orthoclase in China. The abundance of Na and K in carbonate bedrocks is also usually dependent on weathering intensity (Zhu et al., 2008), in low intensity weathering profiles, Na, usually enriched in the upper part of the weathering profiles and K, enriched in the middle and lower parts of the profiles are usually associated with the formation and distribution of illite in the profiles (Zhu et al., 2008). This interpretation was supported by the abundance of K (Table 4.3) in site K5 where Moraetis et al. (2015) established by XRD high abundance of illite compared to site K5 which has lower K abundances than K5.

The abundance of Fe in carbonate soil may come from both primary and secondary Fe-bearing minerals (hematite, goethite and pyrite) (Muhs and Budahn, 2009). The presence of hematite at both sites was confirmed by XRD by Moraetis et al. (2015) and SEM here (Figs. 4.1 and 4.2). Also, hematite has been found to be the dominant Fe mineral in other soils formed on carbonate bedrocks in Croatia (Durn, 2003), and other Caribbean Islands (Muhs and Budahn, 2009; Muhs et al., 2007). The abundance of Fe (Fig. 4.3) and the conservation of Fe (Fig 4.3) in the soil is seen as the retention of hematite in the soil after the dissolution of carbonate minerals from the soil and evidence that the lithology controls the abundance of Fe in carbonate

soils, consistent with the conclusions of (Boero et al., 1992; Boero and Schwertmann, 1989) who studied the mineralogy of terra rossa in northern Italy. The soils at both sites have low abundances of P which are higher than the bedrock. The presence of P in the soil was attributed to the aeolian dust deposition from largely African Sahara consistent with an earlier study that reported abundance of P in the carbonate soils of Mallorca to have been deposited by Saharan dust (Muhs et al., 2010).

At both sites, the bulk chemistry of the soil (Table 4.3) showed that Ca and Mg were considerably dissolved and leached out from the bedrock while the Si, Fe, Al, and K were enriched in the soil also is consistent with our hypothesis that mineral nutrient production is dependent on the dissolution of carbonate minerals leaving the soil matrix enriched with the non-carbonate impurities (Muhs et al., 2010). Carbonate mineral purity shown by the sum CaO + MgO (Table 4.4) shows that the carbonate content in the soils at both sites have enough non-carbonate mineral 'impurities' to support mineral nutrient production through carbonate dissolution compared to other carbonate environments in the Caribbean (Muhs and Budahn, 2009; Muhs et al., 2007) and Mediterranean environments such as Spain (Muhs et al., 2010). However, absence of primary soil forming minerals such as feldspars, hornblende and mica (Moraetis et al., 2015) also indicates that aeolian dust deposition contributes to the soil formation especially at site K5 where Moraetis et al. (2015) reported high abundance of low mobility elements in the soil. this interpretation is also consistent with the findings of Pye (1992) who reported the soil forming contribution of the Saharan dust in Greece.

### 4.3.3 Impacts of Lithology on Soil Formation

Mineral nutrient production, cycling and soil formation processes are principally driven by bedrock weathering (West et al., 2005). In carbonate environments, the soils are typically shallow and lacking in nutrients due to, mostly, congruent dissolution of major carbonate minerals (calcite and dolomite) in the bedrock and the soil coupled with a low abundance of soil-forming minerals in the bedrock (Jiang et al., 2014; Muhs et al., 2010; Wang et al., 2004b). In the K-CZO, the mass transfer analysis of the mobile elements, Ca, Mg, Na and K in the soils at both sites (Figs 4.3

and 4.4) showed that the elements were mostly retained in the soil. The retention of these elements in the soils largely reflects the abundance of the minerals that host them. At both sites, Moraetis et al. (2015) has identified the minerals that host these elements which support our SEM data. At both sites, the bulk chemistry of the soil (Table 4.3) showed that Ca and Mg were considerably dissolved and leached out from the bedrock while the Si, Fe, Al, and K were enriched in the soil, which is also consistent with the hypothesis that soil formation is dependent on the dissolution of carbonate minerals leaving the soil matrix enriched with the non-carbonate impurities (Muhs et al., 2010). Carbonate mineral purity the (SiO2+Al2O3)/(CaO+MgO) (Table 4.4) shows that the carbonate content in the soils at both sites have enough non-carbonate 'impurities' to support soil formation through carbonate dissolution compared to other carbonate environments in the Caribbean (Muhs and Budahn, 2009; Muhs et al., 2007) and Mediterranean environments such as Spain (Muhs et al., 2010). However, the absence of primary soil forming minerals such as hornblende and mica in the bedrock at both sites but are present in the soils (Moraetis et al., 2015) also indicate that aeolian dust deposition contributes to the soil formation especially at site K5 where Moraetis et al. (2015) reported high abundance of low mobility elements in the soil. This interpretation is also consistent with the findings of Pye (1992) who reported the soil forming contribution of the Saharan dust in Greece.

## 4.4 Conclusion

In this study we analysed the production of mineral nutrients in soils at the Koiliaris CZO, Crete and we were able to partially confirm our hypothesis that the mineral nutrients were produced from the dissolution of dominant carbonate minerals in the bedrock, leaving the soils enriched with residual non-carbonate minerals. Also, from the bulk chemistry and mass transfer analysis, we were able to confirm the role of lithology in soil formation in the area. We were also able to confirm that, in addition to lithology, aeolian dust deposition also contributes to the mineral nutrient production and soil formation in the soil. In the next chapters, the bioavailability

(different from their bulk abundance in the soil) of these nutrient elements in the Chinese and Greek soils will be investigated.

# Chapter 5

# Bioavailability of Mineral Elements in the SPECTRA Critical Zone Observatory

**Author contribution declaration:** Rock cutting, and thin sections were conducted by Aminu Lawal under the guidance of Evangelos Mouchos. SEM analysis was also conducted by Aminu Lawal with help from Stuart Kearns. Extraction of exchangeable cations and ICP-OES were carried out by Aminu Lawal with guidance from Adam McAleer

## 5.1 Introduction

The vulnerability of carbonate landscapes to human activities (Durn, 2003; Jiang et al., 2014; Wang et al., 2014; Wang et al., 2004b), in addition to likely low natural input of most mineral nutrients to the soils from bedrock weathering means that agricultural practices in carbonate areas often involve addition of significant quantities of (often artificial) fertiliser, further impacting the already fragile soils. However, although previous work (Liu et al., 2019; Moore et al., 2017) and this thesis (Chapter 3) have established that the soils in the carbonate catchment of Chenqi, in Guizhou province, southwestern China, are relatively nutrient rich, the nutrient elements may not be biologically available for plant uptake. In this Chapter, I examine the link between the bioavailability of mineral nutrients to the abundance and distribution of bulk mineral nutrient pools in the soil. Since this study could not establish correlation between land use and/or slope position with the bulk abundance of mineral nutrient elements (Chapter 3.3.2), I hypothesize that the bioavailability of nutrient elements Ca, Mg and K in the soils developed on the carbonate bedrocks in Chenqi is dependent on the presence and distribution of non-carbonate mineral impurities. Sodium, an element that is also sourced from non-carbonate minerals, but is not absorbed appreciably by plants (Jobbagy and Jackson, 2001) was included in the study to help trace the processes that control the enrichment and distribution of the nutrient bioavailable cations (exchangeable cations) in the soil profiles. The elements were extracted using 1 m ammonium acetate (pH adjusted to 8) and refluxed with 1 M nitric acid (Chapter 2.4.1). Bioavailable nutrient elements contribute to soil fertility and are mainly sorbed on mineral surfaces and organic particles in the soil. These elements are measured using extraction reagents such as $NH_4OAc$, $BrCl_2$ or $SrCl_2$. In this study, $NH_4OAc$ was used as the extraction reagent due to its better suitability for exchangeable K displacement (van der Heijden et al., 2018) compared to other reagents such as $BrCl_2$, $SrCl_2$ and KCl.

## 5.2 Results

The average abundances of the bioavailable elements (average of abundances of depths for each site, Table 5.1) show no significant (within uncertainty) variation between land uses and slope positions and are all within uncertainty of each other. The highest abundances of Ca were observed (Table 5.1) in sites CQ2 and CQ13 (0.40 mg/g and 0.30 mg/g, respectively) in the top slope of the secondary forest and site CQ46 (0.30 mg/g) in the middle slope of the abandoned farmlands. The highest K abundances were in sites CQ46 (0.30 mg/g, middle slope of the abandoned farmlands) and CQ13 (also 0.30 mg/g, top slope of the secondary forest). The elemental ratios (Table 5.2) revealed variations in abundance of the bioavailable nutrient elements in comparison to each other in all the land uses and slope positions.

The vertical distribution of the elements (Figs. 5.1, 5.2 and 5.3) revealed that the distributions and abundances of the elements vary with depth, slope position and land use. In the sloping farmlands, there is a higher topsoil abundance of K and Ca, which decreases with depth. Site CQ7 in the middle slope of the sloping farmlands has higher abundance of all the bioavailable elements at the intermediate depth (50 cm) relative to the depths above and below and at CQ43, all element concentrations peaked at 90 cm with minimum abundances at the surface and middle depths. In the abandoned farmlands, sites CQ38 and CQ55 (bottom and middle slope, respectively), revealed higher abundances of elements at the top and the bottom of the profile, with low abundances in the intermediate depths. Site CQ46 (in the middle slope) and CQ54 (top slope) revealed higher abundances of Ca and K from 30 cm (CQ46) and 100 cm (100 cm) to the bottom of the profile.

In the secondary forest, the vertical abundances of the bioavailable elements follow similar patterns with the other land uses (sloping and abandoned farmlands) with predominantly higher abundance of the nutrient elements in the topsoil, decrease at the intermediate depth and then increasing near the bottom of the profiles.

**Table 5.1**: Bioavailable cation abundances in Chenqi[a]

| Site | Sample | Ca[b] | K | Mg | Na | n[c] |
|---|---|---|---|---|---|---|
| **SFB[d]** | **CQ7** | 0.10 ± 0.08 | 0.06 ± 0.04 | 0.08 ± 0.06 | 0.10 ± 0.06 | 7 |
| | **CQ43** | 0.10 ± 0.30 | 0.20 ± 0.30 | 0.20 ± 0.30 | 0.20 ± 0.30 | 12 |
| | **CQ61** | 0.20 ± 0.10 | 0.10 ± 0.20 | 0.07 ± 0.04 | 0.08 ± 0.05 | 12 |
| **SFM** | **CQ37** | 0.20 ± 0.30 | 0.20 ± 0.30 | 0.20 ± 0.30 | 0.20 ± 0.30 | 6 |
| **AFB** | **CQ38** | 0.03 ± 0.04 | 0.03 ± 0.04 | 0.03 ± 0.04 | 0.03 ± 0.04 | 6 |
| **AFM** | **CQ40** | 0.04 ± 0.02 | 0.05 ± 0.02 | 0.10 ± 0.50 | 0.01 ± 0.01 | 8 |
| | **CQ46** | 0.30 ± 0.20 | 0.30 ± 0.10 | 0.08 ± 0.04 | 0.04 ± 0.03 | 9 |
| | **CQ55** | 0.05 ± 0.04 | 0.05 ± 0.04 | 0.05 ± 0.03 | 0.05 ± 0.03 | 11 |
| **AFT** | **CQ54** | 0.08 ± 0.10 | 0.06 ± 0.05 | 0.04 ± 0.03 | 0.03 ± 0.03 | 13 |
| **SeFM** | **CQ17** | 0.10 ± 0.08 | 0.20 ± 0.30 | 0.20 ± 0.20 | 0.10 ± 0.30 | 6 |
| **SeFT** | **CQ2** | 0.40 ± 0.40 | 0.20 ± 0.20 | 0.20 ± 0.20 | 0.20 ± 0.20 | 7 |
| | **CQ13** | 0.30 ± 0.20 | 0.30 ± 0.10 | 0.08 ± 0.04 | 0.05 ± 0.03 | 9 |
| | **CQ25** | 0.20 ± 0.20 | 0.01 ± 0.01 | 0.01 ± 0.00 | 0.00 ± 0.00 | 5 |
| | **CQ64** | 0.08 ± 0.04 | 0.04 ± 0.03 | 0.05 ± 0.02 | 0.08 ± 0.05 | 10 |

[a] Depths of the sampling sites vary with the cores.

[b] Elements measured by ICP-OES after acid digestion (Chapter 2.4.2) with values presented in mg/g

[c] Uncertainty presented as standard deviation of the number of samples presented in column **n**

[d]SFB = sloping farmlands bottom; SFM = sloping farmlands middle; SFT = sloping farmlands top; AFB = abandoned farmlands bottom; AFM = abandoned farmlands middle; AFT abandoned farmlands top; SeFB = secondary forest bottom; SeFM = secondary forest middle; SeFT = secondary forest top

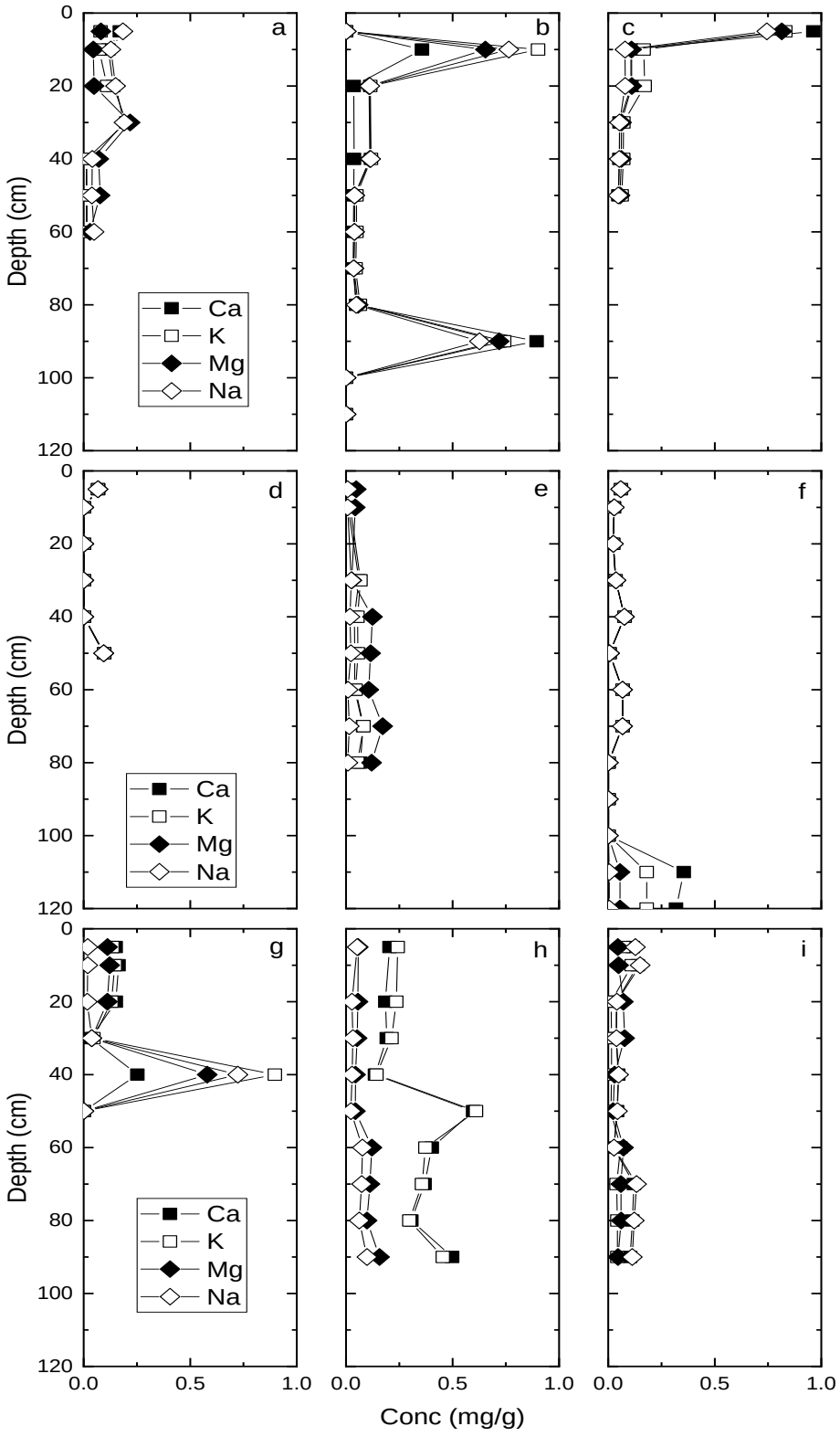


**Figure 5.1:** Vertical abundance of bioavailable cations Ca, K, Mg and Na in Chenqi watershed, a) CQ7 (bottom slope) b) CQ43 (bottom slope) c) CQ37 (middle slope) are from the sloping farmlands (No cores were drilled in the top slope and, therefore, no samples were collected). d) CQ38 (bottom slope) e) CQ40 (middle slope) f) CQ54 (top slope) are from the abandoned farmlands while g) CQ17 (middle slope) h) CQ13 (top slope) i) CQ64 (top slope) are from the secondary forest.

**Table 5.2:** Bioavailable elemental ratios[a]

| Site | Sample | K/Ca[b] | K/Na | K/Mg | n[c] |
|---|---|---|---|---|---|
| **SFB[d]** | **CQ7** | 0.90 ± 0.30 | 0.50 ± 0.10 | 0.70 ± 0.70 | 7 |
| | **CQ43** | 1.50 ± 1.00 | 1.00 ± 0.50 | 1.20 ± 1.20 | 12 |
| | **CQ61** | 0.70 ± 0.50 | 1.50 ± 1.70 | 1.50 ± 4.00 | 12 |
| **SFM** | **CQ37** | 1.30 ± 0.20 | 1.60 ± 0.40 | 1.00 ± 1.00 | 6 |
| **AFB** | **CQ38** | 0.80 ± 0.10 | 7.00 ± 4.00 | 1.00 ± 1.00 | 6 |
| | **CQ40** | 1.30 ± 0.40 | 4.00 ± 1.30 | 0.50 ± 0.40 | 8 |
| | **CQ46** | 1.00 ± 0.10 | 8.70 ± 6.80 | 4.00 ± 3.50 | 9 |
| | **CQ55** | 0.10 ± 0.03 | 1.00 ± 0.06 | 1.00 ± 1.00 | 11 |
| **AFT** | **CQ54** | 0.90 ± 0.20 | 9.00 ± 14.00 | 1.50 ± 2.00 | 13 |
| **SeFM** | **CQ17** | 1.40 ± 1.00 | 4.40 ± 3.00 | 1.40 ± 1.60 | 6 |
| **SeFT** | **CQ2** | 0.80 ± 0.20 | 9.00 ± 10.70 | 1.00 ± 1.00 | 7 |
| | **CQ13** | 1.00 ± 0.10 | 8.00 ± 7.00 | 4.00 ± 3.50 | 9 |
| | **CQ25** | 0.03 ± 0.00 | 7.30 ± 8.30 | 1.00 ± 1.00 | 5 |
| | **CQ64** | 0.60 ± 0.60 | 0.60 ± 0.50 | 0.80 ± 1.80 | 10 |

[a] Depths of the sampling sites vary with the cores.

[b] Elements measured by ICP-OES after acid digestion (Chapter 2.4.2) with values presented in mg/g

[c] Uncertainty presented as standard deviation of the number of samples presented in column **n**

[d]SFB = sloping farmlands bottom; SFM = sloping farmlands middle; SFT = sloping farmlands top; AFB = abandoned farmlands bottom; AFM = abandoned farmlands middle; AFT abandoned farmlands top; SeFB = secondary forest bottom; SeFM = secondary forest middle; SeFT = secondary forest top.

## 5.3 Discussion

Depending on the environment, the distribution of bioavailable elements in soils is usually dependent on different processes such as weathering, atmospheric deposition, leaching and/or vegetation (plant) cycling (Dawson et al., 2020; Derry and Chadwick, 2007; Uhlig et al., 2017; Uhliq and Blanckenburg, 2020) acting together or in isolation (Porder et al., 2007b). Weathering enriches the soil with nutrient elements derived from lithospheric sources such as rocks (Buss et al., 2017; 2010) and controls the depth and distribution of nutrient inputs (Buss et al., 2010; Chapela Lara et al., 2018; Kirkby, 1985; Moore et al., 2017; Moore et al., 2005) while leaching removes the elements or moves them deeper into the soil profiles (Dawson et al., 2020; Porder et al., 2007b; Uhlig et al., 2017). On the other hand, through vegetation cycling (a process in which plants recycle mineral nutrients through litterfall and throughfall), plants scavenge for these elements and concentrate them on the surface through a process known as biolifting and cycle them back through litterfall and throughfall (Chadwick et al., 1999; Dawson et al., 2020; Foley et al., 2005; Uhliq and Blanckenburg, 2020). As such, limiting nutrient elements such as P, K and, in some cases, Ca (which becomes the limiting nutrient element in soils where P and K are either too low or absent) (Tanner et al., 1998; Uhlig et al., 2017; Uhliq and Blanckenburg, 2020) tend to be more concentrated near the surface than (other nutrient) elements such as Cl, Mg and (non-nutrient element) Na (Dawson et al., 2020; Jobbagy and Jackson, 2001; Porder et al., 2007a; Porder et al., 2007b).

Demands for bioavailable nutrient elements by plants in forests (and, often, grasslands) are mostly higher than the supply of the minerals through weathering (Dawson et al., 2020; Howell et al., 2016; Jobbagy and Jackson, 2004; Uhlig et al., 2017; Uhliq and Blanckenburg, 2020) largely because of leaching of the elements and erosion especially in carbonate (karst) environments such as Chenqi. It has been established that carbonate weathering is usually fast and that the major cations (such as Ca, Mg, K and Na) in carbonates and other minerals found in carbonate landscapes are leached from the weathering environments (Dere et al., 2016; Jiang et al., 2020; Jiang et al., 2014; Jin et al., 2010b; Kelly et al., 1998). To augment for this shortfall in supply, atmospheric deposition as well as vegetation (re)cycling of the mineral elements may play an important role (Chadwick et al., 1999; Dawson et al., 2020; Howell et al., 2016; Uhliq and Blanckenburg, 2020) in sustaining nutrient supply in (mostly)

forests and grasslands in both non-eroding (Chadwick et al., 1999) and eroding (Aciego et al., 2017) landscapes. In karst environments such as Chenqi, these processes may control bioavailable nutrient abundance. However, atmospheric mineral nutrient depositions in mountainous settings in Germany and the USA representing different lithologies were found to be lower than the losses (Johnson et al., 2009; Lang et al., 2016) and when atmospheric deposition was considered as the only nutrient source, soil profiles were found to have a net nutrient deficit (Aciego et al., 2017; Chadwick et al., 1999; Uhlig et al., 2017; Uhliq and Blanckenburg, 2020).

### 5.3.1 Effects of Plant Cycling on the Bioavailability of Mineral Nutrients

The lack of clear difference in the abundance of bioavailable cations (Table 5.1) between land uses and slope positions, suggests the likelihood that a different factor other than land use or vegetation cycling is influencing the availability and distribution of the bioavailable cations in Chenqi. However, it has been established that vertically, the topsoil abundance of the mineral-derived bioavailable cations in agricultural systems follows the trend K > Ca > Mg > Na (Chadwick et al., 1999; Dawson et al., 2020; Jobbagy and Jackson, 2001) and shows that vegetation (plant) cycling is the major driver of the vertical distribution of the nutrient elements. Bioavailable elements K and Ca are found in high concentrations in plant tissues in relation to their abundance in soils and rocks (Gordon and Jackson, 2000; Lang et al., 2016) and are therefore recycled through litterfall and throughfall in environments where mineral derived elements are low, consistent with the hypothesis of nutrient uplift reported by Jobbagy and Jackson (2004).

Vertically, the distribution of mineral nutrient elements derived from lithospheric sources shows greater topsoil abundance of K and P compared to other nutrient elements such as Ca and Mg (Jobbagy and Jackson, 2001). For example, Jobbagy and Jackson (2004) reported in a study on Argentinian soils that higher abundance of bioavailable K in the topsoil compared to other bioavailable mineral nutrients such as Ca and Mg explains greater influence of vegetation cycling in relation to other processes such as weathering and leaching that control mineral nutrient abundance in the soil. In the sloping farmlands and the abandoned farmlands of Chenqi, the abundances of the bioavailable nutrient elements (Ca, Mg and K) and Na show similar distributions (Fig 5.1 a-f) in topsoil abundance which decreases with depth to the bottom of the soil profiles. Also, in the sloping farmlands, the

ratios (used to compare the abundances of the bioavailable elements) of the abundances of K to the other bioavailable cations (Table 5.2, Figs 5.4 and 5.5) show variable topsoil (down to 30 cm in some sites) abundance of K with especially Ca and Na but (in most cases) higher than Mg.

Increasing bioavailable K/Ca ratio (Fig. 5.2a) with depth in site CQ7 in the bottom slope of the sloping farmlands suggests that bioavailable K and Ca are contributed to the soil by the bedrock. In forested ecosystems, Uhliq and Blanckenburg (2020) reported that high bulk nutrient element abundance results in low abundances of bioavailable mineral nutrient elements. Lower bioavailable Ca than K with depth in the site CQ7 corresponds to higher bulk Ca than K (Table 3.3, section 3.3.2) in the same site suggesting that the findings of Uhliq and Blanckenburg (2020) can be extended to agricultural soils.

Globally, due to vegetation cycling, bioavailable K and Na in soils were reported to have opposing distribution patterns where K revealed topsoil abundance and Na is enriched at depth (Dawson et al., 2020; Howell et al., 2016; Jobbagy and Jackson, 2001). While K and Ca are essential nutrient elements and, in environments where P is limited, they limit plant productivity, Na as a non-nutrient element, is often excluded by plant roots and is therefore often leached downwards (Dawson et al., 2020; Howell et al., 2016; Jobbagy and Jackson, 2004; Lang et al., 2016). The K and Na in the abandoned farmlands also revealed similar distributions with depth especially in the middle slope of the abandoned farmlands (Fig. 5.2d) but increase with depth in the top slope (Fig. 5.2e and f). Similarly, high Na in the top 30 cm compared to K (Table 5.2, Fig. 5.1 h-i) in the bottom slope of the sloping farmlands was interpreted as coming from the atmospheric deposition. However, in Chenqi, where bulk Na abundance in the soil is attributed to atmospheric deposition (section 3.3.2), the abundance of bioavailable Na in the soil is also likely a result of atmospheric dust deposition rather than vegetation cycling, which is consistent with several studies (Moraetis et al., 2015; Muhs and Budahn, 2009; Muhs et al., 2007) who reported atmospheric deposition as the source of Na in carbonate soils. The abundances of both K and Na in the abandoned farmlands suggest that their distribution does not differ in the early years of abandonment. In a chronosequence study in Argentina, Jobbagy and Jackson (2004) reported that the opposing distribution of bioavailable cations (Ca, K, Mg and Na) only manifests after 15 years. It is likely that, due to the sloping farmlands still being actively farmed and the

abandoned farmlands were abandoned for about 5 years, the effect of vegetation cycling may not yet be manifest.

There is also largely no variation (Table 5.1) in the abundances of the bioavailable nutrients between different sampling pits in the secondary forest. The vertical (Fig. 5.1 h-i) abundances of the elements increase with depth indicating that the nutrient elements are likely leached deeper into the soil or are lost through another process such as weathering or erosion (Bullen and Chadwick, 2016; Chadwick et al., 1999; Chaudhuri et al., 2007; Derry and Chadwick, 2007; Lang et al., 2016; Moore et al., 2005). Chaudhuri et al. (2007) and Moore et al. (2005) asserted that depletion of bioavailable nutrient elements in topsoil and their accumulation at depth in forested ecosystems results from the plants enhancing weathering, leaching and/or erosion (Heartsill Scalley et al., 2012). On the other and, higher abundance of bioavailable Ca in the top of the soil profiles (Fig. 5.1 h-i) relative to bioavailable Mg and Na suggests that in addition to the bedrock, vegetation cycling also contributes to the abundances and distribution of bioavailable Ca, consistent with the findings of Jobbagy and Jackson (2004) who studied the uplift of bioavailable nutrients in forested ecosystems in Argentina. Forested ecosystems were established to have higher topsoil K and Ca abundance compared to Mg and Na (Aciego et al., 2017; Jobbagy and Jackson, 2003; Uhliq and Blanckenburg, 2020) which was attributed to vegetation cycling. Also, the abundance of bioavailable Na (Fig. 5.1 h-i) in the secondary forest largely reveals no variation with depth, indicating that bioavailable Na likely contributed to the soil through atmospheric dust deposition. This interpretation is both consistent with the global distribution of Na in forested ecosystems (Dawson et al., 2020; Jobbagy and Jackson, 2001; Jobbagy and Jackson, 2004; Jobbagy and Jackson, 2003; Uhlig et al., 2017; Uhliq and Blanckenburg, 2020) and this thesis (Chapter 3.3.2).

Although both sloping farmlands and abandoned farmlands are agricultural ecosystems where the use of artificial fertiliser was widespread (and is set to continue) (Green et al., 2019), P abundance in the soil is very low, negligible in the bedrock and largely absent in bioavailable form (Hussey, 2018). Since in the absence of P, K becomes the limiting nutrient element (Tanner et al., 1998; Uhlig et al., 2017), and given that that legacy P in the soil from earlier agricultural activities is also absent, and that P content in plants is low (Hussey,

2018), it is likely that these findings further confirm that the K abundances in both sloping and abandoned farmlands are contributed to the soil by bedrock and vegetation cycling.

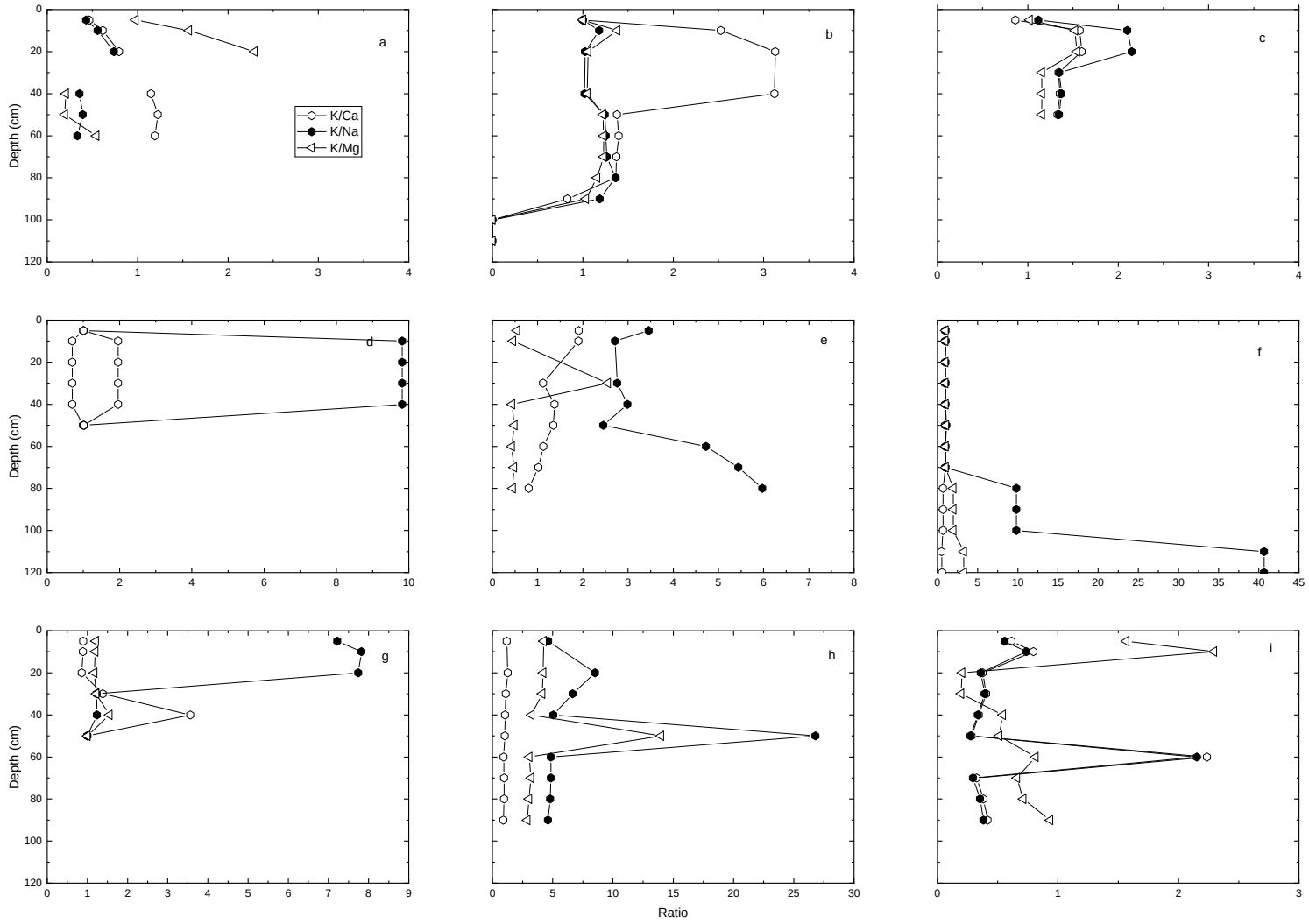

**Figure 5.2:** Ratios of the bioavailable cations Ca, K, Mg and Na in Chenqi watershed, a) CQ7 (bottom slope) b) CQ43 (bottom slope) c) CQ37 (middle slope) are from the sloping farmlands (No cores were drilled in the top slope and, therefore, no samples were collected). d) CQ38 (bottom slope) e) CQ40 (middle slope) f) CQ54 (top slope) are from the abandoned farmlands while g) CQ17 (middle slope) h) CQ13 (top slope) i) CQ64 (top slope) are from the secondary forest.

### 5.3.2 Effects of Lithology on Bioavailability of Mineral Nutrients

In Chapter 3 (Section 3.2.2) it was established that Chenqi has an abundance of rock-derived nutrient elements in the soil. It is therefore conceived that the bedrock contributes to the plant-availability of nutrient elements (Ca, Mg, and K) in the soil. Indeed, the lack of variation between sampling pits (Table 5.1) in the abundances suggests that both land use and vegetation cycling may not be the only processes controlling the distribution and the abundances of the bioavailable elements. In the bottom slope of the sloping farmlands, higher Na at CQ7 suggests atmospheric deposition similar to the findings of Muhs et al. (2007) who established evidence of dust deposition in the carbonate soils of Florida which were primarily formed from aeolian deposition of, mostly, African dust . Higher calcite content in the soil at the site (CQ7) relative to dolomite was interpreted as the reason for higher bulk Ca than Mg in the soil (Chapter 3.2.2, Table 3.2). The content of the aluminosilicates (Table 3.4, Chapter 3.2.2) in the soil at site CQ7 in the bottom slope of the sloping farmlands is lower compared to other sites in the same slope. This low abundance of aluminosilicates in the site did not explain the lowest abundance of bioavailable cations in the site compared to other sites in the slope. Jobbagy and Jackson (2004) established that soils with low abundance of nutrient elements in the soil have high abundance of bioavailable nutrient elements. However, compared to the other sites, CQ43 and CQ61 (both in the bottom slope of the sloping farmlands), CQ7 revealed lower bioavailable K, Mg, and Na in the top 30 cm in the same slope indicating that the findings of Jobbagy and Jackson (2004) may not extend to carbonate soils. Also, site CQ7 has significantly lower Mg/Ca ratios (Chapter 3.2.2, Table 3.2) than sites CQ43 and CQ61 indicating that CQ7 has higher calcite while CQ43 and CQ61 have more dolomite in the soil, suggesting that bioavailability of mineral nutrient elements is influenced by carbonate mineral content in the soil. Chapter 3 (Fig. 3.1, Chapter 3.2.1), as well as Jiang et al. (2020), established that bedrock with more dolomite content has more aluminosilicate impurities and, therefore, more mineral nutrient content than bedrock with more calcite content.

The abundance of the bioavailable elements in the bottom slope of the abandoned farmlands (CQ38) is also similar compared to the middle slope (CQ40 and 55) with only CQ46 revealing higher abundance. The Mg/Ca ratios also showed that the sites in both

slopes of the abandoned farmlands have higher dolomite content than calcite. Also, there is high content of aluminosilicates compared to the carbonate minerals (calcite and dolomite, Chapter 3.2.1, Table 3.2) in the soil, but the abundance of the aluminosilicates suggests that sites with high mineral nutrient content have low bioavailable nutrient abundance. Apart from the bottom enrichment of Ca and K in the top slope, all the slope positions in the abandoned farmlands have revealed low abundance of bioavailable cations supporting the conclusions of Jobbagy and Jackson (2004). Although in their study, Jobbagy and Jackson (2004) excluded soils formed on carbonate bedrocks and agricultural ecosystems, our results indicate that hypothesis (lower bioavailable nutrient elemental abundance compared to higher mineral nutrients) may hold true in both carbonate soils and agricultural ecosystems.

In all the slope positions in the secondary forest, there are higher silicate mineral contents in the soil than carbonate (Chapter 3.2.1, Table 3.2). However, bioavailable cation abundances in the bottom slope increase with depth reaching the highest abundance at 40 cm depth which suggests the contribution of the bedrock to the bioavailable budget in Chenqi. In the middle and the top slopes, abundances of the bioavailable cations are lower than the bottom slope in the secondary forest. However, site CQ25 (top slope) revealed significantly higher Ca abundance than the other sites in all the slope positions in the land use, which was interpreted as the contribution of the bedrock. The Mg/Ca ratios revealed that calcite is more abundant in the secondary forest than dolomite (with the exception of site CQ17) which explains the abundance of bioavailable Ca in the soil.

In all the land uses and slope positions, bioavailable cations are generally low and show no trend in abundance with respect to land use or slope positions. I suggest that vegetation cycling, aeolian deposition and bedrock all contribute to the abundance of bioavailable cations.

## 5.4 Conclusions

In this Chapter, I looked at the role of land use, slope positions, vegetation cycling and bedrock contributions to the bioavailability of mineral nutrient elements. I established that both bedrock and vegetation cycling contribute to the abundances of the bioavailable cations, and that land use and slope positions have no significant control on the abundance and distribution of the bioavailable nutrients. The findings in this thesis extend the conclusions of Jobbagy and Jackson (2004), who reported that higher abundance of mineral nutrients results in low abundances in the bioavailable nutrients in soils to carbonate soils which were excluded in their study. I also established that recovery and distribution of lost bioavailable mineral nutrient elements takes more than 5 years to manifest in both forested and agricultural ecosystems.

# Chapter 6

# Bioavailability of Mineral Elements in Koiliaris Critical Zone Observatory

**Author contribution declaration:** Rock cutting, and thin sections were conducted by Aminu Lawal under the guidance of Evangelos Mouchos. SEM analysis was also conducted by Aminu Lawal with help from Stuart Kearns. Extraction of exchangeable cations and ICP-OES were carried out by Aminu Lawal with guidance from Adam McAleer

## 6.1 Introduction

In this chapter, I extend my investigation into the role of vegetation, lithology, and land use in controlling the abundance of bioavailable mineral nutrients (Ca, K, Mg and Na) in Chenqi catchment of the SPECTRA Critical Zone Observatory (S-CZO) in southwestern China (Chapter 5) to the Koiliaris Critical Zone Observatory (K-CZO) in a Mediterranean environment near Chania on the Island of Crete. In Chenqi, this study established that lithology, vegetation cycling as well as aeolian dust deposition were found to be major contributors to the bioavailable cation abundance and distribution. Also, no correlation was found between land use or slope position and the bulk abundance of mineral nutrient elements in the soil at Chenqi (Chapter 3.3.2). In Chapter 4, lithology and aeolian dust deposition were established to control mineral nutrient production and soil formation in the K-CZO. In this Chapter, I investigate the role of lithology and vegetation on the bioavailability of mineral nutrients in the soil in the Mediterranean climate, with dry summers and wet winters, opposite that of S-CZO, which has wet summers and dry winters (Chapter 2.5.2). In this study, I measured exchangeable cations with depth at two sites studied previously (Moraetis et al., 2015): K4 and K5, a manmade terrace growing olive trees and a mountainous site mainly used for grazing, respectively (Section 2.5.2). The hypothesis is that bioavailability of mineral nutrients is dependent on the distribution of non-carbonate minerals in the soil. The findings in this (and previous) chapters will be compared and analysed in Chapter 7.

## 6. 2 Results

The bioavailable abundances of the elements reveal no variation between the different land uses (Table 6.1). The bioavailable abundances of Ca and Mg fluctuate with increasing depth at site K5, with bioavailable Mg revealing higher abundance at intermediate depth (Table 6.1). In comparison to other bioavailable cations, K abundances in site K4 are lower than K5 in the topsoil but are similar with increasing depth (Table 6.2, Fig. 6.2). Both sites (Table 6.2) revealed higher Mg abundance than K while the abundances of Na are similar in both sites. Figure 6.1 shows that abundance of Na is lower than Ca, Mg and K at both sites and is consistent with depth. Although Mg has the highest abundance at 20 cm at site K4 (Fig. 6.1)

and decreases at the bottom, Mg is higher in abundance at site K5 and does not vary substantially with depth. Both sites also reveal similar bioavailable Ca and K abundances (Fig 6.1, Table 6.1); Ca at both sites is higher in abundance than K.

Elemental ratios used to explain the relationship between the abundances of the bioavailable elements largely show similar distributions. The K/Na ratio is higher at site K4 than K5 (Fig. 6.2, Table 6.2) while K/Ca (higher at 5 cm in site K5) and K/Mg (higher at 26 cm at site K4) reveal similar distributions.

## 6.3 Discussion

### 6.3.1 Effects of Vegetation Cycling on Bioavailability of Nutrient Elements

Nutrient elements K and Na have contrasting importance to plants and K is more abundant in plant tissues than Na (Jobbagy and Jackson, 2004). Jobbagy and Jackson (2001) reported that the K/Na ratio in in plant tissues is much greater than in the soil because Na is not needed as a nutrient by plants and tends to be excluded by plant roots (Dawson et al., 2020). This difference in importance to plants means that bioavailable K, along with other bioavailable mineral elements Ca and Mg, is usually more abundant in topsoil than Na, consistent with the nutrient uplift hypothesis (Jobbagy and Jackson, 2001). In K-CZO however, higher abundance of bioavailable K in the soil than bioavailable Na is likely as a result of the abundance of clay minerals in the soil rather than vegetation cycling because olive trees grown in the Mediterranean region were reported (Restrepo-Diaz et al., 2008a; Restrepo-Diaz et al., 2008b) to have low or deficient K levels in olive leaves and orchards. Removal of K from the olive trees in large quantities by the olive fruits is attributed to the low abundance of K in the tree trunks and leaves (Restrepo-Diaz et al., 2008b) which was interpreted as the likely reason vegetation cycling of bioavailable K in the soil through litterfall or throughfall is low.

In forested ecosystems, bioavailable K has been reported to have higher topsoil abundances than other bioavailable cations Ca and Mg (Dawson et al., 2020; Derry and Chadwick, 2007; Uhlig and von Blanckenburg, 2019; Uhliq and Blanckenburg, 2020) but in K-CZO, bioavailable K is lower than both bioavailable Ca and Mg suggesting that K abundance in the soil results from other processes such as bedrock weathering (explained in the next section) other than vegetation cycling or that K is lost from the surface through erosion or leaching. Also,

Jobbagy and Jackson (2001) who analysed global distribution of bioavailable elements established that bioavailable Na has similar abundances with bioavailable K in top soils which increases with depth in young soils but decreases with depth in old soils. The soil in site K4 is older than K5 (Moraetis et al., 2015) but similar abundances of both bioavailable K and bioavailable Na in the two sites suggest that the conclusions of Jobbagy and Jackson (2001), who did not include carbonate soils in their study, may not hold true on calcareous soils such as the soil in K-CZO.

In forested ecosystems formed on young soils, Ca and Mg are more abundant in the topsoil (Bullen and Chadwick, 2016; Dawson et al., 2020; Howell et al., 2016; Jobbagy and Jackson, 2004) due to vegetation cycling. However, in both sites K4 and K5, I attribute the higher abundance of Ca and Mg in the soil, relative to K, to erosional deposition (Moraetis et al., 2015), contributions from the carbonate bedrock, or an anthropogenic activity such as ploughing that mixes the soil. Therefore, the evidence does not indicate vegetation cycling as a major influence on the abundances of the bioavailable elements at both sites, K4 and K5.

**Table 6.1:** Bioavailable cation abundances in Crete

| Site | Depth[a] | Ca[b] | K | Mg | Na |
|---|---|---|---|---|---|
| **K4** | 5[c] | 0.06 | 0.04 | 0.10 | 0.01 |
| | 10 | 0.10 | 0.05 | 0.20 | 0.01 |
| | 20 | 0.10 | 0.04 | 0.20 | 0.01 |
| | 26 | 0.10 | 0.06 | 0.06 | 0.00 |
| **K5** | 5 | 0.03 | 0.05 | 0.20 | 0.01 |
| | 12 | 0.20 | 0.05 | 0.20 | 0.02 |
| | 20 | 0.10 | 0.04 | 0.10 | 0.01 |
| | 30 | 0.20 | 0.05 | 0.20 | 0.01 |

[a] Elements measured by ICP-OES after acid digestion (Chapter 2.4.2) with values presented in mg/g after three replicate analyses

[c] Depths of the sampling sites vary with the cores

**Table 6.2:** Bioavailable elemental ratios

| Site | Depth[a] | K/Ca[b] | K/Na | K/Mg |
|---|---|---|---|---|
| **K4** | 5[c] | 0.70 | 6.00 | 0.30 |
| | 10 | 0.30 | 4.00 | 0.30 |
| | 20 | 0.30 | 5.00 | 0.20 |
| | 26 | 0.50 | 13.00 | 1.00 |
| **K5** | 5 | 1.60 | 5.00 | 0.30 |
| | 12 | 0.40 | 3.50 | 0.40 |
| | 20 | 0.30 | 6.00 | 0.30 |
| | 30 | 0.30 | 4.00 | 0.30 |

[a] Elements measured by ICP-OES after acid digestion (Chapter 2.4.2) with values presented in mg/g

[b] Depths of the sampling sites vary with the cores

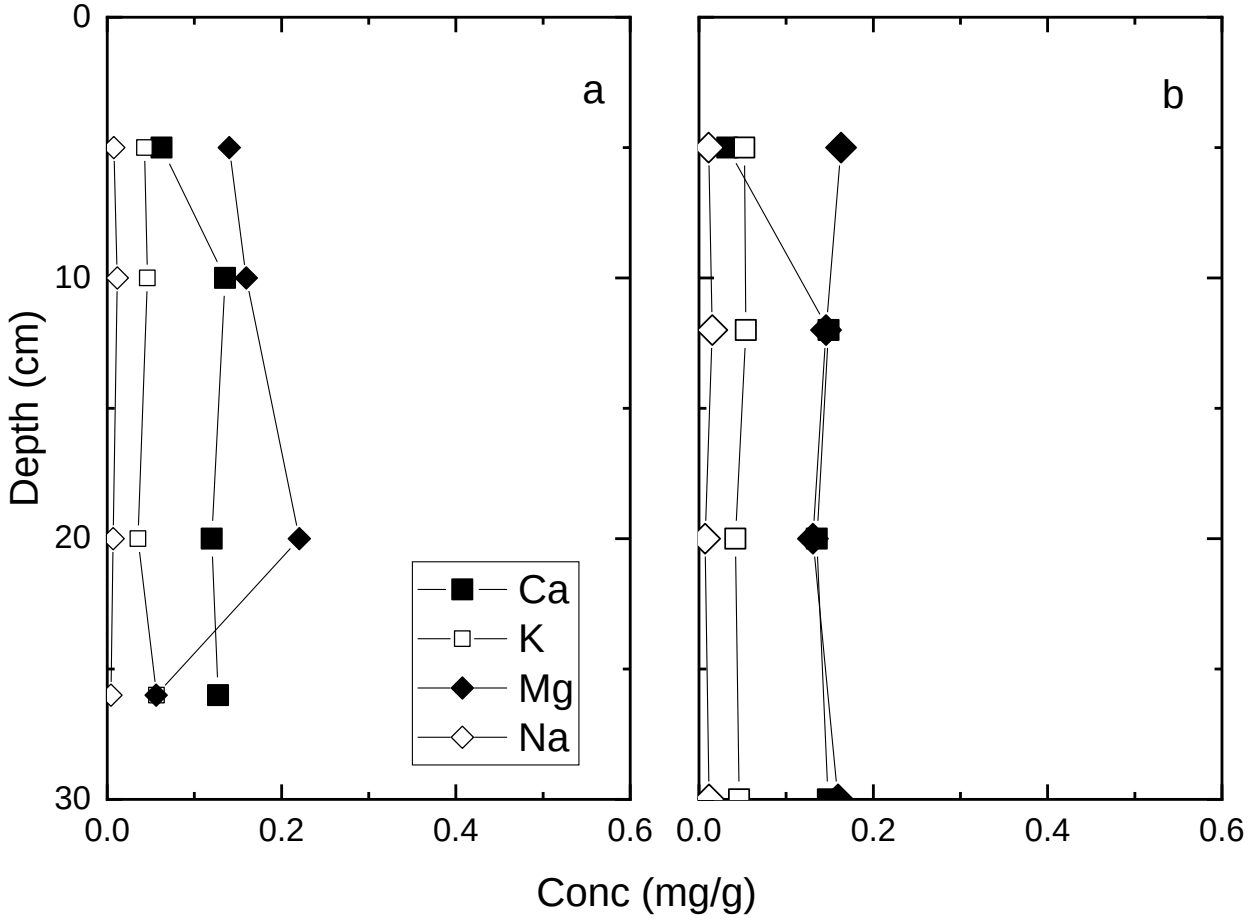


**Figure 6.1:** Abundances of Ca, K, Mg and Na in the soils of sites a) K4 and b) K5 in K-CZO. The depth of sampling varies between the two sites.

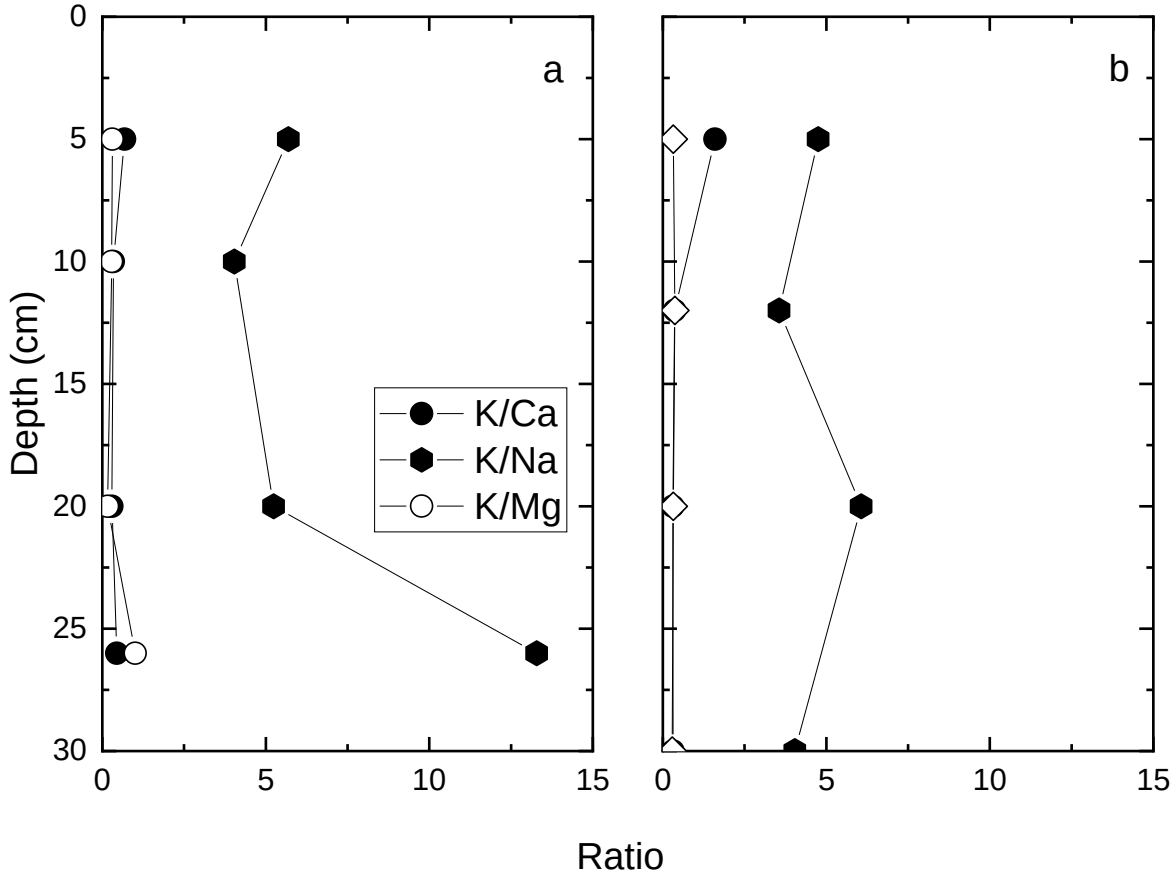

**Figure 6.2:** Abundances of K in relation to Ca, Mg and Na in the soils of sites a) K4 and b) K5 in K-CZO. The depth of sampling varies between the two sites.

### 6.3.2 Effects of Lithology on Bioavailability of Nutrient Elements

In this study (Chapter 4.3.1), the bulk abundance of mineral nutrients in the K-CZO was attributed to both the bedrock and atmospheric dust deposition. The bioavailable mineral nutrient abundances in the K-CZO sites was also interpreted as likely to have been contributed by the bedrock and atmospheric deposition. Abundances of bioavailable Na in the soil is attributed to the aeolian dust deposition due to lack of Na-bearing minerals in both sites K4 and K5 in either the bedrock or the soil as established in this study (Chapter 4.3.1) and Moraetis et al. (2015). Dust deposition has been established as the source of Na in calcareous soils in the other Mediterranean regions in southern Italy (Marzaioli et al., 2010), Croatia (Durn, 2003; Durn et al., 1999), Spain (Muhs et al., 2010) and other regions in the world such as northern Japan (Muhs and Budahn, 2009), Florida (Muhs et al., 2007); and Bermuda (Herwitz and Muhs, 1995). Sources of atmospheric dust to Crete were identified as the nearby Island of Santorini and the Sahara Desert in Africa (Moraetis et al., 2015) which were both found to be rich in Na-bearing minerals (Moraetis et al., 2015; Muhs et al., 2010; Muhs and Budahn, 2009). In addition, as the sites are less than 10 km from the coast, it's also likely that sea spray contributes Na to the soil.

The K abundances in both site K4 and K5 were attributed to the bedrock contribution. The presence of K-bearing minerals was established in the K-CZO bedrock (Chapter 4.2.1 and 4.2.2) and in the soil (Moraetis et al., 2015) at both sites. Although site K4 has lower K-bearing minerals than K5 (Chapter 4.3.1, Table 4.3) (Moraetis et al., 2015) the similarity in the abundances of the bioavailable K at both sites suggests that another process, likely atmospheric dust deposition, contributes to the abundance of bioavailable K in the soil at site K5 more than K4. Site K5 was reported by Moraetis et al. (2015) to have higher exposure to dust deposition and has lower contribution of bedrock to the nutrient budget than K4.

Being a forest, site K4 was expected to have higher abundance of Ca and Mg than K5. Uhlig and von Blanckenburg (2019), Jobbagy and Jackson (2001) and Uhlig et al. (2017) in different studies established that forested ecosystems have higher bioavailable Ca and Mg abundances than agricultural ecosystems. The similarity in the abundances of Ca and Mg at both sites was attributed to the contribution of the bedrock and dust deposition rather than land use or vegetation cycling. Also, the higher silicate mineral contents at site K4 than K5

(Chapter 4.2.1, Table 4.2) which was suggested to result from a longer period of weathering at the site (Moraetis et al., 2015) (Chapter 4.3) may indicate loss of Ca and Mg from the soil due to weathering. However, although site K5 has higher carbonate mineral content in the soils (Chapter 4.2.1, Table 4.2), similarity in the bioavailable Ca and Mg abundances with K4 indicate that higher mineral nutrient abundance in the soil often results in low availability of bioavailable nutrients, consistent with Jobbagy and Jackson (2004), who suggested that high mineral nutrient abundance results in low bioavailability of the nutrients.

## 6.4 Conclusions

In this chapter, the bioavailability of mineral nutrient elements Ca, Mg, K, and Na in the K-CZO was examined and although the two sites studied have different land uses, the contribution of vegetation cycling or land use to the abundance of bioavailable mineral nutrients could not be established. The bioavailable abundances of the elements are likely to have been contributed to the soil from the bedrock and atmospheric dust deposition.

# Chapter 7

## Comparison of Weathering and Nutrient Cycling between the SPECTRA and Koiliaris Critical Zone Observatories

## 7.0 Introduction

Both the SPECTRA (S-CZO) and Koiliaris (K-CZO) Critical Zone Observatories are situated in mountainous karst environments and have experienced intensive agriculture and soil degradation. There are slight differences in the lithology, land use history, MAT and MAP between these two CZOs, but the most notable difference is the opposite seasonality: dry summers and wet winters in the K-CZO and wet summers and dry winters in the S-CZO (Chapter 2.5.2).

In Chapter 3, dissolution and removal of calcite and dolomite in Chenqi, Chenjiazhai and Tianlong (S-CZO, representing degrading, recovering and pristine environments, respectively) was found to leave the soil enriched with elements derived from non-carbonate minerals, consistent with the hypothesis that mineral nutrient production is dependent on the distribution of non-carbonate minerals in the bedrock. Similarly, in Koiliaris (Chapter 4), the major processes controlling the production of mineral nutrients in the soil were found to be lithology and atmospheric dust deposition, with atmospheric deposition being more prominent in one site than the other. Bioavailability of the mineral nutrient elements in the two CZOs were also found to be driven by lithology and aeolian deposition (Chapters 5 and 6). In this chapter, the differences in the lithology of the two CZOs will be discussed (Chapter 7.1) and the lithological and climate controls on weathering will be explored in the context of soil mineral nutrient production and soil mineral nutrient bioavailability (Chapter 7.2). I hypothesize that climate variability, weathering time and slight difference in lithology are likely to influence the impact of bedrock in mineral nutrient production, distribution, and abundance in the two CZOs.

## 7.1 Bedrock Mineralogy

Bedrock composition regulates ecosystems and enhances vegetation in agricultural and forested environments (Hahm et al., 2014; Jiang et al., 2020). Although as established in this study (Chapters 3 and 4), bedrock composition is one of the major controls of mineral nutrient production in both the SPECTRA and Koiliaris CZOs, differences in lithology, age and weathering time may likely contribute to the difference in the extent of the influence of the bedrock in controlling the mineral nutrient production, abundance, and distribution. These differences include soil depth, weathering time, and the aluminosilicate content of the soil.

The bedrock in the S-CZO, formed in the mid-Triassic period (Wang et al., 2004a; Wang et al., 2004b), is older than the bedrock in Koiliaris the K-CZO, which was formed in the Upper Cretaceous (Moraetis et al., 2011) and therefore has had more time to weather.

Typical of karst environments, calcite, dolomite then quartz (Figs 3.1, 4.1 and 4.2) are the dominant and most widely distributed minerals in the bedrocks in both CZOs as established in earlier studies (Moraetis et al., 2015; Wang et al., 2004a) and in this study (Chapters 3 and 4). Both bedrocks have other minerals mostly regarded as impurities such as kaolinite, orthoclase, illite, pyrite, accessory hematite, fluorite and celestine (Figs 3.1, 4.1 4.2 and Appendix 1A; Moore et al., 2017; Moraetis et al., 2015; Wang et al., 2004a). Some minerals in the bedrock in Chenqi (such as celestine, Appendix A1) were not found in Koiliaris. However, the bedrock in Koiliaris also contains minerals such as vermiculite (Moraetis et al., 2015) that were absent in Chenqi. Similarity in the carbonate contents (Tables 3.1 and 4.1) in the bedrocks at both CZOs, likely suggests that factors other than lithology, such as climate and weathering time, may be responsible for differences in the production of mineral nutrients in the two CZOs. However, the slight difference in lithology may cause differences in mineral nutrient production, retention, and distribution by increasing soil acidity through dissolution of celestine or increasing mineral-water contact time due to high water retention capacity of vermiculite.

The bedrock bulk chemistry revealed that the K-CZO has slightly higher dolomite content (Table 4.2) than in S-CZO (Table 3.2) indicating that the bedrock in the K-CZO is likely to have slightly higher porosity than in the S-CZO. The higher porosity enhances dissolution of carbonate minerals by increasing the contact time between the minerals and meteoric water percolating into the bedrock. In both CZOs, the dissolution of carbonate minerals leaves the soil matrix enriched with silicate mineral 'impurities' inherited from the bedrock which control mineral nutrient production and distribution in the soils (Chapters 3 and 4; Moore et al., 2017; Moraetis et al., 2015). The $SiO_2/Al_2O_3$ ratio in the soils normalised to the bedrock $SiO_2/Al_2O_3$ ratio at both sites (averages of 0.5 and 0.9 for the K-CZO and S-CZO, respectively; Tables 7.1 and 7.2) suggests that more aluminosilicates weather to Al-rich clays in the K-CZO than in the S-CZO.

**Table 7.1:** Abundances of quartz relative to other aluminosilicates in both the soil (s) and the bedrock (r) in K-CZO.

| Sites | Depth (cm) | $SiO_2/Al_2O_3$s | $(SiO_2/Al_2O_3)$s/$(SiO_2/Al_2O_3)$r |
|---|---|---|---|
| **K4** | **5** | 6.7 | 0.8 |
| | **10** | 5.6 | 0.7 |
| | **20** | 4.6 | 0.6 |
| | **26** | 5 | 0.6 |
| | **Average** | 5.5 | 0.7 |
| **K5** | **5** | 4 | 0.4 |
| | **12** | 3.7 | 0.3 |
| | **20** | 3.7 | 0.3 |
| | **30** | 3.8 | 0.4 |
| | **Average** | 3.8 | 0.4 |

Both bedrocks have similar carbonate content (Tables 3.1 and 4.1), but the bedrock in the S-CZO has higher iron and aluminosilicate content (Table 3.2) than the K-CZO (Table 4.2) and is thus able to produce more soil matrix (quartz, clays, and metal (hydr)oxides) as well as provide more mineral nutrients to the soil. Except for site K4 in the K-CZO (with Si range 66 – 71%, Table 4.3), the soils at both CZOs have similar abundances of aluminosilicates suggesting that in some parts of the K-CZO, either the bedrock has more abundance and distribution of aluminosilicates, an external source contributes to their elemental budget, or carbonate minerals dissolve faster in the K-CZO than the S-CZO. The climate at the K-CZO (wet winters and dry summers) provides suitable conditions for faster calcite dissolution (lower MAT than S-CZO and in the winter and high precipitation) than in S-CZO and may be the driver of carbonate weathering. Also, the loss of Si in K-CZO to more Al-rich aluminosilicates (Tables 7.1 and 7.2) suggests the likelihood that longer weathering time also contributes to the production of mineral nutrients in the K-CZO more than in the S-CZO.

**Table: 7.2:** Abundances of quartz relative to other aluminosilicates in both the soil and the bedrock in S-CZO

| [a]Site | Sample | $SiO_2/Al_2O_3s$ | $SiO_2/Al_2O_3r$ | $(SiO_2/Al_2O_3)s/(SiO_2/Al_2O_3)r$ |
|---|---|---|---|---|
| **SFB** | **CQ7** | 2.7 | 2.9 | 0.9 |
| | **CQ41** | 3.7 | 4 | 0.9 |
| | **CQ43** | 2.6 | 4 | 0.7 |
| | **CQ45** | 4.8 | 5.7 | 0.8 |
| | **CQ61** | 3.3 | 5.4 | 0.6 |
| **SFM** | **CQ37** | 3.2 | 4 | 0.8 |
| **AFB** | **CQ38** | 2.7 | 3 | 0.9 |
| **AFM** | **CQ1** | 3.3 | 3 | 1.1 |
| | **CQ40** | 3.3 | 4.3 | 0.8 |
| | **CQ46** | 3.3 | 3 | 1.1 |
| | **CQ55** | 4 | 3.6 | 1.1 |
| **AFT** | **CQ54** | 3.8 | 3.3 | 1.2 |
| **SeFB** | **CQ16** | 4 | 4 | 1.0 |
| **SeFM** | **CQ17** | 3.3 | 3.5 | 0.9 |
| **SeFT** | **CQ2** | 3.0 | 3.6 | 0.8 |
| | **CQ13** | 4 | 3.5 | 1.1 |
| | **CQ25** | 2.6 | 3.6 | 0.7 |
| | **CQ48** | 2.9 | 9.3 | 0.3 |
| | **CQ64** | 3.8 | 2.8 | 1.4 |

[a]SFB = sloping farmlands bottom; SFM = sloping farmlands middle; SFT = sloping farmlands top; AFB = abandoned farmlands bottom; AFM = abandoned farmlands middle; AFT abandoned farmlands top; SeFB = secondary forest bottom; SeFM = secondary forest middle; SeFT = secondary forest top

## 7.2 Weathering and Mineral Nutrient Production

The mass transfer profiles of the elements Ca, Mg, K, Na Si, Al, and Fe in the soils of both CZOs largely indicate partial depletion of the elements in the soils, while P mostly showed enrichment. In both the SPECTRA and Koiliaris CZOs, conservation of elements such as Si and Al (Figs 3.3 - 3.5, 3.9 – 3.11, 3.15 – 3.17 and 4.3) indicated that aluminosilicates were retained in the soil after the dissolution of calcite and dolomite. Aside from site K4 in the K-CZO (higher) and Tianlong in the S-CZO (lower), the sites in both CZOs have similar abundances of Si in the soils suggesting similar abundances of aluminosilicates. Although the $(SiO_2/Al_2O_3)_{soil}/(SiO_2/Al_2O_3)_{rock}$ ratio (Table 7.1) in the K-CZO suggests more weathering of aluminosilicates in the K-CZO, there is more abundance of Si-containing minerals (Fig. 7.1) suggesting that the high Si content in the soil is from the more abundant and more widely distributed quartz from the bedrock (Figs 4.1 and 4.3). However, the mass transfer profiles of Si (Fig. 4.3) revealed conservation and enrichment of Si in the soil at the K-CZO suggesting that Si addition from atmospheric dust my distort the effects of weathering time. It is also likely that the high Si abundance in the K-CZO is largely due to the abundance of chert in the bedrock or that dust deposition in the K-CZO is more prominent than in the S-CZO.

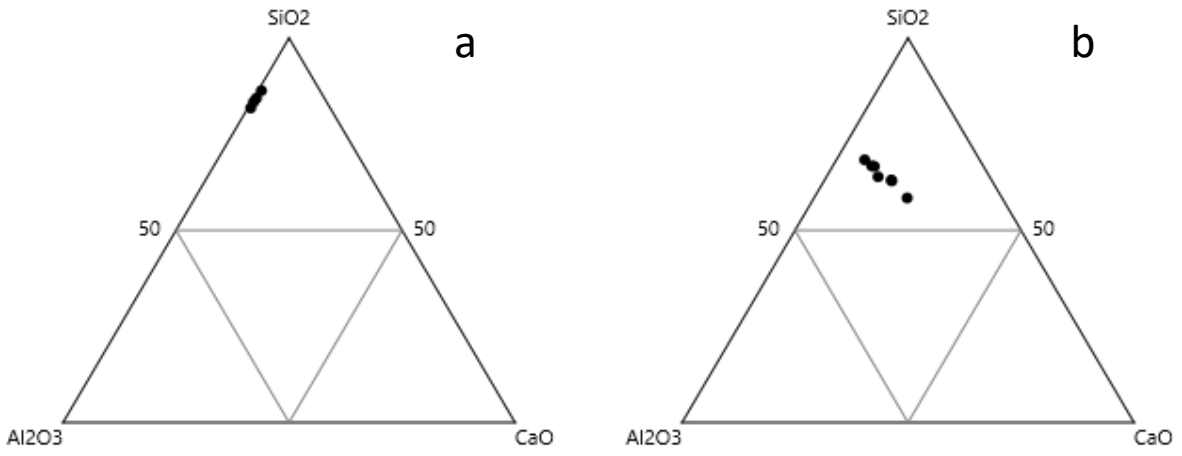


**Figure 7.1:** Ternary plot of a) average SAC in K-CZO and b) in S-CZO indicating the likely higher abundance of quartz in K-CZO with respect to other mineral components in the soil.

The higher abundance of Si in site K4 is also likely a result of insoluble chert in the bedrock (Chapter 4.3) or longer weathering time than site K5 in the K-CZO. There is also the likelihood of the other sites (in both CZOs) having higher clay mineral abundance than site K4. Moraetis et al. (2015) reported higher kaolinite content at site K4 than K5 suggesting that similarity in Si abundance in site K5 with site K4 is likely due to atmospheric dust deposition from the Sahara. The soils in Chenqi and Chenjiazhai are older and have higher (alumino)silicate contents than in the K-CZO sites. Muhs and Budahn (2009) reported that older carbonate soils in Jamaica reveal low Si abundances compared to the younger soils in due increased loss of Si from the soil and formation of more Al-rich minerals. Similarly, it is likely that the lower Si abundance in the pristine forest soil in Tianlong in the S-CZO is because of loss of Si due to weathering of aluminosilicates to more Al-rich clays due to increased soil acidity from decomposing vegetation which, according to Hahm et al. (2014), could influence subsurface porosity and mineral dissolution rates. However, mass transfer profiles of Si in Tianlong revealed conservation of Si which is either due to lower abundance of clay minerals in the soil or lower external addition to the elemental Si budget in Tianlong soil. Since we do not know the bedrock composition in Tianlong, it is likely that the bedrock has lower (alumino)silicates than the bedrock at the other sites at both CZOs.

Mineral nutrient elements such as Fe, K, P, and (non-nutrient) Na were also largely conserved (with P mostly enriched, Figs 3.6 – 3.8, 3.12 – 3.14, 3.18 – 3.20 and 4.4) in the soil in both CZOs indicating that the elements were retained in the soil after the dissolution of the dominant calcite and dolomite. In the S-CZO, past agricultural activities have left no legacy P content in the soil (especially in the degrading Chenqi and the recovering Chenjiazhai watersheds) from fertiliser addition (Hussey, 2018). Tianlong watershed (pristine forest) also has similar P content with the other watersheds in the S-CZO although it has not been affected by anthropogenic perturbation suggesting that conservation and enrichment of P in the soil profiles in the S-CZO indicate that atmospheric dust deposition is also a major contributor to the mineral nutrient abundance in the S-CZO. In the K-CZO, site K4 has similar bulk abundance of P with the sites in the S-CZO while at site K5, P abundance in the soil is higher than in site K4 and the sites at the S-CZO. Similarly, Na abundance (Tables 3.3, 3.5, 3.7 and 4.1) and conservation in the soil profiles (Figs 3.6 – 3.8, 3.12 – 3.14, 3.18 – 3.20 and 4.4) indicate that in both CZOs atmospheric deposition is an important

factor in the abundance of P, Na and Si (in K-CZO) in the soils which was confirmed by higher abundance of Na at site K5 (Table 4.3) in the K-CZO, a site reported (Moraetis et al., 2015) to be exposed to significant aeolian input. In the S-CZO, the sources of aeolian inputs are the neighbouring mining sites (Tang et al., 2016; Yang et al., 2015), while in the K-CZO, the sources are sea spray, Santorini and African dust (Moraetis et al., 2015).

Low abundances of P in the soils of both CZOs are largely attributed to the absence of P-bearing minerals in both bedrocks. However, it is also likely that P is removed from the soil by the dissolved Ca from the carbonate bedrocks. Jiang et al. (2020) reported that dissolved Ca from carbonate bedrocks in forested ecosystems form apatite with P and either percolates into the bedrock or is removed through weathering. Also, Bingham et al. (2020) reported that in agricultural ecosystems, P often precipitates onto soil particles, forming hydroxyapatite or sorbs onto Fe (hydr)oxides. However, in both CZOs, there is no notable relationship between P and Fe (in hematite, the most abundant and widely distributed Fe mineral in both CZOs).

The SEM images (Figs 3.1, 4.1 and 4.2) indicated that hematite is the dominant Fe-bearing mineral in both the CZOs consistent with the findings of Muhs and Budahn (2009) who reported hematite being the dominant Fe mineral in the carbonate soils of Jamaica. All the sites in both CZOs have similar bulk Fe abundance in the soils except for Chenjiazhai which has higher Fe content in the soil. The mostly conservative behaviour of Fe in the soils and the abundance of hematite in the bedrock (Figs 3.1, 4.1 and 4.2) at both CZOs indicates bedrock weathering as the source of Fe. In addition, similarity in soil Fe content in both CZOs indicates that bedrock age and difference in climate have no influence on the Fe content in the soils.

Sites with higher dolomite contents in the soils as shown by the Mg/Ca ratios (Tables 3.4, 3.6, 3.8 and 4.4) also have higher aluminosilicate contents in the soils in both CZOs except for site K5 in Koiliaris which has higher dolomite content than site K4, but lower aluminosilicate contents in the soil. Although SEM data (Figs 3.1, 4.1, 4.2 and Appendix 1) indicated that dolomite-dominated bedrock has a lower distribution of non-carbonate minerals, there is a more even distribution of fractures in the dolomite-dominated rocks which form small crystal interstices (Wang et al., 2004a) and small cavities providing ideal conditions for water retention and promoting higher rock-mineral contact time and more

dissolution. Although dolomite-dominated bedrock has a lower distribution of aluminosilicates than calcite-dominated bedrock, the *soil* formed on dolomite-dominated bedrock has higher aluminosilicate content because the higher porosity in dolomite allows more weathering and removal of carbonate minerals, enriching the soil with more aluminosilicates.

The different dissolution behaviour of calcite in the limestone bedrock makes it easier for the dissolution residues to be carried through by water to accumulate in cracks and karst hollows making soils more likely to accumulate in these cracks than in dolomite bedrock (Wang et al., 2004a; Wang et al., 2004b). This difference in behaviour reduces water-mineral contact time and low carbonate dissolution consistent with the findings of Jiang et al. (2020) who reported dolomite-dominated bedrock in southwestern China produces thicker soils than calcite-dominated bedrock. These processes indicate that bedrock lithology influences weathering reactions and as well as mineral nutrient production, abundance, and distribution within the CZOs.

Both CZOs have similar carbonate mineral abundance in the soil but the difference in the abundances of non-carbonate mineral impurities indicates that bedrock lithology, as established in this study and Moraetis et al. (2015), is the major control in the production of mineral nutrients in both CZOs.

The soils and bedrocks at both CZOs were established in this study (Fig. 4.1 and 4.2) and by Moraetis et al. (2015) to have no minerals of mafic origin, however, Moraetis et al. (2015) also established the abundance of elements such as Mn of mafic origin consistent with the mineralogy of the African dust (Muhs et al., 2007) in the soil at site K5 in the K-CZO. The presence of these elements in the soil was attributed to the dust deposition from the African Sahara.

### 7.3 Controls on Mineral Nutrient Bioavailability

Bioavailability, abundance, and distribution of mineral nutrients in soils have been reported to depend on the abundance of mineral nutrients (Dawson et al., 2020; Jobbagy and Jackson, 2004). In this study, it was established (Chapters 3 and 4) that the soils in both the S-CZO and K-CZO have abundance of bulk mineral nutrients but most of the nutrients are, however, likely not biologically available. Higher abundance of mineral nutrient elements in

the soil has been reported (Jobbagy and Jackson, 2001; Uhlig et al., 2017; Uhliq and Blanckenburg, 2020) to result in lower abundances of lithospheric bioavailable elements in the soil. In addition to lithospheric sources (Uhlig et al., 2017), lower abundances or loss of the bioavailable elements in forested (Howell et al., 2016) and agricultural ecosystems (this thesis) are replenished through vegetation cycling or atmospheric deposition.

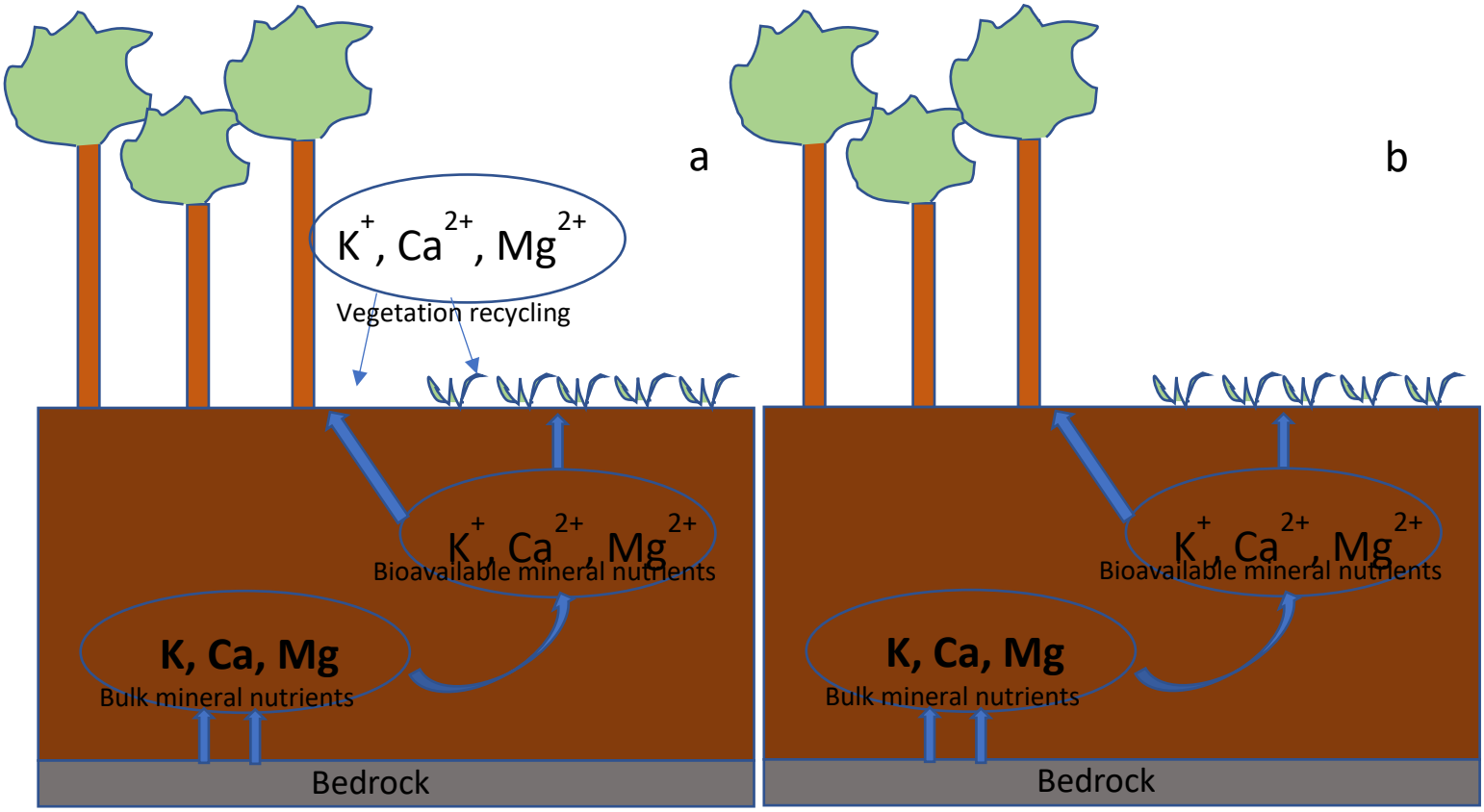


**Figure 7.2:** A conceptual schematic that explains the movement of mineral nutrient element from the bedrock to the soil and to the plant available form. a) Showcases the concept of the movement of the elements in S-CZO and their return back to the soil through vegetation cycling (indicated by smaller arrows to show the low contribution of vegetation cycling to the overall cycling of mineral nutrients in S-CZO). b) Shows similar process in K-CZO but the site has no contribution to the cycling of the elements from the vegetation.

In both the S-CZO and K-CZO, bioavailable mineral nutrient abundances were established in this thesis (Chapters 5 and 6) to be controlled by both the bedrock and atmospheric deposition and not vegetation cycling or fertiliser addition. It was also established (Chapter 6) that trees in Koiliaris have no significant K content in their leaves and trunks (Restrepo-Diaz et al., 2008a) suggesting that recycling of bioavailable K by vegetation does not contribute to the bioavailable nutrient pool in the soil. Although in the S-CZO, both sloping farmlands and abandoned farmlands are agricultural ecosystems where the use of artificial fertiliser was widespread (Green et al., 2019). However, despite having similar abundances of bulk aluminosilicates in the soils at both sites, the K-CZO has lower bioavailable K than the S-CZO. This difference in the abundance of bioavailable K at both sites is likely explained by the difference in vegetation types, karst system and extent of soil degradation. Difference in climate affects the karst system development (Auler and Smart, 2003) and the karst system in the K-CZO is characterised by fast infiltration and low water retention (Moraetis et al., 2011; Nikolaidis et al., 2013) which likely removes K from the soil and makes it unavailable for plants. Also, the olive trees in the K-CZO were reported to have low K content in both leaves and bark and vegetation cycling in the K-CZO is likely lower than in the S-CZO. Although fertiliser addition has no effect in the bulk abundance of mineral nutrients in S-CZO (Chapter 3.3.2), it is likely that the longer abandonment of the sites in the K-CZO, faster water infiltration and low vegetation cycling is responsible for the lower bioavailable K abundance in the K-CZO than in the S-CZO. Hussey (2018) reported that P abundance in the S-CZO soil is very low, negligible in the bedrock and largely absent in bioavailable form confirming the finding in this study (Chapter 5.2.2), that bioavailable P abundances in the soil are largely due to atmospheric dust deposition from mining activities in neighbouring environments (Tang et al., 2016; Yang et al., 2015). Hussey (2018) also reported absence of legacy P in the soil from earlier agricultural activities and low P content in plants. Abundances of P in soils in different environments depends on climate and soil age (Jarvie et al., 2014) and parent material composition (Porder and Hilley, 2010). However, although soil age in both CZOs are different, bulk P abundances are largely similar indicating that the abundance of bulk P in the soil is driven by similar processes such as atmospheric deposition, fertiliser addition and/or biolifting. It was established (Chapter 5.3) that the S-

CZO has no bulk P abundance due to fertiliser addition and bulk P in S-CZO was attributed to atmospheric deposition. It is likely that bulk P abundance from agricultural sources is impacted by the low nutrient buffering capacity of the soils or through rapid removal from the soil before it becomes biologically available (Jarvie et al., 2014). Low abundance of bulk P in both CZOs was, therefore, interpreted as the evidence of lack of bioavailable P in both CZOs.

Similarly, it was established (Chapter 3.3) that fertiliser addition does not contribute to the bulk K abundance in the soils in the S-CZO. It was also expected that after about 50 years of abandonment, there are no bulk K abundances due to fertiliser application in the K-CZO. Therefore, the bioavailable K abundances in both CZOs were attributed to the bedrock lithology.

As established in this study (Chapters 5 and 6) bedrock lithology is one of the major controls on the bioavailable mineral abundances in both CZOs. The bulk abundances of mineral nutrient elements K, Ca, and Mg in both CZOs were attributed to the bedrock. In both CZOs, however, sites with more dolomite contents, reported by Zhu et al. (2020), and established in this study (Chapter 4) to have higher mineral nutrient abundances than sites with more calcite contents. However, the low bioavailability of mineral nutrient elements is found to be low in forested soils that are rich in bulk mineral nutrients (Jobbagy and Jackson, 2004) but this finding was found to hold true in the carbonate soils of both CZOs indicating that the findings of Jobbagy and Jackson (2004) can be extended to agricultural soils in carbonate environments.

## 7.5 Conclusions

In this chapter, controls such as bedrock age, weathering time and climate, on mineral nutrient production, abundance, and distribution in the S-CZO and K-CZO were analysed. It was established that bedrock lithology is the major control in the production, abundance and distribution of mineral elements and their bioavailability in both CZOs. However, bedrock age influences the production, abundance, and distribution of mineral nutrient elements in both CZOs. The difference in climate was found not to have a significant impact on the role of lithology in mineral nutrient production. In addition, in both CZOs,

atmospheric dust deposition contributes to the abundance of mineral nutrient elements in both CZOs. Overall, both CZOs show similarity in the processes that control mineral nutrient in the soil.

# Chapter 8

## Summary, Conclusions and Future Work

## 8.1 Introduction

This chapter summarises the key findings outlined in Chapters 3, 4, 5, 6 and 7 and addresses the impacts of these findings in the wider carbonate CZ context. Potential further work is also presented.

## 8.2 Lithological Controls on Weathering and Mineral Nutrient Production in Karst Terrains

In Chapter 3, bedrock and soil bulk chemical data and soil elemental mass transfer profiles from Chenqi, Chenjiazhai and Tianlong watersheds in the SPECTRA CZO (S-CZO) in southwestern China were presented to identify controls on the production, abundance, and the distribution of mineral nutrients in the soil. It was hypothesized that the abundance of silicate mineral impurities in the dominant carbonate bedrock control the production and distribution of mineral nutrient elements in the soil at S-CZO.

The bedrock lithology in Chenqi (Fig. 3.1., Chen and Bi, 2011; Moore et al., 2017; Wang et al., 2004a), dominated by calcite, dolomite then quartz, also contained aluminosilicates such as illite, kaolinite, and orthoclase; accessory hematite, pyrite and celestine. Presence of some of these minerals (e.g. hematite, Fig. 3.1) along weathering veins, cracks and pores indicated dissolution of the carbonate minerals. Bulk chemistry of the bedrock (Table 3.1) and the soil (Table 3.3) confirms that the primary weathering reaction in the S-CZO is the dissolution of calcite and dolomite leaving the soil matrix enriched with the non-carbonate minerals. In addition, elemental mass transfer profiles (Figs 3.3 – 3.12) suggest conservation of the non-carbonate minerals in the soil. Enrichment of some of the elements (such as P) and abundance of Na, despite the absence of Na-bearing minerals, were attributed to external sources (Muhs et al., 2010; Uhliq and Blanckenburg, 2020) or internal redistribution such as biolifting (Bullen and Chadwick, 2015).

Land use was found to have no influence in elemental mass transfer profiles in the S-CZO. In forested ecosystems in silicate environments, weathering of minerals was often lowest at mid slopes (Egli et al., 2008) but the lack of trends in mass transfer profiles in both the secondary forest (Figs 3.5 and 3.8) in Chenqi and the pristine forest in Tianlong (Figs 3.18 – 3.20) with respect to slope position suggests that land use or slope position does not impact on weathering of carbonate minerals in karst environments. This finding also extends to the

other land uses (sloping farmlands and abandoned farmlands in Chenqi and Chenjiazhai watersheds, Figs 3.3, 3.4, 3.6, 3.7 and 3.9 – 3.12). Artificial fertiliser addition to the soil in the sloping and abandoned farmlands does not appear to contribute to the nutrient abundance due to reported absence of P in the plants (Hussey, 2018) and low abundance in the soil (Tables 3.3, 3.5 and 3.7).

In Chapter 4, bedrock and soil bulk chemical data and mass transfer profiles from the Koiliaris CZO (K-CZO) near Chania on the island of Crete, Greece were presented. In the K-CZO, the dominant calcite and dolomite in the bedrock (Figs 4.1 and 4.2) dissolve and leave the soil matrix enriched with clay minerals, mostly illite, kaolinite and orthoclase and other metal (hydr)oxides such as accessory hematite and pyrite. Other studies (e.g., Moraetis et al., 2015) also reported abundance of muscovite and vermiculite in the soils in Koiliaris. Soil bulk chemistry (Table 4.3) confirms dissolution of carbonate minerals is the primary weathering reaction in Koiliaris, leaving the soil enriched with aluminosilicates and other non-carbonate minerals. Abundances of elements of mafic origin especially at site K5 (Table 4.3, Moraetis et al., 2015), and the conservation of some elements such as Na and P (Figs 4.3 and 4.4) mass transfer profiles in the soil at both sites were attributed to the contribution of external sources such as atmospheric dust deposition

The implication of these findings are as follows:

1. In highly disturbed, intensely cultivated, mountainous agricultural sites, soil formation from bedrock plays a dominant role in soil mineral nutrient abundance and distribution and thus the impacts of land use and erosion may be less significant than generally thought.
2. Influence of mineral nutrient inputs from fertilizer have less long-term significance on the recovery of degraded agricultural sites.

### 8.3 Controls on the Bioavailability of Mineral Nutrient Elements

In Chapters 5 and 6, exchangeable cations were extracted to investigate the controls on bioavailability of the mineral nutrients in both the S-CZO and K-CZO. It was hypothesized that the bioavailability of mineral nutrient elements in these soils is controlled by land use (extent of recovery) and bedrock lithology. The indications (e.g., Chadwick et al., 1999; Lang et al., 2016) that forested ecosystems are losing the ability to efficiently cycle nutrient

elements have led to the assumptions that anthropogenic activities are impacting the nutrient dynamics in both forested and agricultural ecosystems. It was established that abundance and distribution of bioavailable elements is dependent on the distribution of bulk mineral nutrient elements (which is controlled by bedrock lithology) in both forested and agricultural ecosystems. In addition, it was established that vegetation cycling contributes to the bioavailable mineral nutrient abundances in S-CZO but has no significant influence n K-CZO. The findings of this study therefore have the following implications:

The indications (e.g., Chadwick et al., 1999; Lang et al., 2016) that forested ecosystems are losing the ability to efficiently cycle nutrient elements have led to the assumptions that anthropogenic activities are impacting the nutrient dynamics in both forested and agricultural ecosystems.

The findings of this study therefore have the following implications:

1. Ecosystem recovery after abandonment of a disturbed karst CZ likely requires about 15 years to begin to show natural recovery of soil fertility
2. Years of abandonment are a factor in the contribution of vegetation cycling to the recovery of bioavailable mineral nutrients in degraded agricultural ecosystems.

## 8.4 Future Work

This research has established the sources and controls of mineral nutrient production, distribution, and bioavailability in the soils of two agricultural karst CZOs. However, further work is needed to investigate and compare the study sites with more on-agricultural karst CZs within China and globally. There is also the need to study more karst CZs across more diverse climatic zones (e.g cold wet, cold dry etc). There is also a need to further explore the mineralogy of the sites in China and Greece as well as the contributions of Aeolian deposition (both China and Greece) and marine inputs (in Greece).

## 8.5 Closing Remarks

With about 25% of global population, the impacts of karst environments on global socio-economic well-being and environmental sustainability cannot be overemphasized. Intensive agricultural activities in karst regions have been reported to be severely affected by soil

erosion and low nutrient availability which, invariably, lead to poverty, malnourishment, and loss of biodiversity. In this thesis, it has been established that bedrock lithology, atmospheric deposition and longer recovery time are the key drivers of mineral nutrient production and distribution in karst regions rather than land use or erosion.

# References


Aciego, S.M. et al., 2017. Dust outpaces bedrock in nutrient supply to montane forest ecosystems. Nat Commun, 8: 14800.

Amundson, R., Richter, D.D., Humphreys, G.S., Jobbagy, E.G., Gallardet, J., 2007. Coupling between Biota and Earth Materials in the Critical Zone. Elements, 3: 327-332.

Anderson, S.P., Dietrich, W.E., Brimhall, G.H., 2002. Weathering profiles, mass-balance analysis, and rates of solute loss: Linkages between weathering and erosion in a small, steep catchment. Geological Society of America Bulletin, 114: 1143-1158.

Arthur Bettis, E., 2003. Last Glacial loess in the conterminous USA. Quaternary Science Reviews, 22(18-19): 1907-1946.

Auler, A.S., Smart, P.L., 2003. The influence of bedrock-derived acidity in the development of surface and underground karst: evidence from the Precambrian carbonates of semi-arid northeastern Brazil. Earth Surface Processes and Landforms, 28(2): 157-168.

Avila, A., Queralt-Mitjans, I., Alarcón, M., 1997. Mineralogical composition of African dust delivered by red rains over northeastern Spain. Journal of Geophysical Research: Atmospheres, 102(D18): 21977-21996.

Bauer, A., Velde, B.D., 2014. Geochemistry at the Earth's Surface. Springer.

Bingham, S.T. et al., 2020. Rates of hydroxyapatite formation and dissolution in a sandstone aquifer: Implications for understanding dynamic phosphate behaviour within an agricultural catchment. Applied Geochemistry, 115.

Birkeland, P.W., 1999. Soils and Geomorphology. Oxford University Press.

Boero, V., Premoli, A., Melis, P., Barberis, E., Arduino, E., 1992. Influence of Climate on the Iron-Oxide Mineralogy of Terra-Rossa. Clays and Clay Minerals, 40(1): 8-13.

Boero, V., Schwertmann, U., 1989. Iron-Oxide Mineralogy of Terra Rossa and Its Genetic-Implications. Geoderma, 44(4): 319-327.

Brantley, S.L. et al., 2006. Weathering from the soil profile to the watershed: what controls the weathering advance rate? Geochimica Et Cosmochimica Acta, 70(18): A64-A64.

Brantley, S.L., Goldhaber, M.B., Ragnarsdottir, K.V., 2007. Crossing disciplines and scales to understand the critical zone. Elements, 3: 307-314.

Brantley, S.L., Holleran, M.E., Jin, L., Bazilevskaya, E., 2013. Probing deep weathering in the Shale Hills Critical Zone Observatory, Pennsylvania (USA): the hypothesis of nested chemical reaction fronts in the subsurface. Earth Surface Processes and Landforms, 38(11): 1280-1298.

Brimhall, G., Dietrich, W.E., 1987. Constitutive mass balance relations between chemical composition, volume, density, porosity, and strain in metasomatic hydrochemical systems: results on weathering and pedogenisis. Geochimica et Cosmochimica Acta, 51: 567-587.

Bullen, T., Chadwick, O., 2015. Evidence for Nutrient Biolifting in Hawaiian Climosequence Soils as Revealed by Alkaline Earth Metal Stable Isotope Systematics. Procedia Earth and Planetary Science, 13: 312-315.

Bullen, T., Chadwick, O., 2016. Ca, Sr and Ba stable isotopes reveal the fate of soil nutrients along a tropical climosequence in Hawaii. Chemical Geology, 422: 25-45.

Buss, H.L. et al., 2017. Lithological influences on contemporary and long-term regolith weathering at the Luquillo Critical Zone Observatory. Geochimica et Cosmochimica Acta, 196: 224-251.

Buss, H.L., Mathur, R., White, A.F., Brantley, S.L., 2010. Phosphorus and iron cycling in deep saprolite, Luquillo Mountains, Puerto Rico. Chemical Geology, 269: 52-61.

Caquineau, S., 2002. Mineralogy of Saharan dust transported over northwestern tropical Atlantic Ocean in relation to source regions. Journal of Geophysical Research, 107(D15).

Chadwick, O.A., Brimhall, G.H., Hendricks, D.M., 1990. From black box to a grey box: a mass balance interpretation of pedogenesis. Geomorphology, 3: 369-390.

Chadwick, O.A., Derry, L.A., Vitousek, P.M., Huebert, B.J., Hedin, L.O., 1999. Changing sources of nutrients during four million years of ecosystem development. Nature, 397: 491-497.

Chapela Lara, M., Buss, H.L., Pett-Ridge, J.C., 2018. The effects of lithology on trace element and REE behavior during tropical weathering. Chemical Geology, 500: 88-102.

Chaudhuri, S., Clauer, N., Semhi, K., 2007. Plant decay as a major control of river dissolved potassium: A first estimate. Chemical Geology, 243(1-2): 178-190.

Chen, R., Bi, K., 2011. Correlation of karst agricultural geo-environment with non-karst agricultural geo-environment with respect to nutritive elements in Guizhou. Chinese Journal of Geochemistry, 30(4): 563-568.

Cheng, Q., Chen, X., Tao, M., Binley, A., 2019. Characterization of karst structures using quasi-3D electrical resistivity tomography. Environmental Earth Sciences, 78(9).

Dawson, T.E., Hahm, W.J., Crutchfield-Peters, K., 2020. Digging deeper: what the critical zone perspective adds to the study of plant ecophysiology. New Phytol, 226(3): 666-671.

Dere, A.L., White, T.S., April, R.H., Brantley, S.L., 2016. Mineralogical Transformations and Soil Development in Shale across a Latitudinal Climosequence. Soil Science Society of America Journal, 80(3): 623-636.

Derry, L.A., Chadwick, O.A., 2007. Contributions from Earth's Atmosphere to Soil. Elements, 3(5): 333-338.

Drobner, U., Tyler, G., 1998. Conditions controlling relative uptake of potassium and rubidium by plants from soils. Plant and Soil, 201(2): 285-293.

Durn, G., 2003. <Terra Rossa in the Mediterranean Region Parent Materials, Composition and Origin.>. Geologica Croatia, 56: 83-100.

Durn, G., Ottner, F., Slovenec, D., 1999. Mineralogical and geochemical indicators of the polygenetic nature of terra rossa in Istria, Croatia. Geoderma, 91(1-2): 125-150.

Egli, M., Mirabella, A., Sartori, G., 2008. The role of climate and vegetation in weathering and clay mineral formation in late Quaternary soils of the Swiss and Italian Alps. Geomorphology, 102(3-4): 307-324.

Foley, J.A. et al., 2005. Global consequences of land use. Science, 309(5734): 570-574.

Foos, A.M., 1991. Aluminous Lateritic Soils, Eluthera, Bahamas A Modern Analog to Carbonate Paleosols. Journal of Sedimentary Petrology, 61(3): 340-348.

Garrett, R.G., Lalor, G.C., 2005. The Fe/Na ratio, a framework for modelling trace element distributions in Jamaican soils. Geochemistry-Exploration Environment Analysis, 5: 147-157.

Gordon, S.W., Jackson, R.B., 2000. NUTRIENT CONCENTRATIONS IN FINE ROOTS. Ecology, 81(1): 275-280.

Graham, R., Rossi, A., Hubbert, R., 2010. Rock to regolith conversion: Producing hospitable substrates for terrestrial ecosystems. GSA Today: 4-9.

Green, S.M. et al., 2019. Soil functions and ecosystem services research in the Chinese karst Critical Zone. Chemical Geology, 527.

Hahm, W.J., Riebe, C.S., Lukens, C.E., Araki, S., 2014. Bedrock composition regulates mountain ecosystems and landscape evolution. Proc Natl Acad Sci U S A, 111(9): 3338-43.

Heartsill Scalley, T., Scatena, F.N., Moya, S., Lugo, A.E., 2012. Long-term dynamics of organic matter and elements exported as coarse particulates from two Caribbean montane watersheds. Journal of Tropical Ecology, 28(2): 127-139.

Herwitz, S.R., Muhs, D.R., 1995. Bermuda solution pipe soils: A geochemical evaluation of eolian parent materials, Terrestrial and shallow marine geology of the Bahamas and Bermuda.

Howell, D.M., Das Gupta, S., Pinno, B.D., MacKenzie, M.D., 2016. Reclaimed soils, fertilizer, and bioavailable nutrients: Determining similarity with natural benchmarks over time. Canadian Journal of Soil Science.

Hussey, V., 2018. Do oxalic acid exudates from mycorrhizal fungi influence the uptake of phosphorus by primary producers in the karst critical zone of southwest China.

Jarvie, H.P. et al., 2014. Phosphorus retention and remobilization along hydrological pathways in karst terrain. Environ Sci Technol, 48(9): 4860-8.

Jiang, Z. et al., 2020. Bedrock geochemistry influences vegetation growth by regulating the regolith water holding capacity. Nat Commun, 11(1): 2392.

Jin, L. et al., 2010. Mineral weathering and elemental transport during hillslope evolution at the Susquehanna/Shale Hills Critical Zone Observatory. Geochimica et Cosmochimica Acta, 74: 3669-3691.

Jin, L. et al., 2010b. Mineral weathering and elemental transport during hillslope evolution at the Susquehanna/Shale Hills Critical Zone Observatory. Geochimica et Cosmochimica Acta, 74(13): 3669-3691.

Jobbagy, E.G., Jackson, R.B., 2003. Patterns and mechanisms of soil acidification in the conversion of grasslands to forests. Biogeochemistry, 64(2): 205-229.

Jobbagy, Jackson, 2001. The distribution of soil nutrients with depth Global patterns and the imprint of plants. Biogeochemistry, 53.

Jobbagy, Jackson, R.B., 2004. THE UPLIFT OF SOIL NUTRIENTS BY PLANTS BIOGEOCHEMICAL CONSEQUESNCES ACROSS SCALES. Ecology, 85.

Kelly, E.F., Chadwick, O.A., Hilinski, T.E., 1998. The effect of plants on mineral weathering. 42(1-2): 21-53.

Kirkby, M.J., 1985. A basis for soil profile modelling in a geomorphic context. Journal of soil science, 36(1): 97-121.

Kurtz, A.C., Derry, L.A., Chadwick, O.A., 2001. Accretion of Asian dust to Hawaiian soils: Isotopic, elemental, and mineral mass balances. Geochimica Et Cosmochimica Acta, 65(12): 1971-1983.

Lang, F. et al., 2016. Phosphorus in forest ecosystems: New insights from an ecosystem nutrition perspective. Journal of Plant Nutrition and Soil Science, 179(2): 129-135.

Lilli, M.A. et al., 2020. A Multi-Disciplinary Approach to Understand Hydrologic and Geochemical Processes at Koiliaris Critical Zone Observatory. Water, 12(9).

Liu, H. et al., 2019. Rock crevices determine woody and herbaceous plant cover in the karst critical zone. Science China Earth Sciences, 62(11): 1756-1763.

Liu, H. et al., 2019. Rock crevices determine woody and herbaceous plant cover in the karst critical zone. Science China Earth Sciences, 62(11): 1756-1763.

Lu, M. et al., 2011. Minor stimulation of soil carbon storage by nitrogen addition: A meta-analysis. Agriculture, Ecosystems & Environment, 140(1-2): 234-244.

Macleod, D.A., 1980. The Origin of the Red Mediterranean Soils in Epirus, Greece. Journal of Soil Science, 31(1): 125-136.

Marzaioli, R., D'Ascoli, R., De Pascale, R.A., Rutigliano, F.A., 2010. Soil quality in a Mediterranean area of Southern Italy as related to different land use types. Applied Soil Ecology, 44(3): 205-212.

Moore, O., Buss, H., Green, S., Liu, M., Song, Z.L., 2017. The importance of non-carbonate mineral weathering as a soil formation mechanism within a karst weathering profile in the SPECTRA Critical Zone Observatory, Guizhou Province, China. Acta Geochimica, 36(3): 566-571.

Moore, T.R., Trofymow, J.A., Siltanen, M., Prescott, C., Group, C.W., 2005. Patterns of decomposition and carbon, nitrogen, and phosphorus dynamics of litter in upland forest and peatland sites in central Canada. Canadian Journal of Forest Research, 35(1): 133-142.

Moraetis, D. et al., 2011. Identification of hydrologic and geochemical pathways using high frequency sampling, REE aqueous sampling and soil characterization at Koiliaris Critical Zone Observatory, Crete. Applied Geochemistry, 26: S101-S104.

Moraetis, D. et al., 2015. Sediment provenance, soil development, and carbon content in fluvial and manmade terraces at Koiliaris River Critical Zone Observatory. Journal of Soils and Sediments, 15(2): 347-364.

Muhs, D.R. et al., 2008. Geochemical evidence for airborne dust additions to soils in Channel Islands National Park, California. Geological Society of America Bulletin, 120(1-2): 106-126.

Muhs, D.R. et al., 2010. The role of African dust in the formation of Quaternary soils on Mallorca, Spain and implications for the genesis of Red Mediterranean soils. Quaternary Science Reviews, 29(19-20): 2518-2543.

Muhs, D.R., Budahn, J.R., 2009. Geochemical evidence for African dust and volcanic ash inputs to terra rossa soils on carbonate reef terraces, northern Jamaica, West Indies. Quaternary International, 196(1-2): 13-35.

Muhs, D.R., Budahn, J.R., Prospero, J.M., Carey, S.N., 2007. Geochemical evidence for African dust inputs to soils of western Atlantic islands: Barbados, the Bahamas, and Florida. Journal of Geophysical Research, 112: F02009.

Muhs, D.R., Crittenden, R.C., Rosholt, J.N., Bush, C.A., Stewart, K.C., 1987. Genesis of Marine Terrace Soils, Barbados, West-Indies - Evidence from Mineralogy and Geochemistry. Earth Surface Processes and Landforms, 12(6): 605-618.

Nikolaidis, N.P., Bouraoui, F., Bidoglio, G., 2013. Hydrologic and geochemical modeling of a karstic Mediterranean watershed. Journal of Hydrology, 477: 129-138.

Papanikolaou, D., Vassilakis, E., 2010. Thrust faults and extensional detachment faults in Cretan tectono-stratigraphy: Implications for Middle Miocene extension. Tectonophysics, 488(1-4): 233-247.

Peltola, P., Brun, C., Åström, M., Tomilina, O., 2008. High K/Rb ratios in stream waters — Exploring plant litter decay, ground water and lithology as potential controlling mechanisms. Chemical Geology, 257(1-2): 92-100.

Porder, S., Hilley, G.E., 2010. Linking chronosequences with the rest of the world: predicting soil phosphorus content in denuding landscapes. Biogeochemistry, 102(1-3): 153-166.

Porder, S., Hilley, G.E., Chadwick, O.A., 2007a. Chemical weathering, mass loss, and dust inputs across a climate by time matrix in the Hawaiian Islands. Earth and Planetary Science Letters, 258(3-4): 414-427.

Porder, S., Vitousek, P.M., Chadwick, O.A., Chamberlain, C.P., Hilley, G.E., 2007b. Uplift, Erosion, and Phosphorus Limitation in Terrestrial Ecosystems. Ecosystems, 10(1): 159-171.

Porder, S., Vitousek, P.M., Chadwick, O.A., Chamberlain, C.P., Hilley, G.E., 2007. Uplift, Erosion, and Phosphorus Limitation in Terrestrial Ecosystems. Ecosystems, 10(1): 159-171.

Pye, K., 1992. <AEOLIAN DUST TRANSPORT AND DEPOSITION OVER CRETE AND ADJACENT PARTS OF THE MEDITERRANEAN SEA>. Earth Surface Processes and Landforms, 17: 271-288.

Restrepo-Diaz, H., Benlloch, M., Fernández-Escobar, R., 2008a. Plant water stress and K+ starvation reduce absorption of foliar applied K+ by olive leaves. Scientia Horticulturae, 116(4): 409-413.

Restrepo-Diaz, H., Benlloch, M., Navarro, C., Fernández-Escobar, R., 2008b. Potassium fertilization of rainfed olive orchards. Scientia Horticulturae, 116(4): 399-403.

Stamati, F.E., Nikolaidis, N.P., Venieri, D., Psillakis, E., Kalogerakis, N., 2011. Dissolved organic nitrogen as an indicator of livestock impacts on soil biochemical quality. Applied Geochemistry, 26: S340-S343.

Tang, Y., Han, G., Li, F., Wu, Q., 2016. Natural and anthropogenic sources of atmospheric dust at a remote forest area in Guizhou karst region, southwest China. Geochemistry: Exploration, Environment, Analysis, 16(2): 159-163.

Tanner, E.V.J., Vitousek, P.M., Cuevas, E., 1998. Experimental Investigation of Nutrient Limitation of Forest Growth on Wet Tropical Mountains. Ecology, 79(1): 10-22.

Tsiknia, M., Paranychianakis, N.V., Varouchakis, E.A., Moraetis, D., Nikolaidis, N.P., 2014. Environmental drivers of soil microbial community distribution at the Koiliaris Critical Zone Observatory. FEMS Microbiol Ecol, 90(1): 139-52.

Uhlig, D., Schuessler, J.A., Bouchez, J., Dixon, J.L., von Blanckenburg, F., 2017. Quantifying nutrient uptake as driver of rock weathering in forest ecosystems by magnesium stable isotopes. Biogeosciences, 14(12): 3111-3128.

Uhlig, D., von Blanckenburg, F., 2019. How Slow Rock Weathering Balances Nutrient Loss During Fast Forest Floor Turnover in Montane, Temperate Forest Ecosystems. Frontiers in Earth Science, 7.

Uhliq, D., Blanckenburg, v.F., 2020. Mineral nutrients sourced in deep regolith sustain long-term nutrition of mountainous temperate forest ecosystems. American Geophysical Union.

Wang, J. et al., 2014. Erosion-creep-collapse mechanism of underground soil loss for the karst rocky desertification in Chenqi village , Puding county, Guizhou, China.pdf. Environ Earth Sci, 72: 2751-2764.

Wang, S.J. et al., 2004a. How types of carbonate rock assemblages constrain the distribution of karst rocky desertified land in Guizhou Province, PR China: phenomena and mechanisms. Land Degradation & Development, 15(2): 123-131.

Wang, S.J., Liu, Q.M., Zhang, D.F., 2004. Karst Rocky Desertification in Southwestern China Geomorphology, Land use, Impact and Rehabilitation.pdf. Land Degradation and Management, 15: 115-121.

Wang, X., Lou, J., Cai, D., Jiao, L., 2019. Effects of Earth surface processes on the heterogeneity of surface soil elements and the responses of vegetation elements in the Otindag Desert, China. Catena, 183.

West, A.J., Galy, A., Bickle, M., 2005. Tectonic and climatic controls on silicate weathering. Earth and Planetary Science Letters, 235: 211-228.

White, A.F., Schulz, M.S., Lowenstern, J.B., Vivit, D., Bullen, T.D., 2005. The ubiquitous nature of accessory calcite in granitoid rocks: Implications for weathering and solute evolution, and petrogenesis. Geochimica et Cosmochimica Acta, 69(6): 1455-1471.

Yaalon, D.H., 1997. Soils in the Mediterranean region what makes them different? Catena, 28: 157-169.

Yang, Q., Chen, H., Li, B., 2015. Source identification and health risk assessment of metals in indoor dust in the vicinity of phosphorus mining, Guizhou Province, China. Arch Environ Contam Toxicol, 68(1): 20-30.

Zhao, M., Zeng, C., Liu, Z., Wang, S., 2010. Effect of different land use/land cover on karst hydrogeochemistry: A paired catchment study of Chenqi and Dengzhanhe, Puding, Guizhou, SW China. Journal of Hydrology, 388(1-2): 121-130.

Zhu, L.J., He, S.Y., Li, J.Y., 2008. Weathering-pedogenesis of Carbonate Rocks and Its Environmental Effects in Subtropical Region. Acta Geologica Sinica-English Edition, 82(5): 982-993.

Zhu, X. et al., 2020. Impact of bedrock geochemistry on vegetation productivity depends on climate dryness in the Guizhou karst of China. Progress in Physical Geography: Earth and Environment, 45(1): 20-32.

**Appendix A1:** Selected SEM images of the bedrock in Chenqi

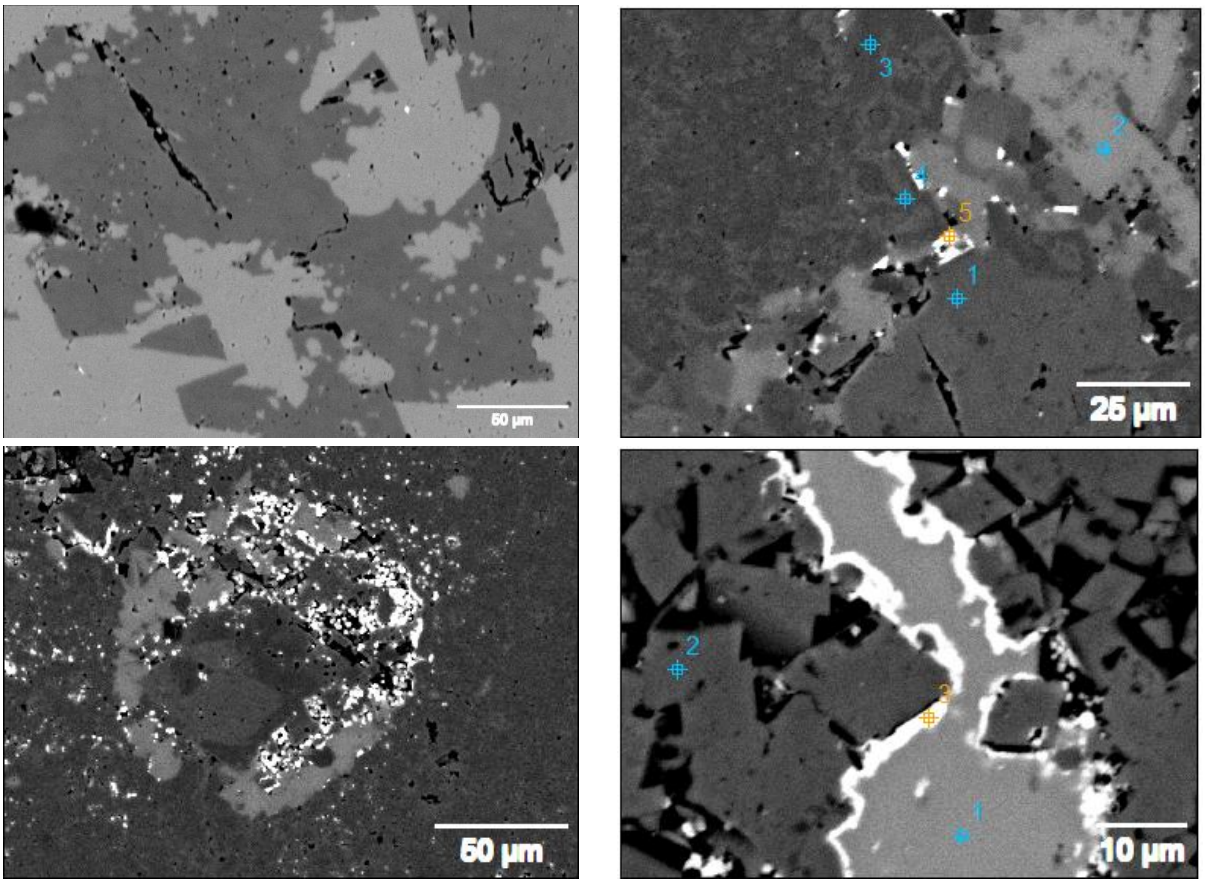


**Appendix A2:** SEM images from the two sites in K-CZO

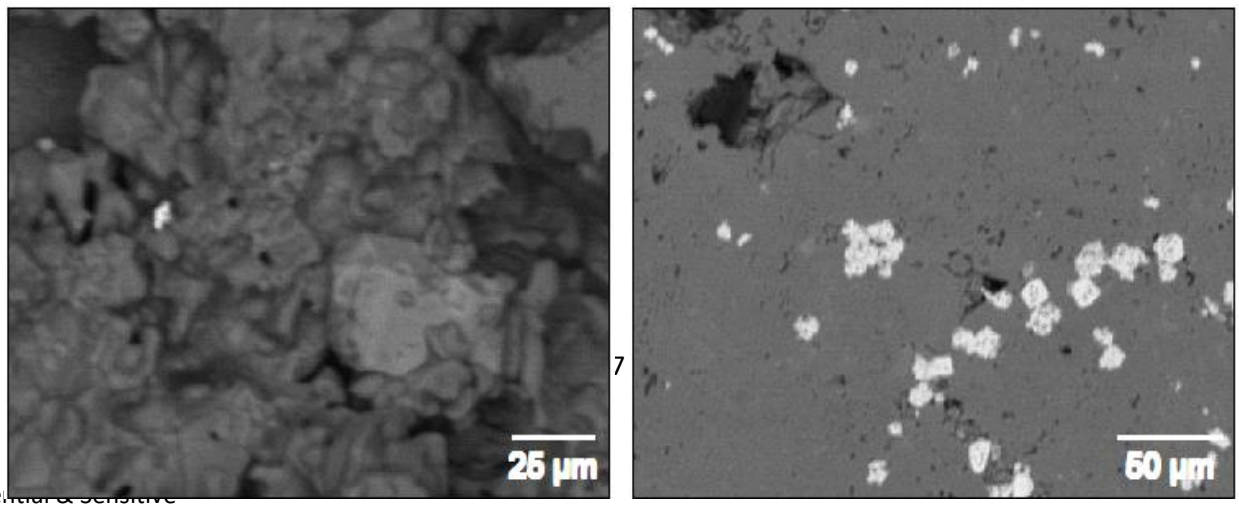

**Appendix B:** Goldschmidt Abstract 2020

## Assessment of Controls on Pedogenesis and Mineral Nutrients in Agricultural Karst Critical Zones in Guizhou, China and Crete, Greece

A.M. LAWAL[1], H.L. BUSS[1], P.J. JOHNES[2], O.W. MOORE[3], S.M. GREEN[4], Z. SONG[5] and N.P. NIKOLAIDIS[6]

[1]School of Earth Sciences, University of Bristol, UK, BS8 1RJ
[2]School of Geographical Sciences, University of Bristol, UK, BS8 1SS
[3]School of Earth and Environment, University of Leeds
[4] Geography, College of Life and Environmental Sciences, Amory Building, University of Exeter, Rennes Drive, Exeter EX4 4QD, UK
[5]Institute of the Surface-Earth System Science Research, Tianjin University, Tianjin 300072, PR China
[6] School of Environmental Engineering, Technical University of Crete, Chania, Greece

The Earth's critical zone (CZ) has been constantly evolving and changing over geological timescales, historically driven by tectonic and climatic forcings. Recently CZ changes have also been driven by anthropogenic factors occasioned by increases in population, which has increased demand for resources and expansion of agriculture, leading to unsustainable land use practices. As a result, about one-third of global arable lands have been eroded and degraded and they are continually being lost at a rate of about 0.5% a year. Soils are especially vulnerable to loss and degradation in karst environments where lithology, climate and landscape may contribute to slow formation of nutrient deficient soils. Here we studied soil formation and mineral nutrient production in karst CZs in Guizhou, China and Crete, Greece as functions of land use, slope position, and lithology. The two sites are/were impacted by intensive agriculture but under different timescales and seasonality.

Bulk chemistry of soil and bedrock were analysed by ICP-OES and mineralogy and rock texture by SEM. The results show no clear effect of land use or slope position on mineral elements mass transfer profiles in these soils, but indicated considerable influence of the bedrock composition as well as atmospheric deposition. The bedrock mineralogy and the mass transfer profiles of the mineral elements showed that loss of carbonate minerals

leaves the soil matrix enriched with silicate-rich mineral 'impurities' which control soil formation and mineral nutrient content in the soils. Enrichment of some mineral elements (Ca, K and P) in the profiles indicated atmospheric deposition and biolifting, a process in which plants scavenge for nutrients and concentrate it in the soil. In Guizhou, China bedrock mineralogy is different from that of Crete, Greece and atmospheric deposition is more prominent in Crete than in Guizhou. We found that small variations in lithology (as some of the minerals found in Guizhou such as mica, pyrite and fluorospar) are absent in Crete) play a dominant role in controlling karst soil mineral nutrient profiles.

**Appendix C:** OSZCAR-TERENO Abstract

# Lithological Influences on Mineral Nutrient Production and Soil Formation in Agricultural Karst Critical Zones

**A.M. LAWAL[1], H.L. BUSS[1], S.M. GREEN [2], Z. SONG [3], and N.P. NIKOLAIDIS[4]**

**[1]School of Earth Sciences, University of Bristol, UK, BS8 1RJ**
**[2] Geography, College of Life and Environmental Sciences, Amory Building, University of Exeter, Rennes Drive, Exeter EX4 4QD, UK**
**[3] Institute of the Surface-Earth System Science Research, Tianjin University, Tianjin 300072, PR China**
**[4] School of Environmental Engineering, Technical University of Crete, Chania, Greece**

Over geological timescales, functions, and shape of the Earth's critical zone (CZ), the region that extends from the top of the vegetation canopy to the bottom of the weathering zone, have been governed by its responses to natural (tectonic and climatic) forcings. Recently, anthropogenic activities, occasioned by increasing population (human and livestock) and demand for resources such as food and fibre, have emerged as major drivers of changes in the critical zone. This demand for resources has led to unsustainable land use practices and loss of soil quality especially in karst environments where lithology contributes to the slow formation of nutrient deficient soils. Here, we studied the influence of lithology on soil formation and mineral nutrients production in karst CZs in Guizhou, China and Crete, Greece. The two sites have been impacted by intensive agricultural activities but under different timescales and seasonality.

Soil and bedrock bulk chemistry were analysed by ICP-OES while mineralogy and rock texture were analysed by SEM. The results indicated the influence of the bedrock composition as well as atmospheric deposition. The bedrock mineralogy and the mass transfer profiles of the mineral elements showed that in situ dissolution of carbonate minerals leaves the soil matrix enriched with aluminosilicates and other non-carbonate mineral impurities which control soil formation and mineral nutrient content in the soils.

Enrichment of some of the mineral elements (Ca, K and P) in the profiles indicated atmospheric deposition and biolifting, a process in which plants scavenge for nutrients and concentrate it in the soil. Variation in bedrock mineralogy (as some of the minerals found in Guizhou such as mica, pyrite and fluorite are absent in Crete) was attributed to the more prominent role of bedrock in Guizhou, China in controlling karst soil mineral nutrient profiles than in Crete, Greece.

**Appendix D:** Selected Unnormalised CQ ICP-OES bulk Chemistry data in Chenqi

| Depth | $SiO_2$ | $Al_2O_3$ | $Fe_2O_3$ | CaO | MgO | $Na_2O$ | $K_2O$ | $P_2O_5$ | Zr |
|---|---|---|---|---|---|---|---|---|---|
| **LoD** | **0.01** | **0.01** | **0.01** | **0.01** | **0.01** | **0.01** | **0.01** | **0.01** | **2** |
| CQ-38-2 0-5 | 50.5 | 13.85 | 6.31 | 1.26 | 1.36 | 0.09 | 3.29 | 0.07 | 191 |
| CQ-38-2 5-10 | 51.5 | 13.8 | 5.73 | 1.28 | 1.33 | 0.1 | 3.36 | 0.06 | 205 |
| CQ-38-2 10-20 | 51.4 | 13.75 | 5.63 | 1.14 | 1.33 | 0.1 | 3.38 | 0.08 | 193 |
| CQ-38-2 20-30 | 52.2 | 14.15 | 6.07 | 1.16 | 1.34 | 0.1 | 3.35 | 0.11 | 184 |
| CQ-38-2 30-40 | 50.8 | 13.75 | 5.88 | 1.13 | 1.31 | 0.1 | 3.29 | 0.1 | 187 |
| CQ-38-2 40-50 | 51.1 | 13.65 | 5.83 | 1.17 | 1.31 | 0.1 | 3.35 | 0.11 | 190 |
| | | | | | | | | | |
| CQ-61-1 0-5 | 55.6 | 15.05 | 7.5 | 0.46 | 1.14 | 0.1 | 2.71 | 0.14 | 297 |
| CQ-61-1 5-10 | 55.3 | 15.05 | 7.29 | 0.49 | 1.09 | 0.11 | 2.68 | 0.13 | 298 |
| CQ-61-1 10-20 | 57.8 | 14.85 | 6.92 | 0.37 | 0.99 | 0.1 | 2.52 | 0.11 | 319 |
| CQ-61-1 20-30 | 57.9 | 16.65 | 8.02 | 0.49 | 1.31 | 0.1 | 2.78 | 0.07 | 353 |
| CQ-61-1 30-40 | 55.1 | 14.95 | 6.89 | 0.59 | 1.38 | 0.1 | 3.25 | <0.01 | 271 |
| CQ-61-1 40-50 | 56.2 | 18.5 | 8.65 | 0.54 | 1.43 | 0.1 | 2.89 | 0.06 | 299 |
| CQ-61-1 50-60 | 51.6 | 17.3 | 7.86 | 0.51 | 1.34 | 0.09 | 2.76 | 0.05 | 271 |
| CQ-61-1 60-70 | 52.8 | 17.05 | 7.93 | 0.52 | 1.32 | 0.1 | 2.79 | 0.04 | 288 |
| CQ-61-1 70-80 | 51.9 | 17.1 | 7.8 | 0.55 | 1.36 | 0.09 | 2.86 | 0.06 | 268 |
| CQ-61-1 80-90 | 50.1 | 17.4 | 8.04 | 0.58 | 1.38 | 0.09 | 2.84 | 0.07 | 273 |
| CQ-61-1 90-100 | 50.2 | 17.7 | 7.96 | 0.6 | 1.43 | 0.09 | 2.87 | 0.04 | 265 |
| CQ-61-1 100-110 | 50.6 | 18.1 | 8.53 | 0.63 | 1.49 | 0.1 | 2.94 | 0.08 | 267 |
| | | | | | | | | | |
| CQ-64-1 0-5 | 57.4 | 13.05 | 5.67 | 0.8 | 1.24 | 0.12 | 3.49 | 0.12 | 298 |
| CQ-64-1 5-10 | 58.4 | 13.6 | 6.08 | 0.7 | 1.3 | 0.12 | 3.49 | 0.13 | 279 |
| CQ-64-1 10-20 | 58.9 | 13.65 | 5.88 | 0.68 | 1.23 | 0.12 | 3.48 | 0.1 | 256 |

| | | | | | | | | | |
|---|---|---|---|---|---|---|---|---|---|
| CQ-64-1 20-30 | 59.9 | 13.8 | 6.04 | 0.71 | 1.24 | 0.12 | 3.47 | 0.08 | 280 |
| CQ-64-1 30-40 | 58.4 | 14.85 | 6.11 | 0.67 | 1.41 | 0.12 | 3.56 | 0.06 | 256 |
| CQ-64-1 40-50 | 58.7 | 14.55 | 6.33 | 0.62 | 1.32 | 0.12 | 3.43 | 0.09 | 261 |
| CQ-64-1 50-60 | 57.6 | 17.05 | 7.36 | 0.75 | 1.75 | 0.11 | 3.82 | 0.09 | 248 |
| CQ-64-1 60-70 | 53.5 | 16 | 7.73 | 0.77 | 1.69 | 0.1 | 3.52 | 0.04 | 244 |
| CQ-64-1 70-80 | 55.2 | 16.35 | 7.23 | 0.86 | 1.62 | 0.11 | 3.48 | 0.13 | 262 |
| CQ-64-1 80-90 | 51.1 | 18.1 | 8.03 | 0.79 | 1.91 | 0.09 | 3.6 | 0.02 | 237 |

**Appendix E:** Selected Unnormalised CQ ICP-OES bulk Chemistry data in K-CZO

| Depth | $SiO_2$ | $Al_2O_3$ | $Fe_2O_3$ | CaO | MgO | $Na_2O$ | $K_2O$ | $P_2O_5$ | Zr |
|---|---|---|---|---|---|---|---|---|---|
| **LoD** | **0.01** | **0.01** | **0.01** | **0.01** | **0.01** | **0.01** | **0.01** | **0.01** | **2** |
| K4 0-5 | 71.27 | 10.68 | 4.83 | 0.61 | 0.72 | 0.06 | 0.82 | 0.18 | 119.00 |
| K4 5-10 | 70.07 | 12.53 | 5.60 | 0.52 | 0.77 | 0.05 | 0.87 | 0.17 | 126.00 |
| K4 15-20 | 66.47 | 14.33 | 6.42 | 0.45 | 0.83 | 0.05 | 0.94 | 0.18 | 137.67 |
| K4 22-26 | 69.43 | 13.40 | 5.98 | 0.44 | 0.78 | 0.05 | 0.89 | 0.16 | 142.33 |
| | | | | | | | | | |
| K5 0-5 | 57.43 | 14.25 | 6.53 | 0.60 | 2.03 | 0.41 | 2.00 | 0.27 | 255.67 |
| K5 7-12 | 57.53 | 15.45 | 7.03 | 0.59 | 2.09 | 0.36 | 2.07 | 0.28 | 252.67 |
| K5 15-20 | 57.17 | 15.40 | 7.02 | 0.62 | 2.08 | 0.35 | 2.05 | 0.28 | 242.33 |
| K5 25-30 | 58.30 | 15.25 | 6.91 | 0.63 | 1.98 | 0.33 | 2.00 | 0.28 | 239.00 |

**Uncategorized References**


Aciego, S.M. et al., 2017. Dust outpaces bedrock in nutrient supply to montane forest ecosystems. Nat Commun, 8: 14800.

Alekseev, A., Alekseeva, T., Kalinin, P., Hajnos, M., 2018. Soils response to the land use and soil climatic gradients at ecosystem scale: Mineralogical and geochemical data. Soil and Tillage Research, 180: 38-47.

Amundson, R., Richter, D.D., Humphreys, G.S., Jobbagy, E.G., Gallardet, J., 2007. Coupling between Biota and Earth Materials in the Critical Zone. Elements, 3: 327-332.

Anderson, R.S., Anderson, S.P., Aufdenkampe, A.K., 2010. Future Directions for Critical Zone Observatory (CZO) Science.

Anderson, S.P., Bales, R.C., Duffy, C.J., 2008. Critical Zone Observatories: Building a network to advance interdisciplinary study of Earth surface processes. Mineralogical Magazine, 72(1): 7-10.

Anderson, S.P., Dietrich, W.E., Brimhall, G.H., 2002. Weathering profiles, mass-balance analysis, and rates of solute loss: Linkages between weathering and erosion in a small, steep catchment. Geological Society of America Bulletin, 114: 1143-1158.

Anderson, S.P., von Blanckenburg, F., White, A.F., 2007. Physical and Chemical Controls on the Critical Zone. Elements, 3: 315-319.

Arthur Bettis, E., 2003. Last Glacial loess in the conterminous USA. Quaternary Science Reviews, 22(18-19): 1907-1946.

Augusto, L., Turpault, M.P., Ranger, J., 2000. Impact of forest tree species on feldspar weathering rates. Geoderma, 96(3): 215-237.

Auler, A.S., Smart, P.L., 2003. The influence of bedrock-derived acidity in the development of surface and underground karst: evidence from the Precambrian carbonates of semi-arid northeastern Brazil. Earth Surface Processes and Landforms, 28(2): 157-168.

Avila, A., Queralt-Mitjans, I., Alarcón, M., 1997. Mineralogical composition of African dust delivered by red rains over northeastern Spain. Journal of Geophysical Research: Atmospheres, 102(D18): 21977-21996.

Banwart, S. et al., 2011. Assessing soil processes and function across an international network of critical zone observatories: Research hypotheses and experimental design. Vadose Zone J, 10: 974-987.

Bauer, A., Velde, B.D., 2014. Geochemistry at the Earth's Surface. Springer.

Berner, R.A., Lasaga, A.C., Garrels, R.M., 1983. The carbonate-silicate geochemical cycle and its effect on the atmospheric carbon dioxide over the past 100 million years. American Journal of Science, 283: 641-683.

Bingham, S.T. et al., 2020. Rates of hydroxyapatite formation and dissolution in a sandstone aquifer: Implications for understanding dynamic phosphate behaviour within an agricultural catchment. Applied Geochemistry, 115.

Birkeland, P.W., 1999. Soils and Geomorphology. Oxford University Press.

Blum, J.D., Gazis, C.A., Jacobson, A.D., Chamberlain, C.P., 1998. Carbonate versus silicate weathering in the Raikhot watershed within the high Himalayan crystalline series. Geology, 26(5): 411-414.

Boero, V., Premoli, A., Melis, P., Barberis, E., Arduino, E., 1992. Influence of Climate on the Iron-Oxide Mineralogy of Terra-Rossa. Clays and Clay Minerals, 40(1): 8-13.

Boero, V., Schwertmann, U., 1989. Iron-Oxide Mineralogy of Terra Rossa and Its Genetic-Implications. Geoderma, 44(4): 319-327.

Brantley, S.L. et al., 2006a. Weathering from the soil profile to the watershed: what controls the weathering advance rate? Geochimica Et Cosmochimica Acta, 70(18): A64-A64.
Brantley, S.L., Goldhaber, M.B., Ragnarsdottir, K.V., 2007. Crossing disciplines and scales to understand the critical zone. Elements, 3: 307-314.
Brantley, S.L., Holleran, M.E., Jin, L., Bazilevskaya, E., 2013. Probing deep weathering in the Shale Hills Critical Zone Observatory, Pennsylvania (USA): the hypothesis of nested chemical reaction fronts in the subsurface. Earth Surface Processes and Landforms, 38(11): 1280-1298.
Brantley, S.L., Lebedeva, M., 2011. Learning to Read the Chemistry of Regolith to Understand the Critical Zone. Annual Review of Earth and Planetary Sciences, 39(1): 387-416.
Brantley, S.L. et al., 2017. Designing a network of critical zone observatories to explore the living skin of the terrestrial Earth. Earth Surface Dynamics, 5(4): 841-860.
Brantley, S.L. et al., 2006b. Frontiers in Exploring the Critical Zone. NSF Workshop.
Brimhall, G., Dietrich, W.E., 1987. Constitutive mass balance relations between chemical composition, volume, density, porosity, and strain in metasomatic hydrochemical systems: results on weathering and pedogenisis. Geochimica et Cosmochimica Acta, 51: 567-587.
Bullen, T., Chadwick, O., 2015. Evidence for Nutrient Biolifting in Hawaiian Climosequence Soils as Revealed by Alkaline Earth Metal Stable Isotope Systematics. Procedia Earth and Planetary Science, 13: 312-315.
Bullen, T., Chadwick, O., 2016. Ca, Sr and Ba stable isotopes reveal the fate of soil nutrients along a tropical climosequence in Hawaii. Chemical Geology, 422: 25-45.
Buss, H.L. et al., 2017. Lithological influences on contemporary and long-term regolith weathering at the Luquillo Critical Zone Observatory. Geochimica et Cosmochimica Acta, 196: 224-251.
Buss, H.L., Mathur, R., White, A.F., Brantley, S.L., 2010. Phosphorus and iron cycling in deep saprolite, Luquillo Mountains, Puerto Rico. Chemical Geology, 269(1-2): 52-61.
Buss, H.L. et al., 2008. Mineral weathering in a deep volcaniclastic saprolite, Luquillo Mountains, Puerto Rico. Geochimica Et Cosmochimica Acta, 72(12): A124-A124.
Calvaruso, C. et al., 2010. Influence of forest trees on the distribution of mineral weathering-associated bacterial communities of the Scleroderma citrinum mycorrhizosphere. Appl Environ Microbiol, 76(14): 4780-7.
Cao, J. et al., 2009. Soil erosion and rocky desertification controlled by karst environment in Guizhou Province. Soil Water Conserv China, 1: 20-23.
Caquineau, S., 2002. Mineralogy of Saharan dust transported over northwestern tropical Atlantic Ocean in relation to source regions. Journal of Geophysical Research, 107(D15).
Chadwick, O.A., Brimhall, G.H., Hendricks, D.M., 1990. From black box to a grey box: a mass balance interpretation of pedogenesis. Geomorphology, 3: 369-390.
Chadwick, O.A., Derry, L.A., Vitousek, P.M., Huebert, B.J., Hedin, L.O., 1999. Changing sources of nutrients during four million years of ecosystem development. Nature, 397: 491-497.
Chapela Lara, M., Buss, H.L., Pett-Ridge, J.C., 2018. The effects of lithology on trace element and REE behavior during tropical weathering. Chemical Geology, 500: 88-102.
Chaudhuri, S., Clauer, N., Semhi, K., 2007. Plant decay as a major control of river dissolved potassium: A first estimate. Chemical Geology, 243(1-2): 178-190.
Chen, R., Bi, K., 2011. Correlation of karst agricultural geo-environment with non-karst agricultural geo-environment with respect to nutritive elements in Guizhou. Chinese Journal of Geochemistry, 30(4): 563-568.
Cheng, Q., Chen, X., Tao, M., Binley, A., 2019. Characterization of karst structures using quasi-3D electrical resistivity tomography. Environmental Earth Sciences, 78(9).
Cuadros, J. et al., 2013. Crystal-chemistry of interstratified Mg/Fe-clay minerals from seafloor hydrothermal sites. Chemical Geology, 360-361: 142-158.
Daoxian, Y., 2001. On the Karst Ecosystem. Acta Geologica Sinica, 75(3).

Dawson, T.E., Hahm, W.J., Crutchfield-Peters, K., 2020. Digging deeper: what the critical zone perspective adds to the study of plant ecophysiology. New Phytol, 226(3): 666-671.
Dere, A.L., White, T.S., April, R.H., Brantley, S.L., 2016. Mineralogical Transformations and Soil Development in Shale across a Latitudinal Climosequence. Soil Science Society of America Journal, 80(3): 623-636.
Derry, L.A., Chadwick, O.A., 2007. Contributions from Earth's Atmosphere to Soil. Elements, 3(5): 333-338.
Drobner, U., Tyler, G., 1998. Conditions controlling relative uptake of potassium and rubidium by plants from soils. Plant and Soil, 201(2): 285-293.
Dupré, B. et al., 2003. Rivers, chemical weathering and Earth's climate. Comptes Rendus Geoscience, 335(16): 1141-1160.
Durn, G., 2003. <Terra Rossa in the Mediterranean Region Parent Materials, Composition and Origin.>. Geologica Croatia, 56: 83-100.
Durn, G., Ottner, F., Slovenec, D., 1999. Mineralogical and geochemical indicators of the polygenetic nature of terra rossa in Istria, Croatia. Geoderma, 91(1-2): 125-150.
Edmond, J.M., Palmer, M.R., Measures, C.I., Grant, B., Stallard, R.F., 1995. The fluvial geochemistry and denudation rate of the Guayana Shield in Venezuela, Colombia, and Brazil. Geochim. Cosmochim. Acta, 59: 3301-3325.
Egli, M., Mirabella, A., Sartori, G., 2008. The role of climate and vegetation in weathering and clay mineral formation in late Quaternary soils of the Swiss and Italian Alps. Geomorphology, 102(3-4): 307-324.
Egli, M., Mirabella, A., Sartori, G., Fitze, P., 2003. Weathering rates as a function of climate: results from a climosequence of the Val Genova (Trentino, Italian Alps). Geoderma, 111(1-2): 99-121.
Foley, J.A. et al., 2005. Global consequences of land use. Science, 309(5734): 570-574.
Foos, A.M., 1991. Aluminous Lateritic Soils, Eluthera, Bahamas A Modern Analog to Carbonate Paleosols. Journal of Sedimentary Petrology, 61(3): 340-348.
Frings, P.J., Buss, H.L., 2019. The Central Role of Weathering in the Geosciences. Elements, 15(4): 229-234.
Gaillardet, J., Dupre, B., Allegre, C.J., 1995. A Global Geochemical Mass Budget Applied to the Congo Basin Rivers - Erosion Rates and Continental-Crust Composition. Geochimica Et Cosmochimica Acta, 59(17): 3469-3485.
Garrels, R.M., MacKenzie, F.T., 1971. Evolution of Sedimentary Rocks. W. Norton, New York, 397 pp.
Garrett, R.G., Lalor, G.C., 2005. The Fe/Na ratio, a framework for modelling trace element distributions in Jamaican soils. Geochemistry-Exploration Environment Analysis, 5: 147-157.
Giardino, J.R., Houser, C., 2015. Introduction to the Critical Zone. Developments in Earth Surface Processes, pp. 1-13.
Gislason, S.R. et al., 2009. Direct evidence of the feedback between climate and weathering. Earth and Planetary Science Letters, 277(1-2): 213-222.
Goddéris, Y., Brantley, S.L., Blum, J.D., 2013. Earthcasting the future Critical Zone. Elementa: Science of the Anthropocene, 1.
Gordon, S.W., Jackson, R.B., 2000. NUTRIENT CONCENTRATIONS IN FINE ROOTS. Ecology, 81(1): 275-280.
Green, S.M. et al., 2019. Soil functions and ecosystem services research in the Chinese karst Critical Zone. Chemical Geology, 527.
Hahm, W.J., Riebe, C.S., Lukens, C.E., Araki, S., 2014. Bedrock composition regulates mountain ecosystems and landscape evolution. Proc Natl Acad Sci U S A, 111(9): 3338-43.
Hayes, N.R., Buss, H.L., Moore, O.W., Krám, P., Pancost, R.D., 2020. Controls on granitic weathering fronts in contrasting climates. Chemical Geology, 535.

Heartsill Scalley, T., Scatena, F.N., Moya, S., Lugo, A.E., 2012. Long-term dynamics of organic matter and elements exported as coarse particulates from two Caribbean montane watersheds. Journal of Tropical Ecology, 28(2): 127-139.
Herwitz, S.R., Muhs, D.R., 1995. Bermuda solution pipe soils: A geochemical evaluation of eolian parent materials, Terrestrial and shallow marine geology of the Bahamas and Bermuda.
Howell, D.M., Das Gupta, S., Pinno, B.D., MacKenzie, M.D., 2016. Reclaimed soils, fertilizer, and bioavailable nutrients: Determining similarity with natural benchmarks over time. Canadian Journal of Soil Science.
Hussey, V., 2018. Do oxalic acid exudates from mycorrhizal fungi influence the uptake of phosphorus by primary producers in the karst critical zone of south west China.
Jarvie, H.P. et al., 2014. Phosphorus retention and remobilization along hydrological pathways in karst terrain. Environ Sci Technol, 48(9): 4860-8.
Jiang, Z. et al., 2020. Bedrock geochemistry influences vegetation growth by regulating the regolith water holding capacity. Nat Commun, 11(1): 2392.
Jiang, Z.C., Lian, Y.Q., Qin, X.Q., 2014. Rocky desertification in Southwest China: Impacts, causes, and restoration. Earth-Science Reviews, 132(132): 1-12.
Jin, L. et al., 2017. REE mobility and fractionation during shale weathering along a climate gradient. Chemical Geology, 466: 352-379.
Jin, L. et al., 2010a. Mineral weathering and elemental transport during hillslope evolution at the Susquehanna/Shale Hills Critical Zone Observatory. Geochimica et Cosmochimica Acta, 74(13): 3669-3691.
Jin, L. et al., 2010b. Mineral weathering and elemental transport during hillslope evolution at the Susquehanna/Shale Hills Critical Zone Observatory. Geochimica et Cosmochimica Acta, 74: 3669-3691.
Jobbagy, Jackson, 2001. The distribution of soil nutrients with depth Global patterns and the imprint of plants. Biogeochemistry, 53.
Jobbagy, Jackson, R.B., 2004. THE UPLIFT OF SOIL NUTRIENTS BY PLANTS BIOGEOCHEMICAL CONSEQUESNCES ACROSS SCALES. Ecology, 85.
Jobbagy, E.G., Jackson, R.B., 2003. Patterns and mechanisms of soil acidification in the conversion of grasslands to forests. Biogeochemistry, 64(2): 205-229.
Johnson, D.W. et al., 2009. Biogeochemical cycling in forest soils of the eastern Sierra Nevada Mountains, USA. Forest Ecology and Management, 258(10): 2249-2260.
Kelly, E.F., Chadwick, O.A., Hilinski, T.E., 1998. The effect of plants on mineral weathering. 42(1-2): 21-53.
Kirkby, M.J., 1985. A basis for soil profile modelling in a geomorphic context. Journal of soil science, 36(1): 97-121.
Kurtz, A.C., Derry, L.A., Chadwick, O.A., 2001. Accretion of Asian dust to Hawaiian soils: Isotopic, elemental, and mineral mass balances. Geochimica Et Cosmochimica Acta, 65(12): 1971-1983.
Lambers, H. et al., 2017. How belowground interactions contribute to the coexistence of mycorrhizal and non-mycorrhizal species in severely phosphorus-impoverished hyperdiverse ecosystems. Plant and Soil, 424(1-2): 11-33.
Lang, F. et al., 2016. Phosphorus in forest ecosystems: New insights from an ecosystem nutrition perspective. Journal of Plant Nutrition and Soil Science, 179(2): 129-135.
Lilli, M.A. et al., 2020. A Multi-Disciplinary Approach to Understand Hydrologic and Geochemical Processes at Koiliaris Critical Zone Observatory. Water, 12(9).
Lin, H., Hopmans, J.W., Richter, D.d., 2011. Interdisciplinary Sciences in a Global Network of Critical Zone Observatories. Vadose Zone Journal, 10(3).
Liu, H. et al., 2019. Rock crevices determine woody and herbaceous plant cover in the karst critical zone. Science China Earth Sciences, 62(11): 1756-1763.

Macleod, D.A., 1980. The Origin of the Red Mediterranean Soils in Epirus, Greece. Journal of Soil Science, 31(1): 125-136.
Maher, K., 2010. The dependence of chemical weathering rates on fluid residence time. Earth and Planetary Science Letters, 294(1-2): 101-110.
Marie-Pierre, T., Claude, N., Christophe, C., 2009. Rhizosphere impact on the dissolution of test minerals in a forest ecosystem. Geoderma, 153(1-2): 147-154.
Marzaioli, R., D'Ascoli, R., De Pascale, R.A., Rutigliano, F.A., 2010. Soil quality in a Mediterranean area of Southern Italy as related to different land use types. Applied Soil Ecology, 44(3): 205-212.
Millennium Assessment Board, 2005. Millennium ecosystem assessment. Washington, DC: New Island, 13: 520.
Minasny, B., McBratney, A.B., Salvador-Blanes, S., 2008. Quantitative models for pedogenesis — A review. Geoderma, 144(1-2): 140-157.
Moore, O., Buss, H., Green, S., Liu, M., Song, Z.L., 2017. The importance of non-carbonate mineral weathering as a soil formation mechanism within a karst weathering profile in the SPECTRA Critical Zone Observatory, Guizhou Province, China. Acta Geochimica, 36(3): 566-571.
Moore, O.W., Buss, H.L., Dosseto, A., 2019. Incipient chemical weathering at bedrock fracture interfaces in a tropical critical zone system, Puerto Rico. Geochimica et Cosmochimica Acta, 252: 61-87.
Moore, T.R., Trofymow, J.A., Siltanen, M., Prescott, C., Group, C.W., 2005. Patterns of decomposition and carbon, nitrogen, and phosphorus dynamics of litter in upland forest and peatland sites in central Canada. Canadian Journal of Forest Research, 35(1): 133-142.
Moraetis, D. et al., 2015. Sediment provenance, soil development, and carbon content in fluvial and manmade terraces at Koiliaris River Critical Zone Observatory. Journal of Soils and Sediments, 15(2): 347-364.
Moraetis, D. et al., 2011. Identification of hydrologic and geochemical pathways using high frequency sampling, REE aqueous sampling and soil characterization at Koiliaris Critical Zone Observatory, Crete. Applied Geochemistry, 26: S101-S104.
Moravec, B., Chorover, J., 2020. Critical Zone Biogeochemistry Linking Structure and Function. AGU.
Muhs, D.R. et al., 2010. The role of African dust in the formation of Quaternary soils on Mallorca, Spain and implications for the genesis of Red Mediterranean soils. Quaternary Science Reviews, 29(19-20): 2518-2543.
Muhs, D.R., Budahn, J.R., 2009. Geochemical evidence for African dust and volcanic ash inputs to terra rossa soils on carbonate reef terraces, northern Jamaica, West Indies. Quaternary International, 196(1-2): 13-35.
Muhs, D.R. et al., 2008. Geochemical evidence for airborne dust additions to soils in Channel Islands National Park, California. Geological Society of America Bulletin, 120(1-2): 106-126.
Muhs, D.R., Budahn, J.R., Prospero, J.M., Carey, S.N., 2007. Geochemical evidence for African dust inputs to soils of western Atlantic islands: Barbados, the Bahamas, and Florida. Journal of Geophysical Research, 112: F02009.
Muhs, D.R., Crittenden, R.C., Rosholt, J.N., Bush, C.A., Stewart, K.C., 1987. Genesis of Marine Terrace Soils, Barbados, West-Indies - Evidence from Mineralogy and Geochemistry. Earth Surface Processes and Landforms, 12(6): 605-618.
Napieralski, S.A. et al., 2019. Microbial chemolithotrophy mediates oxidative weathering of granitic bedrock. Proc Natl Acad Sci U S A.
Nikolaidis, N.P., Bouraoui, F., Bidoglio, G., 2013. Hydrologic and geochemical modeling of a karstic Mediterranean watershed. Journal of Hydrology, 477: 129-138.
Oliva, P., Viers, J., Dupré, B., 2003. Chemical weathering in granitic environments. Chemical Geology, 202(3-4): 225-256.

Papanikolaou, D., Vassilakis, E., 2010. Thrust faults and extensional detachment faults in Cretan tectono-stratigraphy: Implications for Middle Miocene extension. Tectonophysics, 488(1-4): 233-247.
Peltola, P., Brun, C., Åström, M., Tomilina, O., 2008. High K/Rb ratios in stream waters — Exploring plant litter decay, ground water and lithology as potential controlling mechanisms. Chemical Geology, 257(1-2): 92-100.
Pett-Ridge, J., 2009. Contributions of dust to phosphorus cycling in tropical forests of the Luquillo Mountains, Puerto Rico. Biogeochemistry, 94(1): 63-80.
Porder, S., Hilley, G.E., 2010. Linking chronosequences with the rest of the world: predicting soil phosphorus content in denuding landscapes. Biogeochemistry, 102(1-3): 153-166.
Porder, S., Hilley, G.E., Chadwick, O.A., 2007a. Chemical weathering, mass loss, and dust inputs across a climate by time matrix in the Hawaiian Islands. Earth and Planetary Science Letters, 258(3-4): 414-427.
Porder, S. et al., 2015. Linking geomorphology, weathering and cation availability in the Luquillo Mountains of Puerto Rico. Geoderma, 249-250: 100-110.
Porder, S., Vitousek, P.M., Chadwick, O.A., Chamberlain, C.P., Hilley, G.E., 2007b. Uplift, Erosion, and Phosphorus Limitation in Terrestrial Ecosystems. Ecosystems, 10(1): 159-171.
Pye, K., 1992. <AEOLIAN DUST TRANSPORT AND DEPOSITION OVER CRETE AND ADJACENT PARTS OF THE MEDITERRANEAN SEA>. Earth Surface Processes and Landforms, 17: 271-288.
Restrepo-Diaz, H., Benlloch, M., Fernández-Escobar, R., 2008a. Plant water stress and K+ starvation reduce absorption of foliar applied K+ by olive leaves. Scientia Horticulturae, 116(4): 409-413.
Restrepo-Diaz, H., Benlloch, M., Navarro, C., Fernández-Escobar, R., 2008b. Potassium fertilization of rainfed olive orchards. Scientia Horticulturae, 116(4): 399-403.
Robertson, R.H.S., Brindley, G.W., Mackenzie, R.C., 1954. Mineralogy of kaolin clays from Pugu, Tanganyika. American Mineralogist, 39: 118-139.
Sekhar, M., Riotte, J., Ruiz, L., Jouquet, J., Braun, J.J., 2016. Influences of Climate and Agriculture on Water and Biogeochemical Cycles: Kabini Critical Zone Observatory. Proceedings of the Indian National Science Academy, 82(3).
Stamati, F.E., Nikolaidis, N.P., Venieri, D., Psillakis, E., Kalogerakis, N., 2011. Dissolved organic nitrogen as an indicator of livestock impacts on soil biochemical quality. Applied Geochemistry, 26: S340-S343.
Strakhov, N., Fitzsimmons, J.P., Murray, R., 1972. Principles of Lithogenesis. Soil Science, 114(5): 408.
Tang, Y., Han, G., Li, F., Wu, Q., 2016. Natural and anthropogenic sources of atmospheric dust at a remote forest area in Guizhou karst region, southwest China. Geochemistry: Exploration, Environment, Analysis, 16(2): 159-163.
Tang, Y., Lian, B., Dong, H., Liu, D., Hou, W., 2012. Endolithic Bacterial Communities in Dolomite and Limestone Rocks from the Nanjiang Canyon in Guizhou Karst Area (China). Geomicrobiology Journal, 29(3): 213-225.
Tanner, E.V.J., Vitousek, P.M., Cuevas, E., 1998. Experimental Investigation of Nutrient Limitation of Forest Growth on Wet Tropical Mountains. Ecology, 79(1): 10-22.
Tsiknia, M., Paranychianakis, N.V., Varouchakis, E.A., Moraetis, D., Nikolaidis, N.P., 2014. Environmental drivers of soil microbial community distribution at the Koiliaris Critical Zone Observatory. FEMS Microbiol Ecol, 90(1): 139-52.
Uhlig, D., Schuessler, J.A., Bouchez, J., Dixon, J.L., von Blanckenburg, F., 2017. Quantifying nutrient uptake as driver of rock weathering in forest ecosystems by magnesium stable isotopes. Biogeosciences, 14(12): 3111-3128.
Uhlig, D., von Blanckenburg, F., 2019. How Slow Rock Weathering Balances Nutrient Loss During Fast Forest Floor Turnover in Montane, Temperate Forest Ecosystems. Frontiers in Earth Science, 7.

Uhliq, D., Blanckenburg, v.F., 2020. Mineral nutrients sourced in deep regolith sustain long-term nutrition of mountainous temperate forest ecosystems. American Geophysical Union.
van der Heijden, G. et al., 2018. Measuring Plant-Available Mg, Ca, and K Pools in the Soil—An Isotopic Dilution Assay. ACS Earth and Space Chemistry, 2(4): 292-313.
Viers, J., Oliva, P., Dandurand, J.L., Dupré, B., Gaillardet, J., 2014. Chemical Weathering Rates, CO2 Consumption, and Control Parameters Deduced from the Chemical Composition of Rivers, Treatise on Geochemistry, pp. 175-194.
Walker, J.C.G., Hays, P.B., Kasting, J.F., 1981. A negative feedback mechanism for the long-term stabilization of earth's surface temperature. Journal of Geophysical Research, 86(9776-9782).
Wang, J. et al., 2014. Erosion-creep-collapse mechanism of underground soil loss for the karst rocky desertification in Chenqi village , Puding county, Guizhou, China.pdf. Environ Earth Sci, 72: 2751-2764.
Wang, S.J. et al., 2004a. How types of carbonate rock assemblages constrain the distribution of karst rocky desertified land in Guizhou Province, PR China: phenomena and mechanisms. Land Degradation & Development, 15(2): 123-131.
Wang, S.J., Liu, Q.M., Zhang, D.F., 2004b. Karst Rocky Desertification in Southwestern China Geomorphology, Land use, Impact and Rehabilitation.pdf. Land Degradation and Management, 15: 115-121.
Wang, X., Lou, J., Cai, D., Jiao, L., 2019. Effects of Earth surface processes on the heterogeneity of surface soil elements and the responses of vegetation elements in the Otindag Desert, China. Catena, 183.
West, A.J., Galy, A., Bickle, M., 2005. Tectonic and climatic controls on silicate weathering. Earth and Planetary Science Letters, 235: 211-228.
White, A.F., Blum, A.E., 1995. Effects of climate on chemical weathering in watersheds. Geochimica et Cosmochimica Acta, 59(9): 1729-1747.
White, A.F., Buss, H.L., 2014. 7.4 - Natural Weathering Rates of Silicate Minerals. In: Holland, H.D., Turekian, K.K. (Eds.), Treatise on Geochemistry (Second Edition). Elsevier, Oxford, pp. 115-155.
White, A.F., Schulz, M.S., Lowenstern, J.B., Vivit, D., Bullen, T.D., 2005. The ubiquitous nature of accessory calcite in granitoid rocks: Implications for weathering and solute evolution, and petrogenesis. Geochimica et Cosmochimica Acta, 69(6): 1455-1471.
White, T.S. et al., 2017. The role of critical zone observatories in critical zone science.
Yaalon, D.H., 1997. Soils in the Mediterranean region what makes them different? Catena, 28: 157-169.
Yang, Q., Chen, H., Li, B., 2015. Source identification and health risk assessment of metals in indoor dust in the vicinity of phosphorus mining, Guizhou Province, China. Arch Environ Contam Toxicol, 68(1): 20-30.
Ye, W. et al., 2011. Mechanism of cultivation soil egradation in rocky desertification areas under dry wet cycles. Environ Earth Sci, 64: 269-276.
Zhao, M., Zeng, C., Liu, Z., Wang, S., 2010. Effect of different land use/land cover on karst hydrogeochemistry: A paired catchment study of Chenqi and Dengzhanhe, Puding, Guizhou, SW China. Journal of Hydrology, 388(1-2): 121-130.
Zhu, L.J., He, S.Y., Li, J.Y., 2008. Weathering-pedogenesis of Carbonate Rocks and Its Environmental Effects in Subtropical Region. Acta Geologica Sinica-English Edition, 82(5): 982-993.
Zhu, X. et al., 2020. Impact of bedrock geochemistry on vegetation productivity depends on climate dryness in the Guizhou karst of China. Progress in Physical Geography: Earth and Environment, 45(1): 20-32.